FIVE-YEAR WILKINSON MICROWAVE ANISOTROPY PROBE (WMAP[1]) OBSERVATIONS: COSMOLOGICAL INTERPRETATION

E. Komatsu [1], J. Dunkley [2,3,4], M. R. Nolta [5], C. L. Bennett [6], B. Gold [6], G. Hinshaw [7], N. Jarosik [2], D. Larson [6], M. Limon [8] L. Page [2], D. N. Spergel [3,9], M. Halpern [10], R. S. Hill [11], A. Kogut [7], S. S. Meyer [12], G. S. Tucker [13], J. L. Weiland [10], E. Wollack [7], and E. L. Wright [14]

ABSTRACT

The *WMAP* 5-year data provide stringent limits on deviations from the minimal, 6-parameter ΛCDM model. We report these limits and use them to constrain the physics of cosmic inflation via Gaussianity, adiabaticity, the power spectrum of primordial fluctuations, gravitational waves, and spatial curvature. We also constrain models of dark energy via its equation of state, parity-violating interaction, and neutrino properties such as mass and the number of species. We detect no convincing deviations from the minimal model. The 6 parameters and the corresponding 68% uncertainties, derived from the *WMAP* data combined with the distance measurements from the Type Ia supernovae (SN) and the Baryon Acoustic Oscillations (BAO) in the distribution of galaxies, are: $\Omega_b h^2 = 0.02265 \pm 0.00059$, $\Omega_c h^2 = 0.1143 \pm 0.0034$, $\Omega_\Lambda = 0.721 \pm 0.015$, $n_s = 0.960^{+0.014}_{-0.013}$, $\tau = 0.084 \pm 0.016$, and $\Delta_\mathcal{R}^2 = (2.457^{+0.092}_{-0.093}) \times 10^{-9}$ at $k = 0.002$ Mpc^{-1}. From these we derive $\sigma_8 = 0.817 \pm 0.026$, $H_0 = 70.1 \pm 1.3$ km s^{-1} Mpc^{-1}, $\Omega_b = 0.0462 \pm 0.0015$, $\Omega_c = 0.233 \pm 0.013$, $\Omega_m h^2 = 0.1369 \pm 0.0037$, $z_{\rm reion} = 10.8 \pm 1.4$, and $t_0 = 13.73 \pm 0.12$ Gyr. With the *WMAP* data combined with BAO and SN, we find the limit on the tensor-to-scalar ratio of $r < 0.20$ (95% CL), and that $n_s > 1$ is disfavored even when gravitational waves are included, which constrains the models of inflation that can produce significant gravitational waves, such as chaotic or power-law inflation models, or a blue spectrum, such as hybrid inflation models. We obtain tight, simultaneous limits on the (constant) equation of state of dark energy and the spatial curvature of the universe: $-0.11 < 1+w < 0.14$ (95% CL) and $-0.0175 < \Omega_k < 0.0085$ (95% CL). We provide a set of "*WMAP* distance priors," to test a variety of dark energy models with spatial curvature. We test a time-dependent w with a present value constrained as $-0.38 < 1+w_0 < 0.14$ (95% CL). Temperature and dark matter fluctuations are found to obey the adiabatic relation to within 8.6% and 2.0% for the axion-type and curvaton-type dark matter, respectively. The power spectra of TB and EB correlations constrain a parity-violating interaction, which rotates the polarization angle and converts E to B. The polarization angle could not be rotated more than $-5.9° < \Delta\alpha < 2.4°$ (95% CL) between the decoupling and the present epoch. We find the limit on the total mass of massive neutrinos of $\sum m_\nu < 0.61$ eV (95% CL), which is free from the uncertainty in the normalization of the large-scale structure data. The number of relativistic degrees of freedom, expressed in units of the effective number of neutrino species, is constrained as $N_{\rm eff} = 4.4 \pm 1.5$ (68%), consistent with the standard value of 3.04. Finally, quantitative limits on physically motivated primordial non-Gaussianity parameters are $-9 < f_{NL}^{\rm local} < 111$ (95% CL) and $-151 < f_{NL}^{\rm equil} < 253$ (95% CL) for the local and equilateral models, respectively.

Subject headings: cosmic microwave background, cosmology: observations, early universe, dark matter, space vehicles, space vehicles: instruments, instrumentation: detectors, telescopes

1. INTRODUCTION

Measurements of microwave background fluctuations by the Cosmic Background Explorer (*COBE* ; Smoot et al. 1992; Bennett et al. 1994, 1996), the Wilkinson

Electronic address: komatsu@astro.as.utexas.edu
[1] *WMAP* is the result of a partnership between Princeton University and NASA's Goddard Space Flight Center. Scientific guidance is provided by the *WMAP* Science Team.
[1] Univ. of Texas, Austin, Dept. of Astronomy, 2511 Speedway, RLM 15.306, Austin, TX 78712
[2] Dept. of Physics, Jadwin Hall, Princeton University, Princeton, NJ 08544-0708
[3] Dept. of Astrophysical Sciences, Peyton Hall, Princeton University, Princeton, NJ 08544-1001
[4] Astrophysics, University of Oxford, Keble Road, Oxford, OX1 3RH, UK
[5] Canadian Institute for Theoretical Astrophysics, 60 St. George St, University of Toronto, Toronto, ON Canada M5S 3H8
[6] Dept. of Physics & Astronomy, The Johns Hopkins University, 3400 N. Charles St., Baltimore, MD 21218-2686
[7] Code 665, NASA/Goddard Space Flight Center, Greenbelt, MD 20771
[8] Columbia Astrophysics Laboratory, 550 W. 120th St., Mail Code 5247, New York, NY 10027-6902
[9] Princeton Center for Theoretical Physics, Princeton University, Princeton, NJ 08544
[10] Dept. of Physics and Astronomy, University of British Columbia, Vancouver, BC Canada V6T 1Z1
[11] Adnet Systems, Inc., 7515 Mission Dr., Suite A100 Lanham, Maryland 20706
[12] Depts. of Astrophysics and Physics, KICP and EFI, University of Chicago, Chicago, IL 60637
[13] Dept. of Physics, Brown University, 182 Hope St., Providence, RI 02912-1843
[14] UCLA Physics & Astronomy, PO Box 951547, Los Angeles, CA 90095–1547

Microwave Anisotropy Probe (*WMAP*; Bennett et al. 2003a,b), and ground and balloon-borne experiments (Miller et al. 1999, 2002; de Bernardis et al. 2000; Hanany et al. 2000; Netterfield et al. 2002; Ruhl et al. 2003; Mason et al. 2003; Sievers et al. 2003, 2007; Pearson et al. 2003; Readhead et al. 2004; Dickinson et al. 2004; Kuo et al. 2004, 2007; Reichardt et al. 2008; Jones et al. 2006; Montroy et al. 2006; Piacentini et al. 2006) have addressed many of the questions that were the focus of cosmology for the past 50 years: How old is the universe? How fast is it expanding? What is the size and shape of the universe? What is the composition of the universe? What seeded the formation of galaxies and large-scale structure?

By accurately measuring the statistical properties of the microwave background fluctuations, *WMAP* has helped establish a standard cosmology: a flat ΛCDM model composed of atoms, dark matter and dark energy, with nearly scale-invariant adiabatic Gaussian fluctuations. With our most recent measurements, *WMAP* has measured the basic parameters of this cosmology to high precision: with the *WMAP* 5-year data alone, we find the density of dark matter (21.4%), the density of atoms (4.4%), the expansion rate of the universe, the amplitude of density fluctuations, and their scale dependence, as well as the optical depth due to reionization (Dunkley et al. 2008).

Cosmologists are now focused on a new set of questions: What is the nature of the dark energy? What is the dark matter? Did inflation seed the primordial fluctuations? If so, what is the class of the inflationary model? How did the first stars form? Microwave background observations from *WMAP*, *Planck*, and from the upcoming generation of CMB ground and balloon-borne experiments will play an important role in addressing these questions.

This paper will discuss how the *WMAP* results, particularly when combined with other astronomical observations (mainly the distance measurements), are now providing new insights into these questions through constraints on gravitational waves and non-adiabatic (entropic) fluctuations, measurements of primordial non-Gaussianity, accurate determination of the primordial spectral index and the geometry of the universe, and limits on parity-violating interactions.

This paper is one of 7 papers on the analysis of the *WMAP* 5-year data: Hinshaw et al. (2008) report on the data processing, map-making, and systematic error limits, Hill et al. (2008) on the physical optics modeling of beams and the 5-year window functions (beam transfer functions), Gold et al. (2008) on the modeling, understanding, and subtraction of the temperature and polarized foreground emission, Wright et al. (2008) on the catalogue of point sources detected in the 5-year temperature data, Nolta et al. (2008) on the measurements of the temperature and polarization power spectra, and Dunkley et al. (2008) on the parameter estimation methodology, the cosmological parameters inferred from the *WMAP* data alone, and comparison between different cosmological data sets.

This paper is organized as follows. In § 2 we briefly summarize new aspects of our analysis of the *WMAP* 5-year temperature and polarization data. In § 3 we constrain the spatial curvature of the observable universe,

Gaussianity/adiabaticity/scale-invariance of the primordial fluctuations, and the amplitude of primordial gravitational waves. We discuss their implications for the physics of the early, primordial universe. In § 4 we demonstrate that the power spectra of TB and EB correlations[16] which are usually ignored in the cosmological analysis, can be used to constrain a certain parity-violating interaction that couples to photons. In § 5 we explore the nature of dark energy, and in § 6 we study the properties of neutrinos in cosmology. We conclude in § 7.

2. SUMMARY OF 5-YEAR ANALYSIS

2.1. *WMAP 5-year data: temperature and polarization*

With 5 years of observations of Jupiter and an extensive physical optics modeling of beams (Hill et al. 2008), our understanding of the beam transfer function, b_l, has improved significantly: the fractional beam errors, $\Delta b_l/b_l$, have been nearly halved in most Differencing Assemblies (DAs). In some cases, e.g., W4, the errors have been reduced by as much as a factor of 4.

While we use only V and W bands for the cosmological analysis of the temperature data, the treatment of b_l in Q band affects our determination of the point source contamination to the angular power spectrum, A_{ps}[17]. The 5-year estimate of the point source correction, $A_{ps} = 0.011 \pm 0.001 \ \mu\mathrm{K}^2$ sr (Nolta et al. 2008), is slightly lower than the 3-year estimate, $A_{ps} = 0.014 \pm 0.003 \ \mu\mathrm{K}^2$ sr (Hinshaw et al. 2007), partly because more sources have been detected and masked by the 5-year source mask (390 sources have been detected in the 5-year temperature data, whereas 323 sources were detected in the 3-year data (Wright et al. 2008)).

Note that the uncertainty in A_{ps} has been reduced by a factor of 3. The uncertainty in the previous estimate was inflated to include the lower value found by Huffenberger et al. (2006) (0.011) and higher value from our original estimate (0.017). Much of the discrepancy between these estimates is due to the multipole range over which A_{ps} is fit. With the improved beam model from the 5-year analysis, the dependence on the multipole range has disappeared, and thus we no longer need to inflate our uncertainty. See Nolta et al. (2008) for more details.

The method for cleaning foreground emission in both temperature and polarization data is the same as we used for the 3-year data, i.e., the template-based cleaning method described in § 5.3 of Hinshaw et al. (2007) for temperature and § 4.3 of Page et al. (2007) for polarization. Gold et al. (2008) describe the results from the template cleaning of the 5-year data with the new coefficients. In addition, Gold et al. (2008) and Dunkley et al. (2008) explore alternative modelings of the foreground emission. All of these methods give consistent results. Gold et al. (2008) also describe definitions of the new masks, *KQ75* and *KQ85*, that replace the previous masks, *Kp0* and *Kp2*, that are recommended for the

---

[16] Here, "TB" refers to the power spectrum of a cross-correlation between the temperature and B-mode polarization, while "EB" refers to a correlation between the E-mode and B-mode polarization.

[17] This quantity, A_{ps}, is the value of the power spectrum, C_l, from unresolved point sources in Q band, *in units of the antenna temperature*. To convert this value to the thermodynamic units, use $C_{ps} = 1.089 A_{ps}$ (Nolta et al. 2008).

TABLE 1
Summary of the cosmological parameters of ΛCDM model and the corresponding 68% intervals

Class	Parameter	*WMAP* 5-year ML[a]	*WMAP*+BAO+SN ML	*WMAP* 5-year Mean[b]	*WMAP*+BAO+SN Mean
Primary	$100\Omega_b h^2$	2.268	2.263	2.273 ± 0.062	2.265 ± 0.059
	$\Omega_c h^2$	0.1081	0.1136	0.1099 ± 0.0062	0.1143 ± 0.0034
	Ω_Λ	0.751	0.724	0.742 ± 0.030	0.721 ± 0.015
	n_s	0.961	0.961	$0.963^{+0.014}_{-0.015}$	$0.960^{+0.014}_{-0.013}$
	τ	0.089	0.080	0.087 ± 0.017	0.084 ± 0.016
	$\Delta^2_{\mathcal{R}}(k_0{}^e)$	2.41×10^{-9}	2.42×10^{-9}	$(2.41 \pm 0.11) \times 10^{-9}$	$(2.457^{+0.092}_{-0.093}) \times 10^{-9}$
Derived	σ_8	0.787	0.811	0.796 ± 0.036	0.817 ± 0.026
	H_0	72.4 km/s/Mpc	70.3 km/s/Mpc	$71.9^{+2.6}_{-2.7}$ km/s/Mpc	70.1 ± 1.3 km/s/Mpc
	Ω_b	0.0432	0.0458	0.0441 ± 0.0030	0.0462 ± 0.0015
	Ω_c	0.206	0.230	0.214 ± 0.027	0.233 ± 0.013
	$\Omega_m h^2$	0.1308	0.1363	0.1326 ± 0.0063	0.1369 ± 0.0037
	$z_{\rm reion}{}^f$	11.2	10.5	11.0 ± 1.4	10.8 ± 1.4
	$t_0{}^g$	13.69 Gyr	13.72 Gyr	13.69 ± 0.13 Gyr	13.73 ± 0.12 Gyr

[a]Dunkley et al. (2008). "ML" refers to the Maximum Likelihood parameters
[b]Dunkley et al. (2008). "Mean" refers to the mean of the posterior distribution of each parameter
[c]Dunkley et al. (2008). "ML" refers to the Maximum Likelihood parameters
[d]Dunkley et al. (2008). "Mean" refers to the mean of the posterior distribution of each parameter
[e]$k_0 = 0.002$ Mpc^{-1}. $\Delta^2_{\mathcal{R}}(k) = k^3 P_{\mathcal{R}}(k)/(2\pi^2)$ (Eq. [15])
[f]"Redshift of reionization," if the universe was reionized instantaneously from the neutral state to the fully ionized state at $z_{\rm reion}$
[g]The present-day age of the universe

analysis of Gaussianity tests and the power spectrum, respectively.

The method for measuring the TT and TE spectra at higher multipoles, i.e., $l \geq 33$ for TT and $l \geq 24$ for TE, is also the same as we used for the 3-year data (Hinshaw et al. 2007). As for the estimation of the cosmological parameters from these spectra, we now include the weak gravitational lensing effect of CMB due to the intervening matter fluctuations (see Lewis & Challinor 2006, for a review), which was not included in the 3-year analysis. We continue to marginalize over a potential contribution from the Sunyaev–Zel'dovich effect (SZE), using exactly the same template SZE power spectrum that we used for the 3-year analysis: $C_l^{\rm SZE}$ from Komatsu & Seljak (2002) with $\Omega_m = 0.26$, $\Omega_b = 0.044$, $h = 0.72$, $n_s = 0.97$, and $\sigma_8 = 0.80$ (see also § 2.1 of Spergel et al. 2007). We continue to use the V and W band data for estimating the high-l temperature power spectrum, and the Q and V band data for the high-l polarization power spectra.

We have improved our treatment of the temperature and polarization power spectra at lower multipoles, as described below.

Low-l temperature – We use the Gibbs sampling technique and the Blackwell-Rao (BR) estimator to evaluate the likelihood of the temperature power spectrum at $l \leq 32$ (Wandelt et al. 2004; Eriksen et al. 2007b). For the 3-year analysis we used the resolution 4 Internal Linear Combination (ILC) temperature map ($N_{\rm side} = 16$) with a Gaussian smoothing of 9.183° (FWHM). Since the ILC map has an intrinsic Gaussian smoothing of 1°, we have added an extra smoothing of 9.1285°. We then evaluated the likelihood directly in the pixel space for a given C_l. For the 5-year analysis we use a higher resolution map, the resolution 5 ILC map ($N_{\rm side} = 32$) with a smaller Gaussian smoothing of 5° (FWHM). The potential foreground leakage due to smoothing is therefore reduced. The BR estimator has an advantage of being much faster to compute, which is why we have adopted the Gibbs sampling and the BR estimator for the 5-year data release. We have confirmed that both

the resolution 4 pixel-based likelihood and the resolution 5 Gibbs-based likelihood yield consistent results (see Dunkley et al. 2008, for details). Both options are made publicly available in the released likelihood code.

Low-l polarization – While we continue to use the direct evaluation of the likelihood of polarization power spectra in pixel space from coadded resolution 3 ($N_{\rm side} = 8$) polarization maps (Stokes Q and U maps), we now add the Ka band data to the coadded maps; we used only Q and V band data for the 3-year analysis. We believe that we understand the polarized foreground emission (dominated by synchrotron, traced well by the K-band data) in the Ka band data well enough to justify the inclusion of the Ka band (Gold et al. 2008). This, with 2 years more integration, has led to a significant reduction of the noise power spectra (averaged over $l = 2 - 7$) in the polarization EE and BB power spectra by a factor of as much as 2.3 compared to the 3-year analysis. As a result, the EE power spectrum averaged over $l = 2 - 7$ exceeds the noise by a factor of 10, i.e., our measurement of the EE power spectrum at $l = 2 - 7$ is now limited by cosmic variance and the possibility of residual foreground emission and/or systematic errors[18], rather than by noise. In addition, we have added a capability of computing the likelihood of TB and EB power spectra to the released likelihood code. This allows us to test models in which non-zero TB and EB correlations can be generated. We discuss this further in § 4.

We continue to use the Markov Chain Monte Carlo (MCMC) technique to explore the posterior distribution of cosmological parameters given the measured temperature and polarization power spectra. For details on the implementation and convergence criteria, see Dunkley et al. (2008).

2.2. *External data sets: Hubble constant, luminosity and angular diameter distances*

[18] For our limits on the residual polarized foreground contamination, see Dunkley et al. (2008).

TABLE 2
Summary of the 95% confidence limits on deviations from the simple (flat, Gaussian, adiabatic, power-law) ΛCDM model

Section	Name	Type	WMAP 5-year	WMAP+BAO+SN
§ 3.2	Gravitational Wave[a]	No Running Ind.	$r < 0.43$[b]	$r < 0.20$
§ 3.1.3	Running Index	No Grav. Wave	$-0.090 < dn_s/d\ln k < 0.019$[c]	$-0.0728 < dn_s/d\ln k < 0.0087$
§ 3.4	Curvature[d]		$-0.063 < \Omega_k < 0.017$[e]	$-0.0175 < \Omega_k < 0.0085$[f]
	Curvature Radius[g]	Positive Curv.	$R_{\rm curv} > 12 \ h^{-1}{\rm Gpc}$	$R_{\rm curv} > 23 \ h^{-1}{\rm Gpc}$
		Negative Curv.	$R_{\rm curv} > 23 \ h^{-1}{\rm Gpc}$	$R_{\rm curv} > 33 \ h^{-1}{\rm Gpc}$
§ 3.5	Gaussianity	Local	$-9 < f_{NL}^{\rm local} < 111$[h]	N/A
		Equilateral	$-151 < f_{NL}^{\rm equil} < 253$[i]	N/A
§ 3.6	Adiabaticity	Axion	$\alpha_0 < 0.16$[j]	$\alpha_0 < 0.067$[k]
		Curvaton	$\alpha_{-1} < 0.011$[l]	$\alpha_{-1} < 0.0037$[m]
§ 4	Parity Violation	Chern-Simons[n]	$-5.9° < \Delta\alpha < 2.4°$	N/A
§ 5	Dark Energy	Constant w[o]	$-1.37 < 1 + w < 0.32$[p]	$-0.11 < 1 + w < 0.14$
		Evolving $w(z)$[q]	N/A	$-0.38 < 1 + w_0 < 0.14$[r]
§ 6.1	Neutrino Mass[s]		$\sum m_\nu < 1.3$ eV[t]	$\sum m_\nu < 0.61$ eV[u]
§ 6.2	Neutrino Species		$N_{\rm eff} > 2.3$[v]	$N_{\rm eff} = 4.4 \pm 1.5$[w] (68%)

[a]In the form of the tensor-to-scalar ratio, r, at $k = 0.002$ Mpc^{-1}
[b]Dunkley et al. (2008)
[c]Dunkley et al. (2008)
[d](Constant) dark energy equation of state allowed to vary ($w \neq -1$)
[e]With the HST prior, $H_0 = 72 \pm 8$ km/s/Mpc. For $w = -1$, $-0.052 < \Omega_k < 0.013$ (95% CL)
[f]For $w = -1$, $-0.0181 < \Omega_k < 0.0071$ (95% CL)
[g]$R_{\rm curv} = (c/H_0)/\sqrt{|\Omega_k|} = 3/\sqrt{|\Omega_k|} \ h^{-1}{\rm Gpc}$
[h]Cleaned V+W map with $l_{\rm max} = 500$ and the KQ75 mask, after the point source correction
[i]Cleaned V+W map with $l_{\rm max} = 700$ and the KQ75 mask, after the point source correction
[j]Dunkley et al. (2008)
[k]In terms of the adiabaticity deviation parameter, $\delta_{adi}^{(c,\gamma)} = \sqrt{\alpha}/3$ (Eq. [39]), the axion-like dark matter and photons are found to obey the adiabatic relation (Eq. [36]) to 8.6%.
[l]Dunkley et al. (2008)
[m]In terms of the adiabaticity deviation parameter, $\delta_{adi}^{(c,\gamma)} = \sqrt{\alpha}/3$ (Eq. [39]), the curvaton-like dark matter and photons are found to obey the adiabatic relation (Eq. [36]) to 2.0%.
[n]For an interaction of the form given by $(\phi/M)F_{\alpha\beta}\tilde{F}^{\alpha\beta}$, the polarization rotation angle is $\Delta\alpha = M^{-1} \int \frac{dt}{a}\dot{\phi}$
[o]For spatially curved universes ($\Omega_k \neq 0$)
[p]With the HST prior, $H_0 = 72 \pm 8$ km/s/Mpc
[q]For a flat universe ($\Omega_k = 0$)
[r]$w_0 \equiv w(z = 0)$
[s]$\sum m_\nu = 94(\Omega_\nu h^2)$ eV
[t]Dunkley et al. (2008)
[u]For $w = -1$. For $w \neq -1$, $\sum m_\nu < 0.66$ eV (95% CL)
[v]Dunkley et al. (2008)
[w]With the HST prior, $H_0 = 72 \pm 8$ km/s/Mpc. The 95% limit is $1.9 < N_{\rm eff} < 7.8$

TABLE 3
Sound horizon scales determined by the WMAP 5-year data. CMB: the sound horizon scale at the photon decoupling epoch, z_*, imprinted on the CMB power spectrum; Matter: the sound horizon scale at the baryon drag epoch, z_d, imprinted on the matter (galaxy) power spectrum.

	Quantity	Eq.	5-year WMAP
CMB	z_*	(66)	1090.51 ± 0.95
CMB	$r_s(z_*)$	(6)	146.8 ± 1.8 Mpc
Matter	z_d	(3)	1020.5 ± 1.6
Matter	$r_s(z_d)$	(6)	153.3 ± 2.0 Mpc

Aside from the CMB data (including the small-scale CMB measurements), the main external astrophysical results that we shall use in this paper for the joint cosmological analysis are the following distance-scale indicators:

- A Gaussian prior on the present-day Hubble's constant from the Hubble Key Project final results, $H_0 = 72 \pm 8$ km s^{-1} Mpc^{-1} (Freedman et al. 2001).

While the uncertainty is larger than the WMAP's determination of H_0 for the minimal ΛCDM model (see Table 1), this information improves upon limits on the other models, such as models with non-zero spatial curvature.

- The luminosity distances out to Type Ia supernovae with their absolute magnitudes marginalized over uniform priors. We combine measurements from the Hubble Space Telescope (Riess et al. 2004, 2007), the SuperNova Legacy Survey (SNLS) (Astier et al. 2006), and the Equation of State: SupErNovae trace Cosmic Expansion (ESSENCE) survey (Wood-Vasey et al. 2007).

- Gaussian priors on the distance ratios, $r_s/D_V(z)$, at $z = 0.2$ and 0.35 measured from the Baryon Acoustic Oscillations (BAO) in the distribution of galaxies (Percival et al. 2007). The CMB observations measure the acoustic oscillations in the photon-baryon plasma, which can be used to measure the angular diameter distance to the photon decoupling epoch. The same oscillations are imprinted on the distribution of matter, traced by the

distribution of galaxies, which can be used to measure the angular distances to the galaxies that one observes from galaxy surveys. While both CMB and galaxies measure the same oscillations, in this paper we shall use the term, BAO, to refer only to the oscillations in the distribution of matter, for definiteness.

Here, we describe how we use the BAO data in more detail. The BAO can be used to measure not only the angular diameter distance, $D_A(z)$, through the clustering perpendicular to the line of sight, but also the expansion rate of the universe, $H(z)$, through the clustering along the line of sight. This is a powerful probe of dark energy; however, the accuracy of the current data do not allow us to extract $D_A(z)$ and $H(z)$ separately, as one can barely measure BAO in the spherically averaged correlation function (Okumura et al. 2007).

The spherical average gives us the following effective distance measure (Eisenstein et al. 2005):

$$D_V(z) \equiv \left[(1+z)^2 D_A^2(z) \frac{cz}{H(z)} \right]^{1/3}, \quad (1)$$

where $D_A(z)$ is the proper (not comoving) angular diameter distance:

$$D_A(z) = \frac{c}{H_0} \frac{f_k \left[H_0 \sqrt{|\Omega_k|} \int_0^z \frac{dz'}{H(z')} \right]}{(1+z)\sqrt{|\Omega_k|}}, \quad (2)$$

where $f_k[x] = \sin x$, x, and $\sinh x$ for $\Omega_k < 0$ ($k = 1$), $\Omega_k = 0$ ($k = 0$), and $\Omega_k > 0$ ($k = -1$), respectively.

There is an additional subtlety. The peak positions of the (spherically averaged) BAO depend actually on the *ratio* of $D_V(z)$ to the sound horizon size at the so-called drag epoch, z_d, at which baryons were released from photons. Note that there is no reason why the decoupling epoch of photons, z_*, needs to be the same as the drag epoch, z_d. They would be equal only when the energy density of photons and that of baryons were equal at the decoupling epoch – more precisely, they would be equal only when $R(z) \equiv 3\rho_b/(4\rho_\gamma) = (3\Omega_b/4\Omega_\gamma)/(1 + z) \simeq 0.67(\Omega_b h^2/0.023)[1090/(1 + z)]$ was unity at $z = z_*$. Since we happen to live in the universe in which $\Omega_b h^2 \simeq 0.023$, this ratio is less than unity, and thus the drag epoch is slightly later than the photon decoupling epoch, $z_d < z_*$. As a result, the sound horizon size at the drag epoch happens to be slightly larger than that at the photon decoupling epoch. In Table 3 we give the CMB decoupling epoch, BAO drag epoch, as well as the corresponding sound horizon radii that are determined from the *WMAP* 5-year data.

We use a fitting formula for z_d proposed by Eisenstein & Hu (1998):

$$z_d = \frac{1291(\Omega_m h^2)^{0.251}}{1 + 0.659(\Omega_m h^2)^{0.828}} \left[1 + b_1 (\Omega_b h^2)^{b2} \right], \quad (3)$$

where

$$b_1 = 0.313(\Omega_m h^2)^{-0.419} \left[1 + 0.607(\Omega_m h^2)^{0.674} \right], \quad (4)$$

$$b_2 = 0.238(\Omega_m h^2)^{0.223}. \quad (5)$$

In this paper we frequently combine the *WMAP* data with $r_s(z_d)/D_V(z)$ extracted from the Sloan Digital Sky

Survey (SDSS) and the Two Degree Field Galaxy Redshift Survey (2dFGRS) (Percival et al. 2007), where $r_s(z)$ is the comoving sound horizon size given by

$$r_s(z) = \frac{c}{\sqrt{3}} \int_0^{1/(1+z)} \frac{da}{a^2 H(a) \sqrt{1 + (3\Omega_b/4\Omega_\gamma)a}}, \quad (6)$$

where $\Omega_\gamma = 2.469 \times 10^{-5} h^{-2}$ for $T_{\rm cmb} = 2.725$ K, and

$$H(a) = H_0 \left[\frac{\Omega_m}{a^3} + \frac{\Omega_r}{a^4} + \frac{\Omega_k}{a^2} + \frac{\Omega_\Lambda}{a^{3(1+w_{\rm eff}(a))}} \right]^{1/2}. \quad (7)$$

The radiation density parameter, Ω_r, is the sum of photons and relativistic neutrinos,

$$\Omega_r = \Omega_\gamma \left(1 + 0.2271 N_{\rm eff} \right), \quad (8)$$

where $N_{\rm eff}$ is the effective number of neutrino species (the standard value is 3.04). For more details on $N_{\rm eff}$, see § 6.2. When neutrinos are non-relativistic at a, one needs to reduce the value of $N_{\rm eff}$ accordingly. Also, the matter density must contain the neutrino contribution when they are non-relativistic,

$$\Omega_m = \Omega_c + \Omega_b + \Omega_\nu, \quad (9)$$

where Ω_ν is related to the sum of neutrino masses as

$$\Omega_\nu = \frac{\sum m_\nu}{94 h^2 \text{ eV}}. \quad (10)$$

For more details on the neutrino mass, see § 6.1.

All the density parameters refer to the values at the present epoch, and add up to unity:

$$\Omega_m + \Omega_r + \Omega_k + \Omega_\Lambda = 1. \quad (11)$$

Throughout this paper, we shall use Ω_Λ to denote the dark energy density parameter at present:

$$\Omega_\Lambda \equiv \Omega_{de}(z = 0). \quad (12)$$

Here, $w_{\rm eff}(a)$ is the effective equation of state of dark energy given by

$$w_{\rm eff}(a) \equiv \frac{1}{\ln a} \int_0^{\ln a} d\ln a' \ w(a'), \quad (13)$$

and $w(a)$ is the usual dark energy equation of state, i.e., the dark energy pressure divided by the dark energy density:

$$w(a) \equiv \frac{P_{de}(a)}{\rho_{de}(a)}. \quad (14)$$

For vacuum energy (cosmological constant), w does not depend on time, and $w = -1$.

Percival et al. (2007) have determined $r_s(z_d)/D_V(z)$ out to two redshifts, $z = 0.2$ and 0.35, as $r_s(z_d)/D_V(z = 0.2) = 0.1980 \pm 0.0058$ and $r_s(z_d)/D_V(z = 0.35) = 0.1094 \pm 0.0033$, with a correlation coefficient of 0.39. We follow the description given in Appendix A of Percival et al. (2007) to implement these constraints in the likelihood code. We have checked that our calculation of $r_s(z_d)$ using the formulae above (including z_d) matches the value that they quote[19], 111.49 h^{-1} Mpc, to within

---

[19] In Percival et al. (2007) the authors use a different notation for the drag redshift, z_*, instead of z_d. We have confirmed that they have used equation (6) of Eisenstein & Hu (1998) for r_s, which makes an explicit use of the drag redshift (Will Percival, private communication).

0.2 h^{-1} Mpc, for their quoted cosmological parameters, $\Omega_m = 0.25$, $\Omega_b h^2 = 0.0223$, and $h = 0.72$.

We have decided to use these results, as they measure the distances only, and are not sensitive to the growth of structure. This properly enables us to identify the information added by the external astrophysical results more clearly. In addition to these, we shall also use the BAO measurement by Eisenstein et al. (2005)[20], and the flux power spectrum of Lyα forest from Seljak et al. (2006) in the appropriate context.

For the 3-year data analysis in Spergel et al. (2007) we also used the shape of the galaxy power spectra measured from the SDSS main sample as well as the Luminous Red Galaxies (Tegmark et al. 2004b, 2006), and 2dFGRS (Cole et al. 2005). We have found some tension between these data sets, which could be indicative of the degree by which our understanding of non-linearities, such as the non-linear matter clustering, non-linear bias, and non-linear redshift space distortion, is still limited at low redshifts, i.e., $z \lesssim 1$. See Dunkley et al. (2008) for more detailed study on this issue. See also Sanchez & Cole (2007) on the related subject. The galaxy power spectra should provide us with important information on the growth of structure (which helps constrain the dark energy and neutrino masses) as our understanding of non-linearities improves in the future. In this paper we do not combine these data sets because of the limited understanding of the consequences of non-linearities.

3. FLAT, GAUSSIAN, ADIABATIC, POWER-LAW ΛCDM MODEL AND ITS ALTERNATIVES

The theory of inflation, the idea that the universe underwent a brief period of rapid accelerated expansion (Starobinsky 1979; Starobinsky 1982; Kazanas 1980; Guth 1981; Sato 1981; Linde 1982; Albrecht & Steinhardt 1982), has become an indispensable building block of the standard model of our universe.

Models of the early universe must explain the following observations: the universe is nearly flat and the fluctuations observed by *WMAP* appear to be nearly Gaussian (Komatsu et al. 2003), scale-invariant, super-horizon, and adiabatic (Spergel & Zaldarriaga 1997; Spergel et al. 2003; Peiris et al. 2003). Inflation models have been able to explain these properties successfully (Mukhanov & Chibisov 1981; Hawking 1982; Starobinsky 1982; Guth & Pi 1982; Bardeen et al. 1983).

Although many models have been ruled out observationally (see Kinney et al. 2006; Alabidi & Lyth 2006a, for recent surveys), there are more than one hundred candidate inflation models available (see Liddle & Lyth 2000; Bassett et al. 2006; Linde 2008, for reviews). Therefore, we now focus on the question, "*which model is the correct inflation model?*" This must be answered by the observational data.

On the other hand, an inflationary expansion may not be the only way to solve cosmological puzzles and create primordial fluctuations. Contraction of the primordial universe followed by a bounce to expansion can, in principle, make a set of predictions that are qualitatively similar to those of inflation models (Khoury et al. 2001, 2002a,b; Khoury et al. 2003; Buchbinder et al. 2007;

Buchbinder et al. 2007; Koyama & Wands 2007; Koyama et al. 2007; Creminelli & Senatore 2007).

There is also a fascinating possibility that one can learn something about the fundamental physics from cosmological observations. For example, a recent progress in implementing de Sitter vacua and inflation in the context of String Theory (see McAllister & Silverstein 2008, for a review), makes it possible to connect the cosmological observations to the ingredients of the fundamental physics via their predicted properties of inflation such as the shape of the power spectrum, spatial curvature of the universe, and non-Gaussianity of primordial fluctuations.

3.1. *Power spectrum of primordial fluctuations*

3.1.1. *Motivation and Analysis*

The shape of the power spectrum of primordial curvature perturbations, $P_\mathcal{R}(k)$, is one of the most powerful and practical tool for distinguishing among inflation models. Inflation models with featureless scalar-field potentials usually predict that $P_\mathcal{R}(k)$ is *nearly* a power-law (Kosowsky & Turner 1995)

$$\Delta_\mathcal{R}^2(k) \equiv \frac{k^3 P_\mathcal{R}(k)}{2\pi^2} = \Delta_\mathcal{R}^2(k_0) \left(\frac{k}{k_0}\right)^{n_s(k_0)-1+\frac{1}{2} dn_s/d\ln k}.$$
(15)

Here, $\Delta_\mathcal{R}^2(k)$ is a useful quantity, which gives an approximate contribution of $\mathcal{R}$ at a given scale per logarithmic interval in k to the total variance of $\mathcal{R}$, as $\langle \mathcal{R}^2(\mathbf{x}) \rangle = \int d\ln k \, \Delta_\mathcal{R}^2(k)$. It is clear that the special case with $n_s = 1$ and $dn_s/d\ln k = 0$ results in the "scale-invariant spectrum," in which the contributions of $\mathcal{R}$ at any scales per logarithmic interval in k to the total variance are equal. (Hence the term, "scale invariance.") Following the usual terminology, we shall call n_s and $dn_s/d\ln k$ the tilt of the spectrum and the running index, respectively. We shall take k_0 to be 0.002 Mpc^{-1}.

The significance of n_s and $dn_s/d\ln k$ is that different inflation models motivated by different physics make specific, testable predictions for the values of n_s and $dn_s/d\ln k$. For a given shape of the scalar field potential, $V(\phi)$, of a single-field model, for instance, one finds that n_s is given by a combination of the first derivative and second derivative of the potential, $1 - n_s = 3M_{pl}^2(V'/V)^2 - 2M_{pl}^2(V''/V)$ (where $M_{pl}^2 = 1/(8\pi G)$ is the reduced Planck mass), and $dn_s/d\ln k$ is given by a combination of V'/V, V''/V, and V'''/V (see Liddle & Lyth 2000, for a review).

This means that one can reconstruct the shape of $V(\phi)$ up to the first three derivatives in this way. As the expansion rate squared is proportional to $V(\phi)$ via the Friedmann equation, $H^2 = V/(3M_{pl}^2)$, one can reconstruct the expansion history during inflation from measuring the shape of the primordial power spectrum.

How generic are n_s and $dn_s/d\ln k$? They are motivated physically by the fact that most inflation models satisfy the slow-roll conditions, and thus deviations from a pure power-law, scale-invariant spectrum, $n_s = 1$ and $dn_s/d\ln k = 0$, are expected to be small, and the higher-order derivative terms such as V'''' and higher are negligible. On the other hand, there is always a danger of missing some important effects, such as sharp features, when one relies too much on a simple parametrization like this. Therefore, a number of people have investi-

---

[20] We use a Gaussian prior on $A = D_V(z = 0.35)\sqrt{\Omega_m H_0^2}/(0.35c) = 0.469(n_s/0.98)^{-0.35} \pm 0.017$.

TABLE 4
PRIMORDIAL TILT n_s, RUNNING INDEX $dn_s/d\ln k$, AND TENSOR-TO-SCALAR RATIO r

Sec.	Model	Parameter[a]	5-year WMAP[b]	5-year WMAP+CMB[c]	5-year WMAP+ACBAR08[d]	5-year WMAP+BAO+SN
§ 3.1.2	Power-law	n_s	$0.963^{+0.014}_{-0.015}$	0.960 ± 0.014	0.964 ± 0.014	$0.960^{+0.014}_{-0.013}$
§ 3.1.3	Running	n_s	$1.031^{+0.054}_{-0.055}$	$1.059^{+0.051}_{-0.049}$	1.031 ± 0.049	$1.022^{+0.043}_{-0.042}$
		$dn_s/d\ln k$	-0.037 ± 0.028	-0.053 ± 0.025	$-0.035^{+0.024}_{-0.025}$	$-0.032^{+0.021}_{-0.020}{}_i$
§ 3.2.4	Tensor	n_s	0.986 ± 0.022	0.979 ± 0.020	$0.985^{+0.019}_{-0.020}$	0.968 ± 0.015
		r	< 0.43 (95% CL)	< 0.36 (95% CL)	< 0.40 (95% CL)	< 0.20 (95% CL)
§ 3.2.4	Running	n_s	$1.087^{+0.072}_{-0.073}$	$1.127^{+0.075}_{-0.071}$	$1.083^{+0.063}_{-0.062}$	$1.093^{+0.068}_{-0.069}$
	+Tensor	r	< 0.58 (95% CL)	< 0.64 (95% CL)	< 0.54 (95% CL)	< 0.54 (95% CL)[j]
		$dn_s/d\ln k$	-0.050 ± 0.034	$-0.072^{+0.031}_{-0.030}$	-0.048 ± 0.027	$-0.055^{+0.027}_{-0.028}{}_k$

[a]Defined at $k_0 = 0.002$ Mpc^{-1}

[b]Dunkley et al. (2008)

[c]"CMB" includes the small-scale CMB measurements from CBI (Mason et al. 2003; Sievers et al. 2003, 2007; Pearson et al. 2003; Readhead et al. 2004), VSA (Dickinson et al. 2004), ACBAR (Kuo et al. 2004, 2007), and BOOMERanG (Ruhl et al. 2003; Montroy et al. 2006; Piacentini et al. 2006)

[d]"ACBAR08" is the complete ACBAR data set presented in Reichardt et al. (2008). We used the ACBAR data in the multipole range of $900 < l < 2000$

[e]Defined at $k_0 = 0.002$ Mpc^{-1}

[f]Dunkley et al. (2008)

[g]"CMB" includes the small-scale CMB measurements from CBI (Mason et al. 2003; Sievers et al. 2003, 2007; Pearson et al. 2003; Readhead et al. 2004), VSA (Dickinson et al. 2004), ACBAR (Kuo et al. 2004, 2007), and BOOMERanG (Ruhl et al. 2003; Montroy et al. 2006; Piacentini et al. 2006)

[h]"ACBAR08" is the complete ACBAR data set presented in Reichardt et al. (2008). We used the ACBAR data in the multipole range of $900 < l < 2000$

[i]With the Lyα forest data (Seljak et al. 2006), $dn_s/d\ln k = -0.012 \pm 0.012$

[j]With the Lyα forest data (Seljak et al. 2006), $r < 0.28$ (95% CL)

[k]With the Lyα forest data (Seljak et al. 2006), $dn_s/d\ln k = -0.017^{+0.014}_{-0.013}$
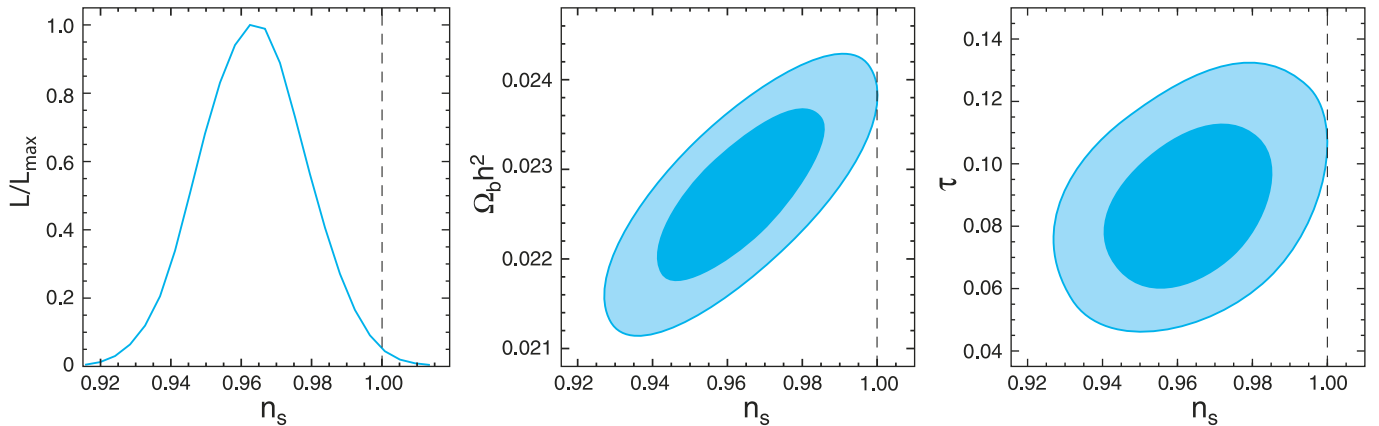

FIG. 1.— Constraint on the primordial tilt, n_s (§ 3.1.2). No running index or gravitational waves are included in the analysis. (*Left*) One-dimensional marginalized constraint on n_s from the WMAP-only analysis. (*Middle*) Two-dimensional joint marginalized constraint (68% and 95% CL), showing a strong degeneracy between n_s and $\Omega_b h^2$. (*Right*) A mild degeneracy with τ. None of these degeneracies improve significantly by including BAO or SN data, as these data sets are not sensitive to $\Omega_b h^2$ or τ; however, the situation changes when the gravitational wave contribution is included (see Fig. 3).

gated various, more general ways of reconstructing the shape of $P_{\mathcal{R}}(k)$ (Matsumiya et al. 2002, 2003; Mukherjee & Wang 2003b,a,c; Bridle et al. 2003; Kogo et al. 2004; Kogo et al. 2005; Hu & Okamoto 2004; Hannestad 2004; Shafieloo & Souradeep 2004; Sealfon et al. 2005; Tocchini-Valentini et al. 2005, 2006; Spergel et al. 2007; Shafieloo & Souradeep 2007; Verde & Peiris 2008), and $V(\phi)$ (Lidsey et al. 1997; Grivell & Liddle 2000; Kadota et al. 2005; Covi et al. 2006; Lesgourgues & Valkenburg 2007; Powell & Kinney 2007).

These studies have indicated that the parametrized form (Eq. [15]) is basically a good fit, and no significant features were detected. Therefore, we do not repeat this type of analysis in this paper, but focus on constraining the parametrized form given by Eq. (15).

Finally, let us comment on the choice of priors. We impose uniform priors on n_s and $dn_s/d\ln k$, but there are other possibilities for the choice of priors. For example, one may impose uniform priors on the slow-roll parameters, $\epsilon = (M_{pl}^2/2)(V'/V)^2$, $\eta = M_{pl}^2(V''/V)$, and $\xi = M_{pl}^4(V'V'''/V^2)$, as well as on the number of e-foldings, N, rather than on n_s and $dn_s/d\ln k$ (Peiris & Easther 2006a,b; Easther & Peiris 2006). It has been found that, as long as one imposes a reasonable lower bound on N, $N > 30$, both approaches yield similar results.

To constrain n_s and $dn_s/d\ln k$, we shall use the *WMAP* 5-year temperature and polarization data, the small-scale CMB data, and/or BAO and SN distance

measurements. In Table 4 we summarize our results presented in § 3.1.2, 3.1.3, and 3.2.4.

3.1.2. Results: Tilt

First, we test the inflation models with $dn_s/d\ln k = 0$, and negligible gravitational waves. The *WMAP* 5-year temperature and polarization data yield $n_s = 0.963^{+0.014}_{-0.015}$, which is slightly above the 3-year value with a smaller uncertainty, $n_s(3\text{yr}) = 0.958 \pm 0.016$ (Spergel et al. 2007). We shall provide the reason for this small upward shift in § 3.1.3.

The scale-invariant, Harrison–Zel'dovich–Peebles spectrum, $n_s = 1$, is at 2.5 standard deviations away from the mean of the likelihood for the WMAP-only analysis. The significance increases to 2.9 standard deviations for WMAP+BAO+SN. Looking at the two-dimensional constraints that include n_s, we find that the most dominant degeneracy that is still left is the degeneracy between n_s and $\Omega_b h^2$ (see Fig. 1). The larger $\Omega_b h^2$ is, the smaller the second peak becomes, and the larger n_s is required to compensate it. Also, the larger $\Omega_b h^2$ is, the larger the Silk damping (diffusion damping) becomes, and the larger n_s is required to compensate it.

This argument suggests that the constraint on n_s should improve as we add more information from the small-scale CMB measurements that probe the Silk damping scales; however, the current data do not improve the constraint very much yet: $n_s = 0.960 \pm 0.014$ from WMAP+CMB, where "CMB" includes the small-scale CMB measurements from CBI (Mason et al. 2003; Sievers et al. 2003, 2007; Pearson et al. 2003; Readhead et al. 2004), VSA (Dickinson et al. 2004), ACBAR (Kuo et al. 2004, 2007), and BOOMERanG (Ruhl et al. 2003; Montroy et al. 2006; Piacentini et al. 2006), all of which go well beyond the *WMAP* angular resolution, so that their small-scale data are statistically independent of the *WMAP* data.

There is still a bit of degeneracy left between n_s and the electron-scattering optical depth, τ (see Fig. 1). While a better measurement of τ from future *WMAP* observations as well as the *Planck* satellite should help reduce the uncertainty in n_s via a better measurement of τ, the effect of $\Omega_b h^2$ is much larger.

We find that the other data sets, such as BAO, SN, and the shape of galaxy power spectrum from SDSS or 2dFGRS, do not improve our constraints on n_s, as these data sets are not sensitive to $\Omega_b h^2$ or τ; however, this will change when we include the running index, $dn_s/d\ln k$ (§ 3.1.3) and/or the tensor-to-scalar ratio, r (§ 3.2.4).

3.1.3. Results: Running index

Next, we explore more general models in which a sizable running index may be generated. (We still do not include gravitational waves; see § 3.2 for the analysis that includes gravitational waves.) We find no evidence for $dn_s/d\ln k$ from WMAP only, $-0.090 < dn_s/d\ln k < 0.019$ (95% CL), or WMAP+BAO+SN $-0.0728 < dn_s/d\ln k < 0.0087$ (95% CL). The improvement from WMAP-only to WMAP+BAO+SN is only modest.

We find a slight upward shift from the 3-year result, $dn_s/d\ln k = -0.055^{+0.030}_{-0.031}$ (68% CL; Spergel et al. 2003), to the 5-year result, $dn_s/d\ln k = -0.037 \pm 0.028$ (68%

CL; WMAP only). This is caused by a combination of three effects:

(i) The 3-year number for $dn_s/d\ln k$ was derived from an older analysis pipeline for the temperature data, namely, the resolution 3 (instead of 4) pixel-based low-l temperature likelihood and a higher point-source amplitude, $A_{ps} = 0.017\ \mu\text{K}^2$ sr.

(ii) With two years more integration, we have a better signal-to-noise near the third acoustic peak, whose amplitude is slightly higher than the 3-year determination (Nolta et al. 2008).

(iii) With the improved beam model (Hill et al. 2008), the temperature power spectrum at $l \gtrsim 200$ has been raised nearly uniformly by $\sim 2.5\%$ (Hill et al. 2008; Nolta et al. 2008).

All of these effects go in the same direction, i.e., to increase the power at high multipoles and reduce a negative running index. We find that these factors contribute to the upward shift in $dn_s/d\ln k$ at comparable levels.

Note that an upward shift in n_s for a power-law model, 0.958 to 0.963 (§ 3.1.2), is not subject to (i) because the 3-year number for n_s was derived from an updated analysis pipeline using the resolution 4 low-l code and $A_{ps} = 0.014\ \mu\text{K}^2$ sr. We find that (ii) and (iii) contribute to the shift in n_s at comparable levels. An upward shift in σ_8 from the 3-year value, 0.761, to the 5-year value, 0.796, can be explained similarly.

We do not find any significant evidence for the running index when the *WMAP* data and small-scale CMB data (CBI, VSA, ACBAR07, BOOMERanG) are combined, $-0.1002 < dn_s/d\ln k < -0.0037$ (95% CL), or the *WMAP* data and the latest results from the analysis of the complete ACBAR data (Reichardt et al. 2008) are combined, $-0.082 < dn_s/d\ln k < 0.015$ (95% CL).

Our best 68% CL constraint from WMAP+BAO+SN shows no evidence for the running index, $dn_s/d\ln k = -0.032^{+0.021}_{-0.020}$. In order to improve upon the limit on $dn_s/d\ln k$, one needs to determine n_s at small scales, as $dn_s/d\ln k$ is simply given by the difference between n_s's measured at two different scales, divided by the logarithmic separation between two scales. The Lyα forest provides such information (see § 7; also Table 4).

3.2. Primordial gravitational waves

3.2.1. Motivation

The presence of primordial gravitational waves is a robust prediction of inflation models, as the same mechanism that generated primordial density fluctuations should also generate primordial gravitational waves (Grishchuk 1975; Starobinsky 1979). The amplitude of gravitational waves relative to that of density fluctuations is model-dependent.

The primordial gravitational waves leave their signatures imprinted on the CMB temperature anisotropy (Rubakov et al. 1982; Fabbri & Pollock 1983; Abbott & Wise 1984; Starobinsky 1985; Crittenden et al. 1993), as well as on polarization (Basko & Polnarev 1980; Bond & Efstathiou 1984; Polnarev 1985; Crittenden et al. 1993, 1995; Coulson et al. 1994). The spin-2 nature of gravitational waves leads to two types of polarization pattern on

the sky (Zaldarriaga & Seljak 1997; Kamionkowski et al. 1997): (i) the curl-free mode (E mode), in which the polarization directions are either purely radial or purely tangential to hot/cold spots in temperature, and (ii) the divergence-free mode (B mode), in which the pattern formed by polarization directions around hot/cold spots possess non-zero vorticity.

In the usual gravitational instability picture, in the linear regime (before shell crossing of fluid elements) velocity perturbations can be written in terms of solely a gradient of a scalar velocity potential u, $\vec{v} = \vec{\nabla} u$. This means that no vorticity would arise, and therefore no B mode polarization can be generated from density or velocity perturbations in the linear regime. However, primordial gravitational waves can generate both E and B mode polarization; thus, the B mode polarization offers a smoking-gun signature for the presence of primordial gravitational waves (Seljak & Zaldarriaga 1997; Kamionkowski et al. 1997). This gives us a strong motivation to look for signatures of the primordial gravitational waves in CMB.

In Table 4 we summarize our constraints on the amplitude of gravitational waves, expressed in terms of the tensor-to-scalar ratio, r, defined by equation (20).

3.2.2. *Analysis*

We quantify the amplitude and spectrum of primordial gravitational waves in the following form:

$$\Delta_h^2(k) \equiv \frac{k^3 P_h(k)}{2\pi^2} = \Delta_h^2(k_0) \left(\frac{k}{k_0}\right)^{n_t}, \qquad (16)$$

where we have ignored a possible scale dependence of $n_t(k)$, as the current data cannot constrain it. Here, by $P_h(k)$ we mean

$$\langle \tilde{h}_{ij}(\mathbf{k})\tilde{h}^{ij}(\mathbf{k}')\rangle = (2\pi)^2 P_h(k)\delta^3(\mathbf{k} - \mathbf{k}'), \qquad (17)$$

where $\tilde{h}_{ij}(\mathbf{k})$ is the Fourier transform of the tensor metric perturbations, $g_{ij} = a^2(\delta_{ij} + h_{ij})$, which can be further decomposed into the two polarization states ($+$ and $\times$) with the appropriate polarization tensor, $e_{ij}^{(+,\times)}$, as

$$\tilde{h}_{ij}(\mathbf{k}) = \tilde{h}_+(\mathbf{k})e_{ij}^+(\mathbf{k}) + \tilde{h}_\times(\mathbf{k})e_{ij}^\times(\mathbf{k}), \qquad (18)$$

with the normalization that $e_{ij}^+ e^{+,ij} = e_{ij}^\times e^{\times,ij} = 2$ and $e_{ij}^+ e^{\times,ij} = 0$. Unless there was a parity-violating interaction term such as $f(\phi)R_{\mu\nu\rho\sigma}\tilde{R}^{\mu\nu\rho\sigma}$ where $f(\phi)$ is an arbitrary function of a scalar field, $R_{\mu\nu\rho\sigma}$ is the Riemann tensor, and $\tilde{R}^{\mu\nu\rho\sigma}$ is a dual tensor (Lue et al. 1999), both polarization states are statistically independent with the same amplitude, meaning

$$\langle |\tilde{h}_+|^2\rangle = \langle |\tilde{h}_\times|^2\rangle \equiv \langle |\tilde{h}|^2|\rangle, \qquad \langle \tilde{h}_\times \tilde{h}_+^*\rangle = 0. \qquad (19)$$

This implies that parity-violating correlations such as the TB and EB correlations must vanish. We shall explore such parity-violating correlations in § 4 in a slightly different context. For limits on the difference between $\langle |\tilde{h}_+|^2\rangle$ and $\langle |\tilde{h}_\times|^2\rangle$ from the TB and EB spectra of the *WMAP* 3-year data, see Saito et al. (2007).

In any case, this definition suggests that $P_h(k)$ is given by $P_h(k) = 4\langle |\tilde{h}|^2\rangle$. Notice a factor of 4. This is the definition of $P_h(k)$ that we have been using consistently

since the first year release (Peiris et al. 2003; Spergel et al. 2003, 2007; Page et al. 2007). We continue to use this definition.

With this definition of $\Delta_h^2(k)$ (Eq. [16]), we define the tensor-to-scalar ratio, r, at $k = k_0$, as

$$r \equiv \frac{\Delta_h^2(k_0)}{\Delta_\mathcal{R}^2(k_0)}, \qquad (20)$$

where $\Delta_\mathcal{R}(k)$ is the curvature perturbation spectrum given by equation (15). We shall take k_0 to be 0.002 Mpc^{-1}. In this paper we sometimes call this quantity loosely the "amplitude of gravitational waves."

What about the tensor spectral tilt, n_t? In single-field inflation models, there exists the so-called consistency relation between r and n_t (see Liddle & Lyth 2000, for a review)

$$n_t = -\frac{r}{8}. \qquad (21)$$

In order to reduce the number of parameters, we continue to impose this relation at $k = k_0 = 0.002 \text{ Mpc}^{-1}$. For a discussion on how to impose this constraint in a more self-consistent way, see Peiris & Easther (2006a).

To constrain r, we shall use the *WMAP* 5-year temperature and polarization data, the small-scale CMB data, and/or BAO and SN distance measurements.

3.2.3. *How CMB constrains the amplitude of gravitational waves*

Let us show how the gravitational wave contribution is constrained by the *WMAP* data (see Fig. 2). In this pedagogical analysis, we vary only r and τ, while adjusting the overall amplitude of fluctuations such that the height of the first peak of the temperature power spectrum is always held fixed. All the other cosmological parameters are fixed at $\Omega_k = 0$, $\Omega_b h^2 = 0.02265$, $\Omega_c h^2 = 0.1143$, $H_0 = 70.1 \text{ km s}^{-1} \text{ Mpc}^{-1}$, and $n_s = 0.960$. Note that the limit on r from this analysis should not be taken as our best limit, as this analysis ignores the degeneracy between r and the other cosmological parameters, especially n_s. The limit on r from the full analysis will be given in § 3.2.4.

(1) (The gray contours in the left panel, and the upper right of the right panel of Fig. 2.) The low-l polarization data (TE/EE/BB) at $l \lesssim 10$ are unable to place meaningful limits on r. A large r can be compensated by a small τ, producing nearly the same EE power spectrum at $l \lesssim 10$. (Recall that the gravitational waves contribute also to EE.) As a result, r that is as large as 10 is still allowed within 68% CL.[21]

(2) (The red contours in the left panel, and the lower left of the right panel of Fig. 2.) Such a high value

---

[21] We have performed a similar, but different, analysis in § 6.2 of Page et al. (2007). In this paper we include both the scalar and tensor contributions to EE, whereas in Page et al. (2007) we have ignored the tensor contribution to EE and found a somewhat tighter limit, $r < 4.5$ (95% CL), from the low-l polarization data. This is because, when the tensor contribution was ignored, the EE polarization could still be used to fix τ, whereas in our case r and τ are fully degenerate when $r \gtrsim 1$ (see Fig. 2), as the EE is also dominated by the tensor contribution for such a high value of r.

of r, however, produces too negative a TE correlation between $30 \lesssim l \lesssim 150$. Therefore, we can improve the limit on r significantly – by nearly an order of magnitude – by simply using the high-l TE data. The 95% upper bound at this point is still as large as $r \sim 2$.[22]

(3) (The blue contours in the left panel, and the upper left of the right panel of Fig. 2.) Finally, the low-l temperature data at $l \lesssim 30$ severely limit the excess low-l power due to gravitational waves, bringing the upper bound down to $r \sim 0.2$. Note that this bound is about a half of what we actually obtain from the full Markov Chain Monte Carlo of the WMAP-only analysis, $r < 0.43$ (95% CL). This is because we have fixed n_s, and thus ignored the degeneracy between r and n_s shown by Fig. 3.

3.2.4. Results

Having understood which parts of the temperature and polarization spectra constrain r, we obtain the upper limit on r from the full exploration of the likelihood space using the Markov Chain Monte Carlo. Figure 3 shows the 1-d constraint on r as well as the 2-d constraint on r and n_s, assuming a negligible running index. With the WMAP 5-year data alone, we find $r < 0.43$ (95% CL). Since the B-mode contributes little here, and most of the information essentially comes from TT and TE, our limit on r is highly degenerate with n_s, and thus we can obtain a better limit on r only when we have a better limit on n_s.

When we add BAO and SN data, the limit improves significantly to $r < 0.20$ (95% CL). This is because the distance information from BAO and SN reduces the uncertainty in the matter density, and thus it helps to determine n_s better because n_s is also degenerate with the matter density. This "chain of degeneracy" helped us improve our limit on r significantly from the previous results. This limit, $r < 0.20$ (95% CL), is the best limit on r to date.[23] With the new data, we are able to get more stringent the limits than our earlier analyses (Spergel et al. 2007) that combined the WMAP data with measurements of the galaxy power spectrum and found $r < 0.30$ (95% CL).

A dramatic reduction in the uncertainty in r has an important implication for n_s as well. Previously $n_s > 1$ was within the 95% CL when the gravitational wave contribution was allowed, owing to the degeneracy between n_s and r. Now, we are beginning to disfavor $n_s > 1$ even when r is non-zero: with WMAP+BAO+SN we find $0.0014 < 1 - n_s < 0.0608$ (95% CL).[24]

However, these stringent limits on r and n_s weaken to $-0.256 < 1 - n_s < 0.025$ (95% CL) and $r < 0.54$ (95% CL) when a sizable running index is allowed. The BAO and SN data helped reduce the uncertainty

in $dn_s/d\ln k$ (Fig. 4), but not enough to improve on the other parameters compared to the WMAP-only constraints. The Lyα forest data can improve the limit on $dn_s/d\ln k$ even when r is present (see § 7; also Table 4).

3.3. Implications for inflation models

How do the WMAP 5-year limits on n_s and r constrain inflationary models?[25] In the context of single-field models, one can write down n_s and r in terms of the derivatives of potential, $V(\phi)$, as (Liddle & Lyth 2000):

$$1 - n_s = 3M_{pl}^2 \left(\frac{V'}{V}\right)^2 - 2M_{pl}^2 \frac{V''}{V}, \qquad (22)$$

$$r = 8M_{pl}^2 \left(\frac{V'}{V}\right)^2, \qquad (23)$$

where $M_{pl} = 1/\sqrt{8\pi G}$ is the reduced Planck mass, and the derivatives are evaluated at the mean value of the scalar field at the time that a given scale leaves the horizon. These equations may be combined to give a relation between n_s and r:

$$r = \frac{8}{3}(1 - n_s) + \frac{16M_{pl}^2}{3}\frac{V''}{V}. \qquad (24)$$

This equation indicates that it is the *curvature* of the potential that divides models on the n_s-r plane; thus, it makes sense to classify inflation models on the basis of the sign and magnitude of the curvature of the potential (Peiris et al. 2003).[26]

What is the implication of our bound on r for inflation models? Equation (24) suggests that a large r can be generated when the curvature of the potential is positive, i.e., $V'' > 0$, at the field value that corresponds to the scales probed by the WMAP data. Therefore, it is a set of *positive curvature models* that we can constrain from the limit on r. On the other hand, negative curvature models are more difficult to constrain from r, as they tend to predict small r (Peiris et al. 2003). We shall not discuss negative curvature models in this paper.

Here we shall pick three, simple but representative, forms of $V(\phi)$ that can produce $V'' > 0$[27]:

(a) Monomial (chaotic-type) potential, $V(\phi) \propto \phi^\alpha$. This form of the potential was proposed by, and is best known for, Linde's chaotic inflation models (Linde 1983). This model also approximates a pseudo Nambu-Goldstone boson potential (natural inflation; Freese et al. 1990; Adams et al.

---

[22] See Polnarev et al. (2007); Miller et al. (2007) for a way to constrain r from the TE power spectrum alone.

[23] This is the one-dimensional marginalized 95% limit. From the joint two-dimensional marginalized distribution of n_s and r, we find $r < 0.25$ (95% CL) at $n_s = 0.98$. See Fig. 3.

[24] This is is the one-dimensional marginalized 95% limit. From the joint two-dimensional marginalized distribution of n_s and r, we find $n_s < 1.005$ (95% CL) at $r = 0.16$. See Fig. 3.

---

[25] For recent surveys of inflation models in light of the WMAP 3-year data, see Alabidi & Lyth (2006a); Kinney et al. (2006).

[26] This classification scheme is similar to, but different from, the most widely used one, which is based upon the field value (small-field, large-field, hybrid) (Dodelson et al. 1997; Kinney 1998).

[27] These choices are used to sample the space of positive curvature models. Realistic potentials may be much more complicated: see, for example, Destri et al. (2008) for the WMAP 3-year limits on trinomial potentials. Also, the classification scheme based upon derivatives of potentials sheds little light on the models with non-canonical kinetic terms such as k-inflation (Armendariz-Picon et al. 1999; Garriga & Mukhanov 1999), ghost inflation (Arkani-Hamed et al. 2004), or DBI inflation (Silverstein & Tong 2004; Alishahiha et al. 2004), as the tilt, n_s, depends also on the derivative of the effective speed of sound of a scalar field (for recent constraints on this class of models from the WMAP 3-year data, see Bean et al. 2007, 2008).
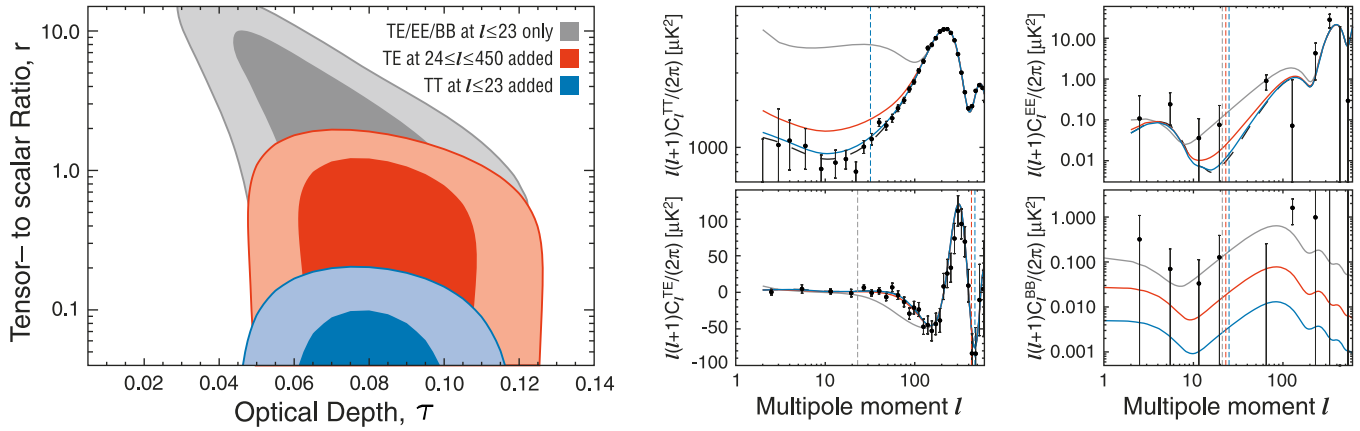
FIG. 2.— How the *WMAP* temperature and polarization data constrain the tensor-to-scalar ratio, r. (*Left*) The contours show 68% and 95% CL. The gray region is derived from the low-l polarization data (TE/EE/BB at $l \leq 23$) only, the red region from the low-l polarization plus the high-l TE data at $l \leq 450$, and the blue region from the low-l polarization, the high-l TE, and the low-l temperature data at $l \leq 32$. (*Right*) The gray curves show $(r, \tau) = (10, 0.050)$, the red curves $(r, \tau) = (1.2, 0.075)$, and the blue curves $(r, \tau) = (0.20, 0.080)$, which are combinations of r and τ that give the upper edge of the 68% CL contours shown on the left panel. The vertical lines indicate the maximum multipoles below which the data are used for each color. The data points with 68% CL errors are the WMAP 5-year measurements (Nolta et al. 2008). (Note that the BB power spectrum at $l \sim 130$ is consistent with zero within 95% CL.)

FIG. 3.— Constraint on the tensor-to-scalar ratio, r, at $k = 0.002$ Mpc^{-1} (§ 3.2.4). No running index is assumed. See Fig. 4 for r with the running index. In all panels we show the WMAP-only results in blue and WMAP+BAO+SN in red. (*Left*) One-dimensional marginalized distribution of r, showing the WMAP-only limit, $r < 0.43$ (95% CL), and WMAP+BAO+SN, $r < 0.20$ (95% CL). (*Middle*) Joint two-dimensional marginalized distribution (68% and 95% CL), showing a strong degeneracy between n_s and r. (*Right*) Degeneracy between n_s and $\Omega_m h^2$. The BAO and SN data help to break this degeneracy which, in turn, reduces the degeneracy between r and n_s, resulting in a factor of 2.2 better limit on r.

1993) with the negative sign, $V(\phi) \propto 1 - \cos(\phi/f)$, when $\phi/f \ll 1$, or with the positive sign, $V(\phi) \propto 1 + \cos(\phi/f)$, when $\phi/f \sim 1$.[28] This model can also approximate the Landau-Ginzburg type of spontaneous symmetry breaking potential, $V(\phi) \propto (\phi^2 - v^2)^2$, in the appropriate limits.

(b) Exponential potential, $V(\phi) \propto \exp[-(\phi/M_{pl})\sqrt{2/p}]$. A unique feature of this potential is that the dynamics of inflation is exactly solvable, and the solution is a power-law expansion, $a(t) \propto t^p$, rather than an exponential one. For this reason this type of model is called power-law inflation (Abbott & Wise 1984; Lucchin & Matarrese 1985). They often appear in models of scalar-tensor theories of gravity (Accetta et al. 1985; La & Steinhardt 1989; Futamase & Maeda 1989; Steinhardt & Accetta 1990; Kalara et al.

1990).

(c) ϕ^2 plus vacuum energy, $V(\phi) = V_0 + m^2\phi^2/2$. These models are known as Linde's hybrid inflation (Linde 1994). This model is a "hybrid" because the potential combines the chaotic-type (with $\alpha = 2$) with a Higgs-like potential for the second field (which is not shown here). This model behaves as if it were a single-field model until the second field terminates inflation when ϕ reaches some critical value. When $\phi \gg (2V_0)^{1/2}/m$ this model is the same as the model (a) with $\alpha = 2$, although one of Linde's motivation was to avoid having such a large field value that exceeds M_{pl}.

These potentials[29] make the following predictions for

---

[28] The positive sign case, $V(\phi) \propto 1 + \cos(\phi/f)$, belongs to a negative curvature model when $\phi/f \ll 1$. See Savage et al. (2006) for constraints on this class of models from the *WMAP* 3-year data.
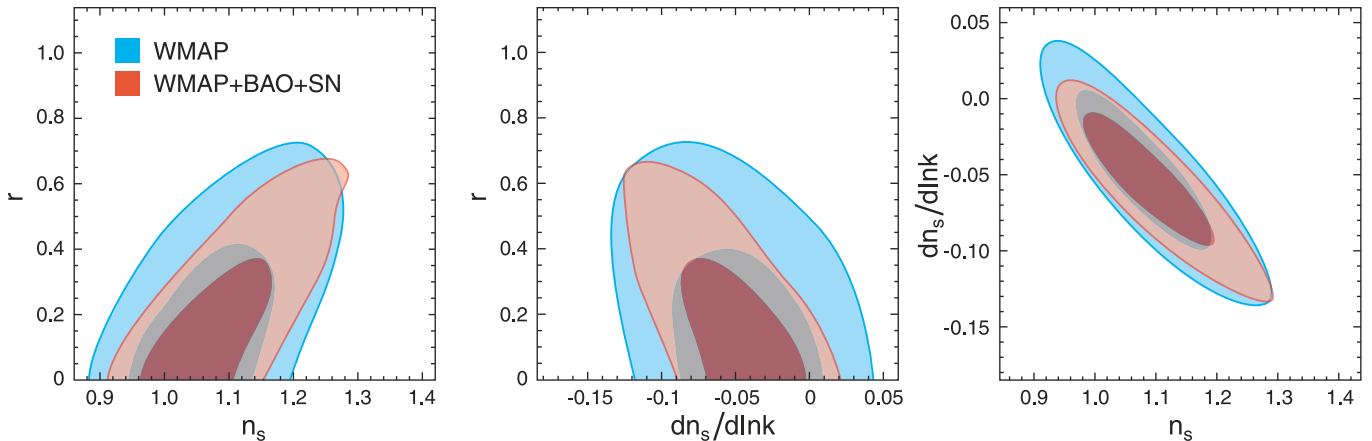
[29] In the language of § 3.4 in Peiris et al. (2003), the models (a) and (b) belong to "small positive curvature models," and the model (c) to "large positive curvature models" for $\tilde{\phi} \ll 1$, "small positive curvature models" for $\tilde{\phi} \gg 1$, and "intermediate positive curvature models" for $\tilde{\phi} \sim 1$.

FIG. 4.— Constraint on the tensor-to-scalar ratio, r, the tilt, n_s, and the running index, $dn_s/d\ln k$, when all of them are allowed to vary (§ 3.2.4). In all panels we show the WMAP-only results in blue and WMAP+BAO+SN in red. (*Left*) Joint two-dimensional marginalized distribution of n_s and r at $k = 0.002$ Mpc^{-1} (68% and 95% CL). (*Middle*) n_s and $dn_s/d\ln k$. (*Right*) $dn_s/d\ln k$ and r. We find no evidence for the running index. While the inclusion of the running index weakens our constraint on n_s and r, the data do not support any need for treating the running index as a free parameter.

r and n_s as a function of their parameters:

(a) $r = 8(1 - n_s)\frac{\alpha}{\alpha+2}$

(b) $r = 8(1 - n_s)$

(c) $r = 8(1 - n_s)\frac{\tilde{\phi}^2}{2\tilde{\phi}^2 - 1}$

Here, for (c) we have defined a dimensionless variable, $\tilde{\phi} \equiv m\phi/(2V_0)^{1/2}$. This model approaches to the model (a) with $\alpha = 2$ for $\tilde{\phi} \gg 1$, and yields the scale-invariant spectrum, $n_s = 1$, when $\tilde{\phi} = 1/\sqrt{2}$.

We summarize our findings below, and in Fig. 5:

(a) Assuming that the monomial potentials are valid to the end of inflation including the reheating of the universe, one can relate n_s and r to the number of e-folds of inflation, $N \equiv \ln(a_{\rm end}/a_{WMAP})$, between the expansion factors at the end of inflation, $a_{\rm end}$, and the epoch when the wavelength of fluctuations that we probe with *WMAP* left the horizon during inflation, a_{WMAP}. The relations are (Liddle & Lyth 2000):

$$r = \frac{4\alpha}{N}, \qquad 1 - n_s = \frac{\alpha + 2}{2N}. \qquad (25)$$

We take $N = 50$ and 60 as a reasonable range (Liddle & Leach 2003). For $\alpha = 4$, i.e., inflation by a massless self-interacting scalar field $V(\phi) = (\lambda/4)\phi^4$, we find that both $N = 50$ and 60 are far away from the 95% region, and they are excluded convincingly at more than 99% CL. For $\alpha = 2$, i.e., inflation by a massive free scalar field $V(\phi) = (1/2)m^2\phi^2$, the model with $N = 50$ lies outside of the 68% region, whereas the model with $N = 60$ is at the boundary of the 68% region. Therefore, both of these models are consistent with the data within the 95% CL. While this limit applies to a single massive free field, Easther & McAllister (2006) show that a model with many massive axion fields (*N*-flation model; Dimopoulos et al. 2005) can shift the predicted n_s further away from unity,

$$1 - n_s^{\rm N.f.} = (1 - n_s^{\rm s.f.})\left(1 + \frac{\beta}{2}\right), \qquad (26)$$

where "N.f" refers to "*N* fields," and "s.f." to "single field," and β is a free parameter of the model. Easther & McAllister (2006) argue that $\beta \sim 1/2$ is favoured, for which $1 - n_s$ is larger than the single-field prediction by as much as 25%. The prediction for the tensor-to-scalar ratio, r, is the same as the single-field case (Alabidi & Lyth 2006b). Therefore, this model lies outside of the 95% region for $N = 50$. As usual, however, these monomial potentials can be made a better fit to the data by invoking a non-minimal coupling between the inflaton and gravity, as the non-minimal coupling can reduce r to negligible levels (Komatsu & Futamase 1999; Hwang & Noh 1998; Tsujikawa & Gumjudpai 2004).

(b) For an exponential potential, r and n_s are uniquely determined by a single parameter, p, that determines a power-law index of the expansion factor, $a(t) \propto t^p$, as

$$r = \frac{16}{p}, \qquad 1 - n_s = \frac{2}{p}. \qquad (27)$$

We find that $p < 60$ is excluded at more than 99% CL, $60 < p < 70$ is within the 99% region but outside of the 95% region, and $p > 70$ is within the 95% region. The models with $p \sim 120$ lie on the boundary of the 68% region, but other parameters are not within the 68% CL. This model can be thought of as a single-field inflation with $p \gg 1$, or multi-field inflation with n fields, each having $p_i \sim 1$ or even $p_i < 1$ (assisted inflation; Liddle et al. 1998). In this context, therefore, one can translate the above limits on p into the limits on the number of fields. The data favour $n \sim 120/p_i$ fields.

(c) For this model we can divide the parameter space into 3 regions, depending upon the value of $\tilde{\phi}$ that corresponds to the field value when the wavelength of fluctuations that we probe with *WMAP* left the horizon. When $\tilde{\phi} \ll 1$, the potential is dominated by a constant term, which we call "Flat Potential
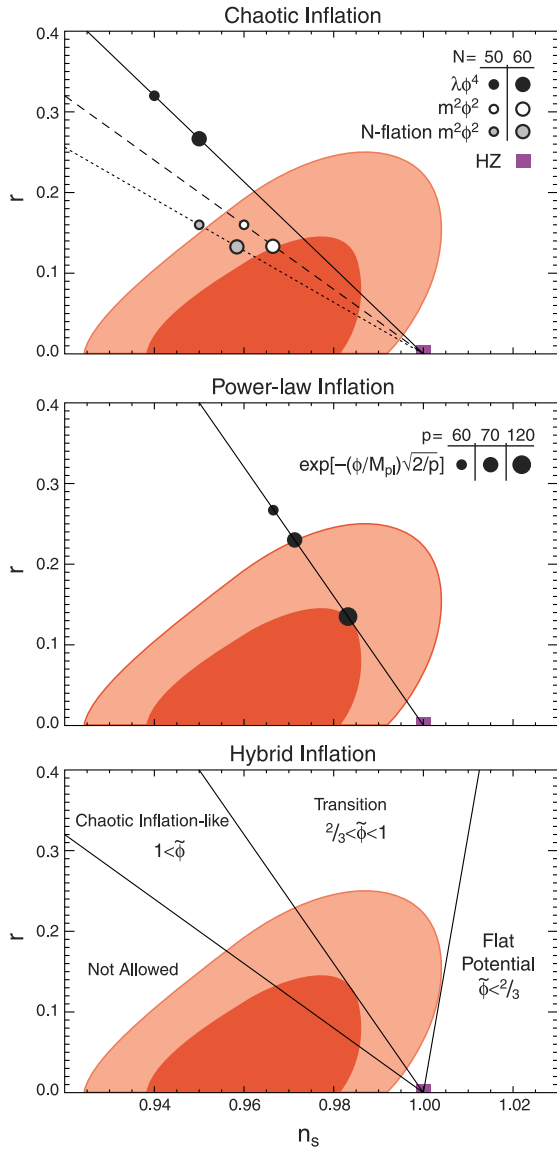
FIG. 5.— Constraint on three representative inflation models whose potential is positively curved, $V'' > 0$ (§ 3.3). The contours show the 68% and 95% CL derived from WMAP+BAO+SN. (*Top*) The monomial, chaotic-type potential, $V(\phi) \propto \phi^\alpha$ (Linde 1983), with $\alpha = 4$ (solid) and $\alpha = 2$ (dashed) for single-field models, and $\alpha = 2$ for multi-axion field models with $\beta = 1/2$ (Easther & McAllister 2006) (dotted). The symbols show the predictions from each of these models with the number of e-folds of inflation equal to 50 and 60. The $\lambda\phi^4$ potential is excluded convincingly, the $m^2\phi^2$ single-field model lies outside of (at the boundary of) the 68% region for $N = 50$ (60), and the $m^2\phi^2$ multi-axion model with $N = 50$ lies outside of the 95% region. (*Middle*) The exponential potential, $V(\phi) \propto \exp[-(\phi/M_{pl})\sqrt{2/p}]$, which leads to a power-law inflation, $a(t) \propto t^p$ (Abbott & Wise 1984; Lucchin & Matarrese 1985). All models but $p \sim 120$ are outside of the 68% region. The models with $p < 60$ are excluded at more than 99% CL, and those with $p < 70$ are outside of the 95% region. For multi-field models these limits can be translated into the number of fields as $p \to np_i$, where p_i is the p-parameter of each field (Liddle et al. 1998). The data favour $n \sim 120/p_i$ fields. (*Bottom*) The hybrid-type potential, $V(\phi) = V_0 + (1/2)m^2\phi^2 = V_0(1 + \tilde\phi^2)$, where $\tilde\phi \equiv m\phi/(2V_0)^{1/2}$ (Linde 1994). The models with $\tilde\phi < 2/3$ drive inflation by the vacuum energy term, V_0, and are disfavoured at more than 95% CL, while those with $\tilde\phi > 1$ drive inflation by the quadratic term, and are similar to the chaotic type (the left panel with $\alpha = 2$). The transition regime, $2/3 < \tilde\phi < 1$ are outside of the 68% region, but still within the 95% region.

Regime." When $\tilde\phi \gg 1$, the potential is indistinguishable from the chaotic-type (model (a)) with $\alpha = 2$. We call this region "Chaotic Inflation-like Regime." When $\tilde\phi \sim 1$, the model shows a transitional behaviour, and thus we call it "Transition Regime." We find that the flat potential regime with $\tilde\phi \lesssim 2/3$ lies outside of the 95% region. The transition regime with $2/3 \lesssim \tilde\phi \lesssim 1$ is within the 95% region, but outside of the 68% region. Finally, the chaotic-like regime contains the 68% region. Since inflation in this model ends by the second field whose dynamics depends on other parameters, there is no constraint from the number of e-folds.

These examples show that the *WMAP* 5-year data, combined with the distance information from BAO and SN, begin to disfavour a number of popular inflation models.

3.4. *Curvature of the observable universe*

3.4.1. *Motivation*

The flatness of the observable universe is one of the predictions of conventional inflation models. How much curvature can we expect from inflation? The common view is that inflation naturally produces the spatial curvature parameter, Ω_k, on the order of the magnitude of quantum fluctuations, i.e., $\Omega_k \sim 10^{-5}$. On the other hand, the current limit on Ω_k is of order 10^{-2}; thus, the current data are not capable of reaching the level of Ω_k that is predicted by the common view.

Would a detection of Ω_k rule out inflation? It is possible that the value of Ω_k is just below our current detection limit, even within the context of inflation: inflation may not have lasted for so long, and the curvature radius of our universe may just be large enough for us not to see the evidence for curvature within our measurement accuracy, yet. While this sounds like fine-tuning, it is a possibility.

This is something we can test by constraining Ω_k better. There is also a revived (and growing) interest in measurements of Ω_k, as Ω_k is degenerate with the equation of state of dark energy, w. Therefore, a better determination of Ω_k has an important implication for our ability to constrain the nature of dark energy.

3.4.2. *Analysis*

Measurements of the CMB power spectrum alone do not strongly constrain Ω_k. More precisely, any experiments that measure the angular diameter or luminosity distance to a *single* redshift are not able to constrain Ω_k uniquely, as the distance depends not only on Ω_k, but also on the expansion history of the universe. For a universe containing matter and vacuum energy, it is essential to combine *at least two* absolute distance indicators, or the expansion rates, out to different redshifts, in order to constrain the spatial curvature well. Note that CMB is also sensitive to Ω_Λ via the late-time integrated Sachs-Wolfe (ISW) effect, as well as to Ω_m via the signatures of gravitational lensing in the CMB power spectrum. These properties can be used to break the degeneracy between Ω_k and Ω_m (Stompor & Efstathiou 1999) or Ω_Λ (Ho et al. 2008).

It has been pointed out by a number of people (e.g., Eisenstein et al. 2005) that a combination of distance

measurements from BAO and CMB is a powerful way to constrain Ω_k. One needs more distances, if dark energy is not a constant but dynamical.

In this section, we shall make one important assumption that the dark energy component is vacuum energy, i.e., a cosmological constant. We shall study the case in which the equation of state, w, and Ω_k are varied simultaneously, in § 5.

3.4.3. Results

Figure 6 shows the limits on Ω_Λ and Ω_k. While the *WMAP* data alone cannot constrain Ω_k (see the left panel), the *WMAP* data combined with the HST's constraint on H_0 tighten the constraint significantly, to $-0.052 < \Omega_k < 0.013$ (95% CL). The *WMAP* data combined with SN yield $\sim 50\%$ better limits, $-0.0344 < \Omega_k < 0.0043$ (95% CL), compared to WMAP+HST. Finally, the WMAP+BAO yields the smallest statistical uncertainty, $-0.0170 < \Omega_k < 0.0068$ (95% CL), which is a factor of 2.6 and 1.7 better than WMAP+HST and WMAP+SN, respectively. This shows how powerful the BAO is in terms of constraining the spatial curvature of the universe; however, this statement needs to be re-evaluated when dynamical dark energy is considered, e.g., $w \neq -1$. We shall come back to this point in § 5.

Finally, when *WMAP*, BAO, and SN are combined, we find $-0.0181 < \Omega_k < 0.0071$ (95% CL). As one can see from the right panel of Fig. 6, the constraint on Ω_k is totally dominated by that from WMAP+BAO; thus, the size of the uncertainty does not change very much from WMAP+BAO to WMAP+BAO+SN. Note that the above result indicates that we have reached 1.3% accuracy (95% CL) in determining Ω_k, which is rather good. The future BAO surveys at $z \sim 3$ are expected to yield an order of magnitude better determination, i.e., 0.1% level, of Ω_k (Knox 2006).

It is instructive to convert our limit on Ω_k to the limits on the curvature radius of the universe. As Ω_k is defined as $\Omega_k = -kc^2/(H_0^2 R_{\rm curv}^2)$, where $R_{\rm curv}$ is the present-day curvature radius, one can convert the upper bounds on Ω_k into the lower bounds on $R_{\rm curv}$, as $R_{\rm curv} = (c/H_0)/\sqrt{|\Omega_k|} = 3/\sqrt{|\Omega_k|}\ h^{-1}{\rm Gpc}$. For negatively curved universes, we find $R_{\rm curv} > 36\ h^{-1}{\rm Gpc}$, whereas for positively curved universes, $R_{\rm curv} > 22\ h^{-1}{\rm Gpc}$. Incidentally these values are greater than the particle horizon at present, $9.7\ h^{-1}{\rm Gpc}$ (computed for the same model).

The 68% limits from the 3-year data (Spergel et al. 2007) were $\Omega_k = -0.012 \pm 0.010$ from WMAP-3yr+BAO (where BAO is from the SDSS LRG of Eisenstein et al. (2005)), and $\Omega_k = -0.011 \pm 0.011$ from WMAP-3yr+SN (where SN is from the SNLS data of Astier et al. (2006)). The 68% limit from WMAP-5yr+BAO+SN (where both BAO and SN have more data than for the 3-year analysis) is $\Omega_k = -0.0052 \pm 0.0064$. A significant improvement in the constraint is due to a combination of the better *WMAP*, BAO, and SN data.

We conclude that, *if* dark energy is vacuum energy (cosmological constant) with $w = -1$, we do not find any deviation from a spatially flat universe.

3.4.4. Implications for the duration of inflation

What does this imply for inflation? Since we do not detect any finite curvature radius, inflation had to last for a long enough period in order to make the observable universe sufficiently flat within the observational limits. This argument allows us to find a lower bound on the *total* number of e-foldings of the expansion factor during inflation, from the beginning to the end, $N_{\rm tot} \equiv \ln(a_{\rm end}/a_{\rm begin})$ (see also § 4.1 of Weinberg 2008).

When the curvature parameter, Ω_k, is much smaller than unity, it evolves with the expansion factor, a, as $\Omega_k \propto a^{-2}$, a^2, and a during inflation, radiation, and matter era, respectively. Therefore, the observed Ω_k is related to Ω_k at the beginning of inflation as[30]

$$\frac{\Omega_k^{\rm obs}}{\Omega_k^{\rm begin}} = \left(\frac{a_{\rm today}}{a_{\rm eq}}\right)\left(\frac{a_{\rm eq}}{a_{\rm end}}\right)^2\left(\frac{a_{\rm begin}}{a_{\rm end}}\right)^2 \quad (28)$$

$$= (1 + z_{\rm eq})\left(\frac{T_{\rm end}g_{*,{\rm end}}^{1/3}}{T_{\rm eq}g_{*,{\rm eq}}^{1/3}}\right)^2 e^{-2N_{\rm tot}}, \quad (29)$$

where g_* is the effective number of relativistic degrees of freedom contributing to entropy, $z_{\rm eq}$ is the matter-radiation equality redshift, and $T_{\rm end}$ and $T_{\rm eq}$ are the reheating temperature of the universe at the end of inflation[31] and the temperature at the equality epoch, respectively. To within 10% accuracy, we take $1 + z_{\rm eq} = 3200$, $T_{\rm eq} = 0.75$ eV, and $g_{*,eq} = 3.9$. We find

$$N_{\rm tot} = 47 - \frac{1}{2}\ln\frac{\Omega_k^{\rm obs}/0.01}{\Omega_k^{\rm begin}} + \ln\frac{T_{\rm end}}{10^8\ {\rm GeV}} + \frac{1}{3}\ln\frac{g_{*,{\rm end}}}{200}.$$
$$(30)$$

Here, it is plausible that $g_{*,{\rm end}} \sim 100$ in the Standard Model of elementary particles, and ~ 200 when the supersymmetric partners are included. The difference between these two cases gives the error of only $\Delta N_{\rm tot} = -0.2$, and thus can be ignored.

The curvature parameter at the beginning of inflation must be below of order unity, as inflation would not begin otherwise. However, it is plausible that $\Omega_k^{\rm begin}$ was not too much smaller than 1; otherwise, we have to explain why it was so small before inflation, and probably we would have to explain it by inflation before inflation. In that case $N_{\rm tot}$ would refer to the sum of the number of e-foldings from two periods of inflation. From this argument we shall take $\Omega_k^{\rm begin} \sim 1$.

The reheating temperature can be anywhere between 1 MeV and 10^{16} GeV. It is more likely that it is between 1 TeV and 10^8 GeV for various reasons, but the allowed region is still large. If we scale the result to a reasonably conservative lower limit on the reheating temperature, $T_{\rm end} \sim 1$ TeV, then we find, from our limit on the curvature of the universe,

$$N_{\rm tot} > 36 + \ln\frac{T_{\rm end}}{1\ {\rm TeV}}. \quad (31)$$

A factor of 10 improvement in the upper limit on $|\Omega_k^{\rm begin}|$ will raise this limit by $\Delta N_{\rm tot} = 1.2$.

Again, $N_{\rm tot}$ here refers to the total number of e-foldings of inflation. In § 3.3 we use $N \equiv \ln(a_{\rm end}/a_{WMAP})$, which

---

[30] To simplify our discussion, we ignore the dark energy contribution, and assume that the universe is dominated matter at the present epoch. This leads to a small error in the estimated lower bound on $N_{\rm tot}$.

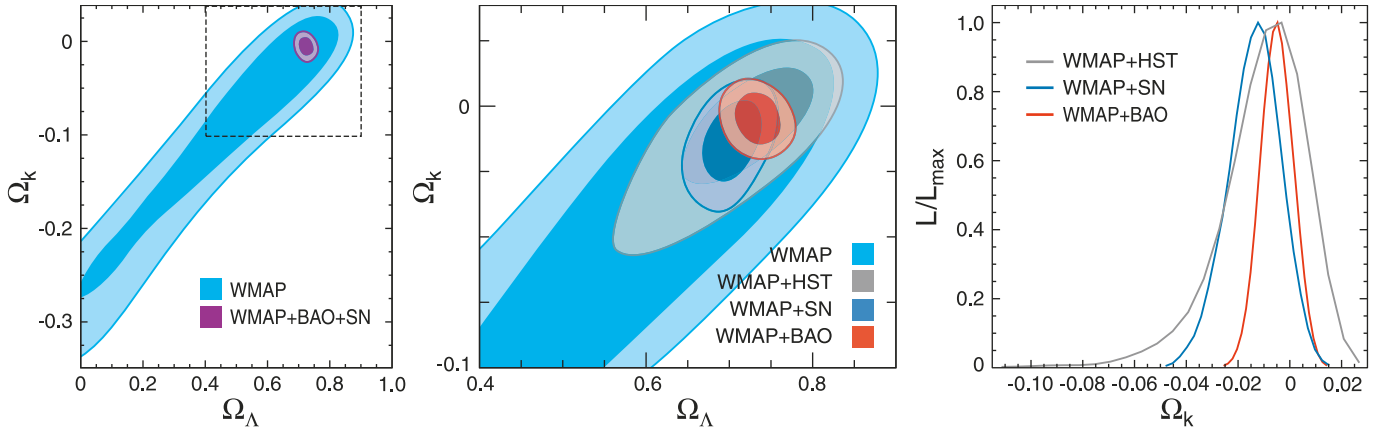[31] For simplicity we assume that reheating occurred as soon as inflation ended.

FIG. 6.— Joint two-dimensional marginalized constraint on the vacuum energy density, Ω_Λ, and the spatial curvature parameter, Ω_k (§ 3.4.3). The contours show the 68% and 95% CL. (*Left*) The WMAP-only constraint (light blue) compared with WMAP+BAO+SN (purple). Note that we have a prior on Ω_Λ, $\Omega_\Lambda > 0$. This figure shows how powerful the extra distance information is for constraining Ω_k. (*Middle*) A blow-up of the region within the dashed lines in the left panel, showing WMAP-only (light blue), WMAP+HST (gray), WMAP+SN (dark blue), and WMAP+BAO (red). The BAO provides the most stringent constraint on Ω_k. (*Right*) One-dimensional marginalized constraint on Ω_k from WMAP+HST, WMAP+SN, and WMAP+BAO. We find the best limit, $-0.0181 < \Omega_k < 0.0071$ (95% CL), from WMAP+BAO+SN, which is essentially the same as WMAP+BAO. See Fig. 12 for the constraints on Ω_k when dark energy is dynamical, i.e., $w \neq -1$, with time-independent w.

is the number of e-foldings between the end of inflation and the epoch when the wavelength of fluctuations that we probe with *WMAP* left the horizon during inflation. Therefore, by definition N is less than $N_{\rm tot}$.

3.5. *Primordial non-Gaussianity*

3.5.1. *Motivation and Background*

In the simplest model of inflation, the distribution of primordial fluctuations is close to a Gaussian with random phases. The level of deviation from a Gaussian distribution and random phases, called *non-Gaussianity*, predicted by the simplest model of inflation is well below the current limit of measurement. Thus, any detection of non-Gaussianity would be a significant challenge to the currently favored models of the early universe.

The assumption of Gaussianity is motivated by the following view: the probability distribution of quantum fluctuations, $P(\varphi)$, of free scalar fields in the ground state of the Bunch-Davies vacuum, φ, is a Gaussian distribution; thus, the probability distribution of primordial curvature perturbations (in the comoving gauge), $\mathcal{R}$, generated from φ (in the flat gauge) as $\mathcal{R} = -[H(\phi)/\dot{\phi}_0]\varphi$ (Mukhanov & Chibisov 1981; Hawking 1982; Starobinsky 1982; Guth & Pi 1982; Bardeen et al. 1983), would also be a Gaussian distribution. Here, $H(\phi)$ is the expansion rate during inflation, and ϕ_0 is the mean field, i.e., $\phi = \phi_0 + \varphi$.

This argument suggests that non-Gaussianity can be generated when (a) scalar fields are not free, but have some interactions, (b) there are non-linear corrections to the relation between $\mathcal{R}$ and φ, and (c) the initial state is not in the Bunch-Davies vacuum.

For (a) one can think of expanding a general scalar field potential $V(\phi)$ to the cubic order or higher, $V(\phi) = \bar{V} + V'\varphi + (1/2)V''\varphi^2 + (1/6)V'''\varphi^3 + \ldots$. The cubic (or higher-order) interaction terms can yield non-Gaussianity in φ (Falk et al. 1993). When perturbations in gravitational fields are included, there are many more interaction terms that arise from expanding the Ricci scalar to the cubic order, with coefficients containing derivatives of V and ϕ_0, such as $\dot{\phi}_0 V''$, $\dot{\phi}_0^{\,3}/H$, etc.

(Maldacena 2003).

For (b) one can think of this relation, $\mathcal{R} = -[H(\phi)/\dot{\phi}_0]\varphi$, as the leading-order term of a Taylor series expansion of the underlying non-linear (gauge) transformation law between $\mathcal{R}$ and φ. Salopek & Bond (1990) show that, in the single-field models, $\mathcal{R} = 4\pi G \int_{\phi_0}^{\phi_0+\varphi} d\phi \, (\partial \ln H/\partial\phi)^{-1}$. Therefore, even if φ is precisely Gaussian, $\mathcal{R}$ can be non-Gaussian due to non-linear terms such as φ^2 in a Taylor series expansion of this relation. One can write this relation in the following form, up to second order in $\mathcal{R}$,

$$\mathcal{R} = \mathcal{R}_{\rm L} - \frac{1}{8\pi G}\left(\frac{\partial^2 \ln H}{\partial\phi^2}\right)\mathcal{R}_{\rm L}^2, \qquad (32)$$

where $\mathcal{R}_{\rm L}$ is a linear part of the curvature perturbation. We thus find that the second term makes $\mathcal{R}$ non-Gaussian, even when $\mathcal{R}_{\rm L}$ is precisely Gaussian. This formula has also been found independently by other researchers, extended to multi-field cases, and often referred to as the "δN formalism" (Sasaki & Stewart 1996; Lyth et al. 2005; Lyth & Rodriguez 2005).

The observers like us, however, do not measure the primordial curvature perturbations, $\mathcal{R}$, directly. A more observationally relevant quantity is the curvature perturbation during the matter era, Φ. At the linear order these quantities are related by $\Phi = (3/5)\mathcal{R}_{\rm L}$ (e.g., Kodama & Sasaki 1984), but the actual relation is more complicated at the non-linear order (see Bartolo et al. 2004, for a review). In any case, this argument has motivated our defining the "*local* non-linear coupling parameter," $f_{NL}^{\rm local}$, as (Komatsu & Spergel 2001)[32]

$$\Phi = \Phi_{\rm L} + f_{NL}^{\rm local}\Phi_{\rm L}^2. \qquad (33)$$

If we take equation (32), for example, we find $f_{NL}^{\rm local} = -(5/24\pi G)(\partial^2 \ln H/\partial\phi^2)$ (Komatsu 2001). Here, we have followed the terminology proposed by Babich et al. (2004) and called $f_{NL}^{\rm local}$ the "local" parameter, as both

---

[32] Note that $f_{NL}^{\rm local}$ can be related to the quantities discussed in earlier, pioneering work: $-\Phi_3/2$ (Gangui et al. 1994), $-A_{\rm infl}/2$ (Wang & Kamionkowski 2000), and $-\alpha$ (Verde et al. 2000).

sides of equation (33) are evaluated at the same location in space. (Hence the term, "local".)

Let us comment on the magnitude of the second term in equation (33). Since $\Phi \sim 10^{-5}$, the second term is smaller than the first term by $10^{-5} f_{NL}^{\rm local}$; thus, the second term is only 0.1% of the first term for $f_{NL}^{\rm local} \sim 10^2$. As we shall see below, the existing limits on $f_{NL}^{\rm local}$ have reached this level of Gaussianity already, and thus it is clear that we are already talking about a tiny deviation from Gaussian fluctuations. This limit is actually better than the current limit on the spatial curvature, which is only on the order of 1%. Therefore, Gaussianity tests offer a stringent test of early universe models.

In the context of single-field inflation in which the scalar field is rolling down the potential slowly, the quantities, H, V, and ϕ, are changing slowly. Therefore, one generically expects that $f_{NL}^{\rm local}$ is small, on the order of the so-called slow-roll parameters ϵ and η, which are typically of order 10^{-2} or smaller. In this sense, the single-field, slow-roll inflation models are expected to result in a tiny amount of non-Gaussianity (Salopek & Bond 1990; Falk et al. 1993; Gangui et al. 1994; Maldacena 2003; Acquaviva et al. 2003). These contributions from the epoch of inflation are much smaller than those from the ubiquitous, second-order cosmological perturbations, i.e., the non-linear corrections to the relation between Φ and $\mathcal{R}$, which result in $f_{NL}^{\rm local}$ of order unity (see Bartolo et al. 2004, for a review).

One can use the cosmological observations, such as the CMB data, to constrain $f_{NL}^{\rm local}$ (Verde et al. 2000; Komatsu & Spergel 2001). While the temperature anisotropy, $\Delta T/T$, is related to Φ via the Sachs–Wolfe formula as $\Delta T/T = -\Phi/3$ at the linear order on very large angular scales (Sachs & Wolfe 1967), there are non-linear corrections (non-linear Sachs–Wolfe effect, non-linear Integrated Sachs–Wolfe effect, gravitational lensing, etc) to this relation, which add terms of order unity to $f_{NL}^{\rm local}$ by the time we observe it in CMB (Pyne & Carroll 1996; Mollerach & Matarrese 1997). On smaller angular scales one must include the effects of acoustic oscillations of photon-baryon plasma by solving the Boltzmann equations. The second-order corrections to the Boltzmann equations can also yield $f_{NL}^{\rm local}$ of order unity (Bartolo et al. 2006, 2007).

Any detection of $f_{NL}^{\rm local}$ at the level that is currently accessible would have a profound implication for the physics of inflation. How can a large $f_{NL}^{\rm local}$ be generated? We essentially need to break either (a) single field, or (b) slow-roll. For example, a multi-field model known as the curvaton scenario can result in much larger values of $f_{NL}^{\rm local}$ (Linde & Mukhanov 1997; Lyth et al. 2003), so can the models with field-dependent (variable) decay widths for reheating of the universe after inflation (Dvali et al. 2004b,a). A more violent, non-linear reheating process called "preheating" can give rise to a large $f_{NL}^{\rm local}$, depending upon potential of the second field to which inflation decays (Enqvist et al. 2005; Jokinen & Mazumdar 2006; Chambers & Rajantie 2008).

Although breaking of slow-roll usually results in a premature termination of inflation, it is possible to break it temporarily for a brief period, without terminating inflation, by some features (steps, dips, etc) in the shape of the potential. In such a scenario, a large non-Gaussianity may be generated at a certain limited scale at which the feature exists (Kofman et al. 1991; Wang & Kamionkowski 2000; Komatsu et al. 2003). The structure of non-Gaussianity from features is much more complex and model-dependent than $f_{NL}^{\rm local}$ (Chen et al. 2007; Chen et al. 2008).

There is also a possibility that non-Gaussianity can be used to test alternatives to inflation. In a collapsing universe followed by a bounce, there exists a duality relation, with regard to the slow-roll parameter, between this scenario and the conventional inflationary scenario. As a result, $f_{NL}^{\rm local}$ in these scenarios (e.g., New Ekpyrotic scenario) is given by the *inverse* of slow-roll parameters; thus, $f_{NL}^{\rm local}$ as large as of order 10 to 10^2 is a fairly generic prediction of this class of models (Koyama et al. 2007; Buchbinder et al. 2007; Lehners & Steinhardt 2007).

Using the angular bispectrum,[33] the harmonic transform of the angular 3-point correlation function, Komatsu et al. (2002) have obtained the first observational limit on $f_{NL}^{\rm local}$ from the *COBE* 4-year data (Bennett et al. 1996), finding $-3500 < f_{NL}^{\rm local} < 2000$ (95% CL). The uncertainty was large due to a relatively large beam size of *COBE*, which allowed us to go only to the maximum multipole of $l_{\rm max} = 20$. Since the signal-to-noise ratio of $f_{NL}^{\rm local}$ is proportional to $l_{\rm max}$, it was expected that the *WMAP* data would yield a factor of ~ 50 improvement over the *COBE* data (Komatsu & Spergel 2001).

The full bispectrum analysis was not feasible with the *WMAP* data, as the computational cost scales as $N_{\rm pix}^{5/2}$, where $N_{\rm pix}$ is the number of pixels, which is on the order of millions for the *WMAP* data. The "KSW" estimator (Komatsu et al. 2005) has solved this problem by inventing a cubic statistic that combines the triangle configurations of the bispectrum optimally so that it is maximally sensitive to $f_{NL}^{\rm local}$.[34] The computational cost of the KSW estimator scales as $N_{\rm pix}^{3/2}$. We give a detailed description of the method that we use in this paper in Appendix A.

We have applied this technique to the *WMAP* 1-year and 3-year data, and found $-58 < f_{NL}^{\rm local} < 134$ ($l_{\rm max} = 265$; Komatsu et al. 2003) and $-54 < f_{NL}^{\rm local} < 114$ ($l_{\rm max} = 350$; Spergel et al. 2007), respectively, at 95% CL. Creminelli et al. performed an independent analysis of the *WMAP* data and found similar limits: $-27 < f_{NL}^{\rm local} < 121$ ($l_{\rm max} = 335$; Creminelli et al. 2006) and $-36 < f_{NL}^{\rm local} < 100$ ($l_{\rm max} = 370$; Creminelli et al. 2007) for the 1-year and 3-year data, respectively. These constraints are slightly better than the *WMAP* team's, as their estimator for $f_{NL}^{\rm local}$ was improved from the original KSW estimator.

While these constraints are obtained from the KSW-like fast bispectrum statistics, many groups have used the *WMAP* data to measure $f_{NL}^{\rm local}$ using various other statistics, such as the Minkowski functionals (Komatsu et al. 2003; Spergel et al. 2007; Gott et al. 2007; Hikage et al. 2008), real-space 3-point function (Gaztañaga

---

[33] For a pedagogical introduction to the bispectrum (3-point function) and trispectrum (4-point function) and various topics on non-Gaussianity, see Komatsu (2001); Bartolo et al. (2004).

[34] Since the angular bispectrum is the harmonic transform of the angular three-point function, it forms a triangle in the harmonic space. While there are many possible triangles, the "squeezed triangles," in which the two wave vectors are long and one is short, are most sensitive to $f_{NL}^{\rm local}$ (Babich et al. 2004).

& Wagg 2003; Chen & Szapudi 2005), integrated bispectrum (Cabella et al. 2006), 2-1 cumulant correlator power spectrum (Chen & Szapudi 2006), local curvature (Cabella et al. 2004), and spherical Mexican hat wavelet (Mukherjee & Wang 2004). The sub-orbital CMB experiments have also yielded constraints on $f_{NL}^{\rm local}$: MAXIMA (Santos et al. 2003), VSA (Smith et al. 2004), Archeops (Curto et al. 2007), and BOOMERanG (De Troia et al. 2007).

We stress that it is important to use different statistical tools to measure $f_{NL}^{\rm local}$ if any signal is found, as different tools are sensitive to different systematics. The analytical predictions for the Minkowski functionals (Hikage et al. 2006) and the angular trispectrum (the harmonic transform of the angular 4-point correlation function; Okamoto & Hu 2002; Kogo & Komatsu 2006) as a function of $f_{NL}^{\rm local}$ are available now. Studies on the forms of the trispectrum from inflation models have just begun, and some important insights have been obtained (Boubekeur & Lyth 2006; Huang & Shiu 2006; Byrnes et al. 2006; Seery & Lidsey 2007; Seery et al. 2007; Arroja & Koyama 2008). It is now understood that the trispectrum is at least as important as the bispectrum in discriminating inflation models: some models do not produce any bispectra but produce significant trispectra, and other models produce similar amplitudes of the bispectra but produce very different trispectra (Huang & Shiu 2006; Buchbinder et al. 2007).

In this paper we shall use the estimator that further improves upon Creminelli et al. (2006) by correcting an inadvertent numerical error of a factor of 2 in their derivation (Yadav et al. 2007). Yadav & Wandelt (2007) used this estimator to measure $f_{NL}^{\rm local}$ from the *WMAP* 3-year data. We shall also use the Minkowski functionals to find a limit on $f_{NL}^{\rm local}$.

In addition to $f_{NL}^{\rm local}$, we shall also estimate the "*equilateral* non-linear coupling parameter*,*" $f_{NL}^{\rm equil}$, which characterizes the amplitude of the three-point function (i.e., the bispectrum) of the equilateral configurations, in which the lengths of all the three wave vectors forming a triangle in Fourier space are equal. This parameter is useful and highly complementary to the local one: while $f_{NL}^{\rm local}$ characterizes mainly the amplitude of the bispectrum of the squeezed configurations, in which two wave vectors are large and nearly equal and the other wave vector is small, and thus it is fairly insensitive to the equilateral configurations, $f_{NL}^{\rm equil}$ is mainly sensitive to the equilateral configurations with little sensitivity to the squeezed configurations. In other words, it is possible that one may detect $f_{NL}^{\rm local}$ without any detection of $f_{NL}^{\rm equil}$, and *vice versa*.

These two parameters cover a fairly large class of models. For example, $f_{NL}^{\rm equil}$ can be generated from inflation models in which the scalar field takes on the non-standard (non-canonical) kinetic form, such as $\mathcal{L} = P(X, \phi)$, where $X = (\partial\phi)^2$. In this class of models, the effective sound speed of ϕ can be smaller than the speed of light, $c_s^2 = [1 + 2X(\partial^2 P/\partial X^2)/(\partial P/\partial X)]^{-1} < 1$. One then obtains $f_{NL}^{\rm equil} \sim -1/c_s^2 < 0$, in the limit of $c_s \ll 1$ (Seery & Lidsey 2005; Chen et al. 2007; Cheung et al. 2007). Such models can be realized in the context of String Theory via the non-canonical kinetic ac-

tion called the Dirac-Born-Infeld (DBI) form (Alishahiha et al. 2004), and in the context of an infrared modification of gravity called the ghost condensation (Arkani-Hamed et al. 2004).

The observational limits on $f_{NL}^{\rm equil}$ have been obtained from the *WMAP* 1-year and 3-year data as $-366 < f_{NL}^{\rm equil} < 238$ ($l_{\rm max} = 405$; Creminelli et al. 2006) and $-256 < f_{NL}^{\rm equil} < 332$ ($l_{\rm max} = 475$; Creminelli et al. 2007), respectively.

There are other forms, too. Warm inflation might produce a different form of $f_{\rm NL}$(Moss & Xiong 2007; Moss & Graham 2007). Also, the presence of particles at the beginning of inflation, i.e., a departure of the initial state of quantum fluctuations from the Bunch-Davies vacuum, can result in an enhanced non-Gaussianity in the "flattened" triangle configurations (Holman & Tolley 2007). We do not consider these forms of non-Gaussianity in this paper.

In this paper we do not discuss the non-Gaussian signatures that cannot be characterized by $f_{NL}^{\rm local}$, $f_{NL}^{\rm equil}$, or b_{src} (the point source bispectrum amplitude). There have been many studies on non-Gaussian signatures in the *WMAP* data in various forms (Chiang et al. 2003, 2007; Naselsky et al. 2007; Park 2004; de Oliveira-Costa et al. 2004; Tegmark et al. 2003; Larson & Wandelt 2004; Eriksen et al. 2004; Eriksen et al. 2004; Eriksen et al. 2004, 2007a; Copi et al. 2004; Schwarz et al. 2004; Copi et al. 2006, 2007; Gordon et al. 2005; Bielewicz et al. 2005; Jaffe et al. 2005, 2006; Vielva et al. 2004; Cruz et al. 2005, 2006, 2007b,a; Cayón et al. 2005; Bridges et al. 2007; Wiaux et al. 2008; Räth et al. 2007; Land & Magueijo 2005b,a, 2007; Rakić & Schwarz 2007; Park et al. 2007; Bernui et al. 2007; Hajian & Souradeep 2003; Hajian et al. 2005; Hajian & Souradeep 2006; Prunet et al. 2005; Hansen et al. 2004; Hansen et al. 2004), many of which are related to the large-scale features at $l \lesssim 20$. We expect these features to be present in the *WMAP* 5-year temperature map, as the structure of CMB anisotropy in the *WMAP* data on such large angular scales has not changed very much since the 3-year data.

3.5.2. *Analysis*

The largest concern in measuring primordial non-Gaussianity from the CMB data is the potential contamination from the Galactic diffuse foreground emission. To test how much the results would be affected by this, we measure f_{NL} parameters from the raw temperature maps as well as from the foreground-reduced maps.

We shall mainly use the *KQ75* mask, the new mask that is recommended for tests of Gaussianity (Gold et al. 2008). The important difference between the new mask and the previous *Kp0* mask (Bennett et al. 2003c) is that the new mask is defined by the *difference* between the K band map and the Internal Linear Combination (ILC) map, and that between the Q band and ILC. Therefore, the CMB signal was absent when the mask was defined, which removes any concerns regarding a potential bias in the distribution of CMB on the masked sky.[35]

---

[35] Previously, the *Kp0* mask was defined by the K band map, which contains CMB as well as the foreground emission. By cutting bright pixels in the K band map, it could be possible to cut also

TABLE 5
Clean-map estimates and the corresponding 68%
intervals of the local form of primordial
non-Gaussianity, $f_{NL}^{\rm local}$, the point source bispectrum
amplitude, b_{src} (in units of 10^{-5} $\mu{\rm K}^3$ ${\rm sr}^2$), and
Monte-Carlo estimates of bias due to point sources,
$\Delta f_{NL}^{\rm local}$

Band	Mask	$l_{\max}$	$f_{NL}^{\rm local}$	$\Delta f_{NL}^{\rm local}$	b_{src}
V+W	KQ85	400	50 ± 29	1 ± 2	0.26 ± 1.5
V+W	KQ85	500	61 ± 26	2.5 ± 1.5	0.05 ± 0.50
V+W	KQ85	600	68 ± 31	3 ± 2	0.53 ± 0.28
V+W	KQ85	700	67 ± 31	3.5 ± 2	0.34 ± 0.20
V+W	Kp0	500	61 ± 26	2.5 ± 1.5	
V+W	KQ75p1[a]	500	53 ± 28	4 ± 2	
V+W	KQ75	400	47 ± 32	3 ± 2	-0.50 ± 1.7
V+W	KQ75	500	55 ± 30	4 ± 2	0.15 ± 0.51
V+W	KQ75	600	61 ± 36	4 ± 2	0.53 ± 0.30
V+W	KQ75	700	58 ± 36	5 ± 2	0.38 ± 0.21

[a]This mask replaces the point-source mask in KQ75 with the
one that does not mask the sources identified in the WMAP
K-band data

TABLE 6
Null tests, frequency dependence, and
raw-map estimates of the local form of
primordial non-Gaussianity, $f_{NL}^{\rm local}$, for
$l_{\max} = 500$

Band	Foreground	Mask	$f_{NL}^{\rm local}$
Q−W	Raw	KQ75	-0.53 ± 0.22
V−W	Raw	KQ75	-0.31 ± 0.23
Q−W	Clean	KQ75	0.10 ± 0.22
V−W	Clean	KQ75	0.06 ± 0.23
Q	Raw	KQ75p1[a]	-42 ± 45
V	Raw	KQ75p1	38 ± 34
W	Raw	KQ75p1	43 ± 33
Q	Raw	KQ75	-42 ± 48
V	Raw	KQ75	41 ± 35
W	Raw	KQ75	46 ± 35
Q	Clean	KQ75p1	9 ± 45
V	Clean	KQ75p1	47 ± 34
W	Clean	KQ75p1	60 ± 33
Q	Clean	KQ75	10 ± 48
V	Clean	KQ75	50 ± 35
W	Clean	KQ75	62 ± 35
V+W	Raw	KQ85	9 ± 26
V+W	Raw	Kp0	48 ± 26
V+W	Raw	KQ75p1	41 ± 28
V+W	Raw	KQ75	43 ± 30

[a]This mask replaces the point-source mask in
KQ75 with the one that does not mask the sources
identified in the WMAP K-band data

TABLE 7
Clean-map estimates and the
corresponding 68% intervals of the
equilateral form of primordial
non-Gaussianity, $f_{NL}^{\rm equil}$, and
Monte-Carlo estimates of bias due to
point sources, $\Delta f_{NL}^{\rm equil}$

Band	Mask	$l_{\max}$	$f_{NL}^{\rm equil}$	$\Delta f_{NL}^{\rm equil}$
V+W	KQ75	400	77 ± 146	9 ± 7
V+W	KQ75	500	78 ± 125	14 ± 6
V+W	KQ75	600	71 ± 108	27 ± 5
V+W	KQ75	700	73 ± 101	22 ± 4

To carry out tests of Gaussianity, one should use the
KQ75 mask, which is slightly more conservative than
Kp0, as the KQ75 mask cuts slightly more sky: we retain
71.8% of the sky with KQ75, while 76.5% with Kp0. To
see how sensitive we are to the details of the mask, we
also tried Kp0 as well as the new mask that is recom-
mended for the power spectrum analysis, KQ85, which
retains 81.7% of the sky. The previous mask that corre-
sponds to KQ85 is the Kp2 mask, which retains 84.6%
of the sky.

In addition, we use the KQ75p1 mask, which replaces
the point source mask of KQ75 with the one that does
not mask the sources identified in the WMAP K-band
data. Our point source selection at K band removes more
sources and sky in regions with higher CMB flux. We
estimate the amplitude of this bias by using the KQ75p1
mask which does not use any WMAP data for the point
source identification. The small change in $f_{NL}^{\rm local}$ shows
that this is a small bias.

The unresolved extra-galactic point sources also con-
tribute to the bispectrum (Refregier et al. 2000; Komatsu
& Spergel 2001; Argüeso et al. 2003; Serra & Cooray
2008), and they can bias our estimates of primordial non-
Gaussianity parameters such as $f_{NL}^{\rm local}$ and $f_{NL}^{\rm equil}$. We
estimate the bias by measuring $f_{NL}^{\rm local}$ and $f_{NL}^{\rm equil}$ from
Monte Carlo simulations of point sources, and list them
as $\Delta f_{NL}^{\rm local}$ and $\Delta f_{NL}^{\rm equil}$ in Table 5 and 7. As the errors in
these estimates of the bias are limited by the number of
Monte Carlo realizations (which is 300), one may obtain
a better estimate of the bias using more realizations.

We give a detailed description of our estimators for
$f_{NL}^{\rm local}$, $f_{NL}^{\rm equil}$, and b_{src}, the amplitude of the point source
bispectrum, as well as of Monte Carlo simulations in Ap-
pendix A.

the bright CMB pixels, introducing the negative skewness in the
distribution of CMB. Since we did not include isolated "islands"
on the high Galactic latitudes, some of which could be bright CMB
spots, in the final mask when we defined the Kp0 mask, the skew-
ness bias mentioned above should not be as large as one would
expect, if any. Nevertheless, with the new definition of mask, the
masked maps are free from this type of bias. For more details on
the definition of the mask, see Gold et al. (2008).

3.5.3. Results: Bispectrum

In Table 5 we show our measurement of $f_{NL}^{\rm local}$ from
the template-cleaned V+W map (Gold et al. 2008) with
4 different masks, KQ85, Kp0, KQ75p1, and KQ75, in
the increasing order of the size of the mask. For KQ85
and KQ75 we show the results from different maximum
multipoles used in the analysis, $l_{\max} = 400, 500, 600$, and
700. The WMAP 5-year temperature data are limited by
cosmic variance to $l \sim 500$.

We find that both KQ85 and Kp0 for $l_{\max} = 500$ show
evidence for $f_{NL}^{\rm local} > 0$ at more than 95% CL, $9 < f_{NL}^{\rm local} <$
113 (95% CL), before the point source bias correction,
and $6.5 < f_{NL}^{\rm local} < 110.5$ (95% CL) after the correction.
For a higher $l_{\max}$, $l_{\max} = 700$, we still find evidence for
$f_{NL}^{\rm local} > 0$, $1.5 < f_{NL}^{\rm local} < 125.5$ (95% CL), after the
correction.[36]

This evidence is, however, reduced when we use larger
masks, KQ75p1 and KQ75. For the latter we find

[36] The uncertainty for $l_{\max} > 500$ is slightly larger than that for
$l_{\max} = 500$ due to a small sub-optimality of the estimator of $f_{NL}^{\rm local}$
(Yadav et al. 2007).

TABLE 8
POINT SOURCE BISPECTRUM AMPLITUDE, b_{src}, FOR
$l_{\max} = 900$

Band	Foreground	Mask	b_{src} $[10^{-5}$ μK^3 $sr^2]$
Q	Raw	$KQ75p1^a$	11.1 ± 1.3
V	Raw	$KQ75p1$	0.83 ± 0.31
W	Raw	$KQ75p1$	0.16 ± 0.24
V+W	Raw	$KQ75p1$	0.28 ± 0.16
Q	Raw	$KQ75$	6.0 ± 1.3
V	Raw	$KQ75$	0.43 ± 0.31
W	Raw	$KQ75$	0.12 ± 0.24
V+W	Raw	$KQ75$	0.14 ± 0.16
V+W	Raw	$KQ85$	0.20 ± 0.15
Q	Clean	$KQ75p1$	8.7 ± 1.3
V	Clean	$KQ75p1$	0.75 ± 0.31
W	Clean	$KQ75p1$	0.16 ± 0.24
V+W	Clean	$KQ75p1$	0.28 ± 0.16
Q	Clean	$KQ75$	4.3 ± 1.3
V	Clean	$KQ75$	0.36 ± 0.31
W	Clean	$KQ75$	0.13 ± 0.24
V+W	Clean	$KQ75$	0.14 ± 0.16
V+W	Clean	$KQ85$	0.13 ± 0.15

^{a}This mask replaces the point-source mask in $KQ75$ with the one that does not mask the sources identified in the *WMAP* K-band data

TABLE 9
χ^2 ANALYSIS OF THE MINKOWSKI
FUNCTIONALS FOR THE
TEMPLATE-CLEANED V+W MAP. THE
RESULTS FROM THE AREA, CONTOUR
LENGTH, AND EULER CHARACTERISTICS
ARE COMBINED

$N_{\rm side}$	$\chi^2_{WMAP}/$dof	$F(> \chi^2_{WMAP})$
256	51.5/45	0.241
128	40.0/45	0.660
64	54.2/45	0.167
32	46.8/45	0.361
16	44.7/45	0.396
8	61.3/45	0.104

$-5 < f_{NL}^{\rm local} < 115$ (95% CL) before the source bias correction, and $-9 < f_{NL}^{\rm local} < 111$ (95% CL) after the correction, which we take as our best estimate. This estimate improves upon our previous estimate from the 3-year data, $-54 < f_{NL}^{\rm local} < 114$ (95% CL; Spergel et al. 2007, for $l_{\max} = 350$), by cutting much of the allowed region for $f_{NL}^{\rm local} < 0$. To test whether the evidence for $f_{NL}^{\rm local} > 0$ can also be seen with the $KQ75$ mask, we need more years of *WMAP* observations.

In Table 6 we summarize the results from various tests. As a null test, we have measured $f_{NL}^{\rm local}$ from the difference maps such as Q−W and V−W, which are sensitive to non-Gaussianity in noise and the residual foreground emission. Since the difference maps do not contain the CMB signal, which is a source of a large cosmic variance in the estimation of $f_{NL}^{\rm local}$, the errors in the estimated $f_{NL}^{\rm local}$ are much smaller. Before the foreground cleaning ("Raw" in the second column) we see negative values of $f_{NL}^{\rm local}$, which is consistent with the foreground emission having positively skewed temperature distribution and $f_{NL}^{\rm local} > 0$ mainly generating negative skewness. We do not find any significant signal of $f_{NL}^{\rm local}$ at more than 99% CL for raw maps, or at more than 68% CL for cleaned maps, which indicates that the temperature maps are
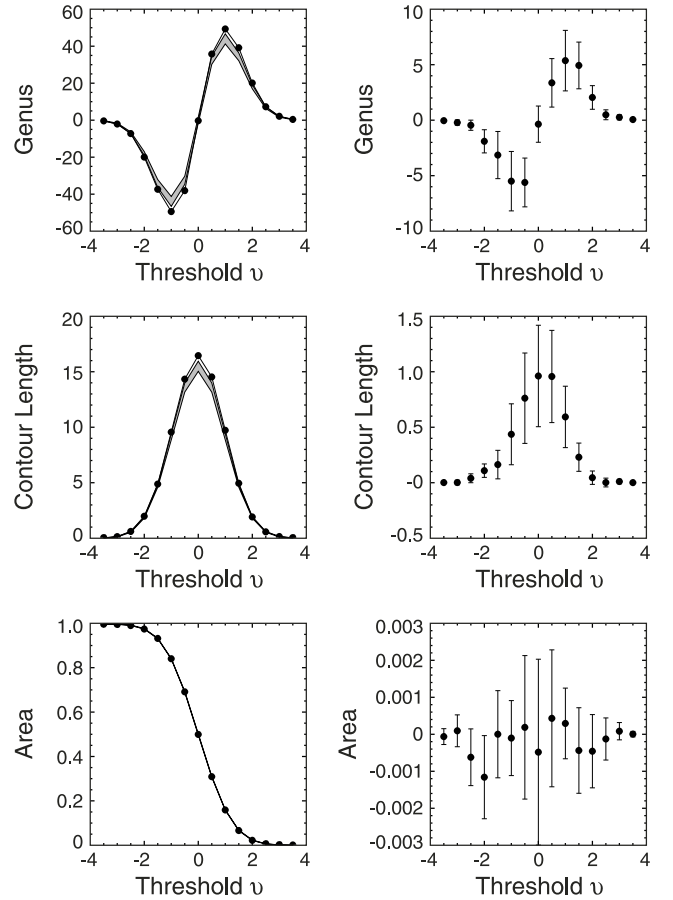

FIG. 7.— Minkowski functionals from the *WMAP* 5-year data, measured from the template-cleaned V+W map at $N_{\rm side} = 128$ (28′ pixels) outside of the $KQ75$ mask. From the top to bottom panels, we show the Euler characteristics (also known as the genus), the contour length, and the cumulative surface area, as a function of the threshold (the number of σ's of hot and cold spots), $\nu \equiv \Delta T/\sigma_0$. (*Left*) The data (symbols) are fully consistent with the mean and dispersion of Gaussian realizations that include CMB and noise. The gray bands show the 68% intervals of Gaussian realizations. (*Right*) The residuals between the *WMAP* data and the mean of the Gaussian realizations. Note that the residuals are highly correlated from bin to bin. From this result we find $f_{NL}^{\rm local} = -57 \pm 60$ (68% CL). From $N_{\rm side} = 64$ we find $f_{NL}^{\rm local} = -68 \pm 69$ (68% CL).

quite clean outside of the $KQ75$ mask.

From the results presented in Table 6, we find that the raw-map results yield more scatter in $f_{NL}^{\rm local}$ estimated from various data combinations than the clean-map results. From these studies we conclude that the clean-map results are robust against the data combinations, as long as we use only the V and W band data.

In Table 7 we show the equilateral bispectrum, $f_{NL}^{\rm equil}$, from the template-cleaned V+W map with the $KQ75$ mask. We find that the point source bias is much more significant for $f_{NL}^{\rm equil}$: we detect the bias in $f_{NL}^{\rm equil}$ at more than the 5σ level for $l_{\max} = 600$ and 700. After correcting for the bias, we find $-151 < f_{NL}^{\rm equil} < 253$ (95% CL; $l_{\max} = 700$) as our best estimate. Our estimate improves upon the previous one, $-256 < f_{NL}^{\rm equil} < 332$ (95% CL; Creminelli et al. 2006, for $l_{\max} = 475$), by reducing the allowed region from both above and below by a similar amount.

Finally, the bispectrum from very high multipoles, e.g.,

$l_{max} = 900$, can be used to estimate the amplitude of residual point source contamination. One can use this information to check for a consistency between the estimate of the residual point sources from the power spectrum and that from the bispectrum. In Table 8 we list our estimates of b_{src}. The raw maps and cleaned maps yield somewhat different values, indicating a possible leakage from the diffuse foreground to an estimate of b_{src}. Our best estimate in the Q band is $b_{src} = 4.3 \pm 1.3 \ \mu K^3 \ sr^2$ (68% CL). See Nolta et al. (2008) for the comparison between b_{src}, C_{ps}, and the point-source counts.

Incidentally, we also list b_{src} from the $KQ75p1$ mask, whose source mask is exactly the same as we used for the first-year analysis. We find $b_{src} = 8.7 \pm 1.3 \ \mu K^3 \ sr^2$ in the Q band, which is in an excellent agreement with the first-year result, $b_{src} = 9.5 \pm 4.4 \ \mu K^3 \ sr^2$ (Komatsu et al. 2003).

3.5.4. Results: Minkowski Functionals

For the analysis of the Minkowski functionals, we follow the method described in Komatsu et al. (2003) and Spergel et al. (2007). In Fig. 7 we show all of the three Minkowski functionals (Gott et al. 1990; Mecke et al. 1994; Schmalzing & Buchert 1997; Schmalzing & Gorski 1998; Winitzki & Kosowsky 1998) that one can define on a two-dimensional sphere: the cumulative surface area (bottom), the contour length (middle), and the Euler characteristics (which is also known as the genus; top), as a function the "threshold," ν, which is the number of σ's of hot and cold spots, defined by

$$\nu \equiv \frac{\Delta T}{\sigma_0}, \qquad (34)$$

where σ_0 is the standard deviation of the temperature data (which includes both signal and noise) at a given resolution of the map that one works with. We compare the Minkowski functionals measured from the WMAP data with the mean and dispersion of Gaussian realizations that include CMB signal and noise. We use the $KQ75$ mask and the V+W-band map.

While Fig. 7 shows the results at resolution 7 ($N_{side} = 128$), we have carried out Gaussianity tests using the Minkowski functionals at six different resolutions from resolution 3 ($N_{side} = 8$) to resolution 8 ($N_{side} = 256$). We find no evidence for departures from Gaussianity at any resolutions, as summarized in Table 9: in this table we list the values of χ^2 of the Minkowski functionals relative to the Gaussian predictions:

$$\chi^2_{WMAP} = \sum_{ij} \sum_{\nu_1 \nu_2} \left[F^i_{WMAP} - \langle F^i_{sim} \rangle \right]_{\nu_1}$$

$$\times (\Sigma^{-1})^{ij}_{\nu_1 \nu_2} \left[F^j_{WMAP} - \langle F^j_{sim} \rangle \right]_{\nu_2}, \quad (35)$$

where F^i_{WMAP} and F^i_{sim} are the ith Minkowski functionals measured from the WMAP data and Gaussian simulations, respectively, the angular bracket denotes the average over realizations, and $\Sigma^{ij}_{\nu_1 \nu_2}$ is the covariance matrix estimated from the simulations. We use 15 different thresholds from $\nu = -3.5$ to $\nu = +3.5$, as indicated by the symbols in Fig. 7, and thus the number of degrees of freedom in the fit is $15 \times 3 = 45$. We show the values of χ^2_{WMAP} and the degrees of freedom in the second column, and the probability of having χ^2 that is larger than

the measured value, $F(> \chi^2_{WMAP})$, in the third column. The smallest probability is 0.1 (at $N_{side} = 8$), and thus we conclude that the Minkowski functionals measured from the WMAP 5-year data are fully consistent with Gaussianity.

What do these results imply for f^{local}_{NL}? We find that the absence of non-Gaussianity at $N_{side} = 128$ and 64 gives the 68% limits on f^{local}_{NL} as $f^{local}_{NL} = -57 \pm 60$ and -68 ± 69, respectively. The 95% limit from $N_{side} = 128$ is $-178 < f^{local}_{NL} < 64$. The errors are larger than those from the bispectrum analysis given in § 3.5.3 by a factor of two, which is partly because we have not used the Minkowski functional at all six resolutions to constrain f^{local}_{NL}. For a combined analysis of the WMAP 3-year data, see Hikage et al. (2008).

It is intriguing that the Minkowski functionals prefer a *negative* value of f^{local}_{NL}, $f^{local}_{NL} \sim -60$, whereas the bispectrum prefers a *positive* value, $f^{local}_{NL} \sim 60$. In the limit that non-Gaussianity is weak, the Minkowski functionals are sensitive to three "skewness parameters:" (1) $\langle (\Delta T)^3 \rangle$, (2) $\langle (\Delta T)^2 [\partial^2(\Delta T)] \rangle$, and (3) $\langle [\partial(\Delta T)]^2 [\partial^2(\Delta T)] \rangle$, all of which can be written in terms of the weighted sum of the bispectrum; thus, the Minkowski functionals are sensitive to some selected configurations of the bispectrum (Hikage et al. 2006). It would be important to study where an apparent "tension" between the Minkowski functionals and the KSW estimator comes from. This example shows how important it is to use different statistical tools to identify the origin of non-Gaussian signals on the sky.

3.6. Adiabaticity of primordial fluctuations
3.6.1. Motivation

"Adiabaticity" of primordial fluctuations offers important tests of inflation as well as clues to the origin of matter in the universe. The negative correlation between the temperature and E-mode polarization (TE) at $l \sim 100$ is a generic signature of adiabatic super-horizon fluctuations (Spergel & Zaldarriaga 1997; Peiris et al. 2003). The improved measurement of the TE power spectrum as well as the temperature power spectrum from the WMAP 5-year data, combined with the distance information from BAO and SN, now provide tight limits on deviations of primordial fluctuations from adiabaticity.

Adiabaticity may be defined loosely as the following relation between fluctuations in radiation density and those in matter density:

$$\frac{3\delta\rho_r}{4\rho_r} = \frac{\delta\rho_m}{\rho_m}. \qquad (36)$$

This version[37] of the condition guarantees that the entropy density (dominated by radiation, $s_r \propto \rho_r^{3/4}$) per matter particle is unperturbed, i.e., $\delta(s_r/n_m) = 0$.

There are two situations in which the adiabatic condition may be satisfied: (1) there is only one degree of freedom in the system, e.g., both radiation and matter were created from decay products of a single scalar field

---

[37] A more general relation is $\delta\rho_x/\dot{\rho}_x = \delta\rho_y/\dot{\rho}_y$, where x and y refer to some energy components. Using the energy conservation equation, $\dot{\rho}_x = -3H(1 + w_x)\rho_x$ (where w_x is the equation of state for the component x), one can recover Eq. (36), as $w_r = 1/3$ and $w_m = 0$. For a recent discussion on this topic, see, e.g., Weinberg (2003).

that was solely responsible for generating fluctuations, and (2) matter and radiation were in thermal equilibrium before any non-zero conserving quantum number (such as baryon number minus lepton number, $B - L$) was created (e.g., Weinberg 2004).

Therefore, detection of any non-adiabatic fluctuations, i.e., any deviation from the adiabatic condition (Eq. [36]), would imply that there were multiple scalar fields during inflation, *and* either matter (baryon or dark matter) was never in thermal equilibrium with radiation, or a non-zero conserving quantum number associated with matter was created well before the era of thermal equilibrium. In any case, the detection of non-adiabatic fluctuations between matter and radiation has a profound implication for the physics of inflation and, perhaps more importantly, the origin of matter.

For example, axions, a good candidate for dark matter, generate non-adiabatic fluctuations between dark matter and photons, as axion density fluctuations could be produced during inflation independent of curvature perturbations (which were generated from inflaton fields, and responsible for CMB anisotropies that we observe today), *and* were not in thermal equilibrium with radiation in the early universe (see Kolb & Turner 1990; Sikivie 2008, for reviews). We can therefore place stringent limits on the properties of axions by looking at a signature of deviation from the adiabatic relation in the CMB temperature and polarization anisotropies.

In this paper we focus on the non-adiabatic perturbations between cold dark matter (CDM) and CMB photons. Non-adiabatic perturbations between baryons and photons are exactly the same as those between CDM and photons, up to an overall constant; thus, we shall not consider them separately in this paper. For neutrinos and photons we consider only adiabatic perturbations. In other words, we consider only three standard neutrino species (i.e., no sterile neutrinos), and assume that the neutrinos were in thermal equilibrium before the lepton number was generated.

The basic idea behind this study is not new, and adiabaticity has been constrained extensively using the *WMAP* data since the first year release, including general (phenomenological) studies without references to specific models (Peiris et al. 2003; Crotty et al. 2003; Bucher et al. 2004; Moodley et al. 2004; Lazarides et al. 2004; Kurki-Suonio et al. 2005; Beltrán et al. 2005; Dunkley et al. 2005; Bean et al. 2006; Trotta 2007; Keskitalo et al. 2007), as well as constraints on specific models such as double inflation (Silk & Turner 1987; Polarski & Starobinsky 1992, 1994), axion (Weinberg 1978; Wilczek 1978; Seckel & Turner 1985; Linde 1985; Linde 1991; Turner & Wilczek 1991), and curvaton (Lyth & Wands 2003; Moroi & Takahashi 2001, 2002; Bartolo & Liddle 2002), all of which can be constrained from the limits on non-adiabatic fluctuations (Gordon & Lewis 2003; Gordon & Malik 2004; Beltran et al. 2004; Lazarides 2005; Parkinson et al. 2005; Beltran et al. 2005, 2007; Kawasaki & Sekiguchi 2007).

We shall use the *WMAP* 5-year data, combined with the distance information from BAO and SN, to place more stringent limits on two types of non-adiabatic CDM fluctuations: (i) axion-type, and (ii) curvaton-type. Our study given below is similar to the one by Kawasaki & Sekiguchi (2007) for the *WMAP* 3-year data.

3.6.2. *Analysis*

We define the non-adiabatic, or entropic, perturbation between the CDM and photons, $\mathcal{S}_{c,\gamma}$, as

$$\mathcal{S}_{c,\gamma} \equiv \frac{\delta\rho_c}{\rho_c} - \frac{3\delta\rho_\gamma}{4\rho_\gamma}, \tag{37}$$

and report on the limits on the ratio of the power spectrum of $\mathcal{S}_{c,\gamma}$, $P_\mathcal{S}(k)$, to the curvature perturbation, $P_\mathcal{R}(k)$, at a given pivot wavenumber, k_0, given by (e.g., Bean et al. 2006)

$$\frac{\alpha(k_0)}{1 - \alpha(k_0)} \equiv \frac{P_\mathcal{S}(k_0)}{P_\mathcal{R}(k_0)}. \tag{38}$$

We shall take k_0 to be 0.002 Mpc^{-1}.

While α parametrizes the ratio of the entropy power spectrum to the curvature power spectrum, it may be more informative to quantify "how much the adiabatic relation (Eq. [36]) can be violated." To quantify this, we introduce the adiabaticity deviation parameter, δ_{adi}, given by

$$\delta_{adi}^{(c,\gamma)} \equiv \frac{\delta\rho_c/\rho_c - 3\delta\rho_\gamma/(4\rho_\gamma)}{\frac{1}{2}[\delta\rho_c/\rho_c + 3\delta\rho_\gamma/(4\rho_\gamma)]}, \tag{39}$$

which can be used to say, "dark matter and photons obey the adiabatic relation to $100\delta_{adi}^{(c,\gamma)}\%$." The numerator is just the definition of the entropy perturbation, $\mathcal{S}_{c,\gamma}$, whereas the denominator is given by

$$\frac{1}{2}\left(\frac{\delta\rho_c}{\rho_c} + \frac{3\delta\rho_\gamma}{4\rho_\gamma}\right) = 3\mathcal{R} + O(\mathcal{S}). \tag{40}$$

Therefore, we find, up to the first order in $\mathcal{S}/\mathcal{R}$,

$$\delta_{adi}^{(c,\gamma)} \approx \frac{\mathcal{S}}{3\mathcal{R}} \approx \frac{\sqrt{\alpha}}{3}, \tag{41}$$

for $\alpha \ll 1$.

There could be a significant correlation between $\mathcal{S}_{c,\gamma}$ and $\mathcal{R}$ (Langlois 1999; Langlois & Riazuelo 2000; Gordon et al. 2001). We take this into account by introducing the cross-correlation coefficient, as

$$-\beta(k_0) \equiv \frac{P_{S,\mathcal{R}}(k_0)}{\sqrt{P_\mathcal{S}(k_0)P_\mathcal{R}(k_0)}}, \tag{42}$$

where $P_{\mathcal{S},\mathcal{R}}(k)$ is the cross-correlation power spectrum.

Here, we have a negative sign on the left hand side because of the following reason. In our notation that we used for Gaussianity analysis, the sign convention of the curvature perturbation is such that it gives temperature anisotropy on large scales (the Sachs–Wolfe limit) as $\Delta T/T = -(1/5)\mathcal{R}$. On the other hand, those who investigate correlations between $\mathcal{S}$ and $\mathcal{R}$ usually use an opposite sign convention for the curvature perturbation, such that the temperature anisotropy is given by

$$\frac{\Delta T}{T} = \frac{1}{5}\tilde{\mathcal{R}} - \frac{2}{5}\mathcal{S} \tag{43}$$

on large angular scales (Langlois 1999), where $\tilde{\mathcal{R}} \equiv -\mathcal{R}$, and define the correlation coefficient by

$$\beta(k_0) = \frac{P_{S,\tilde{\mathcal{R}}}(k_0)}{\sqrt{P_\mathcal{S}(k_0)P_{\tilde{\mathcal{R}}(k_0)}}}. \tag{44}$$
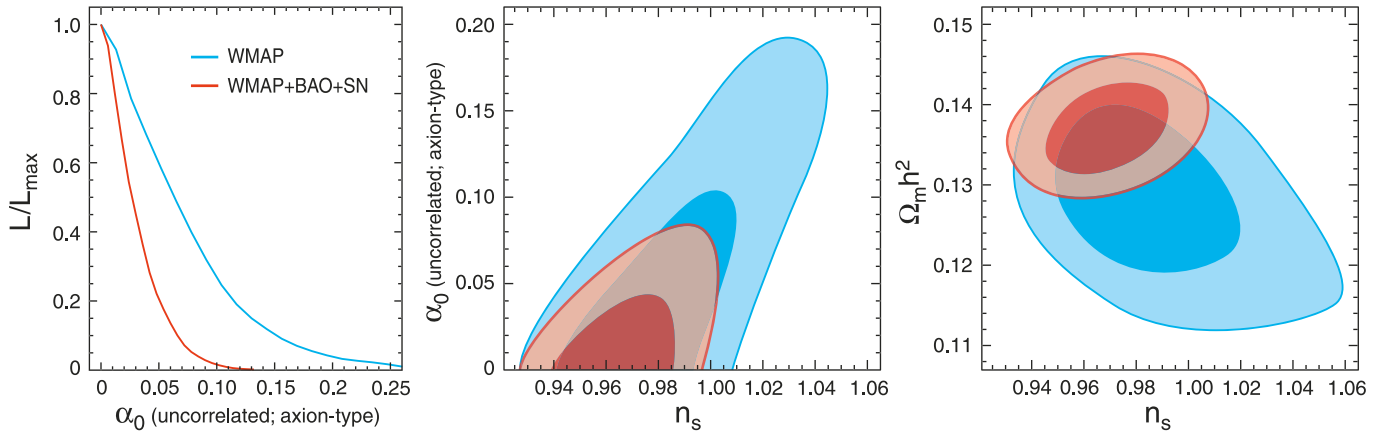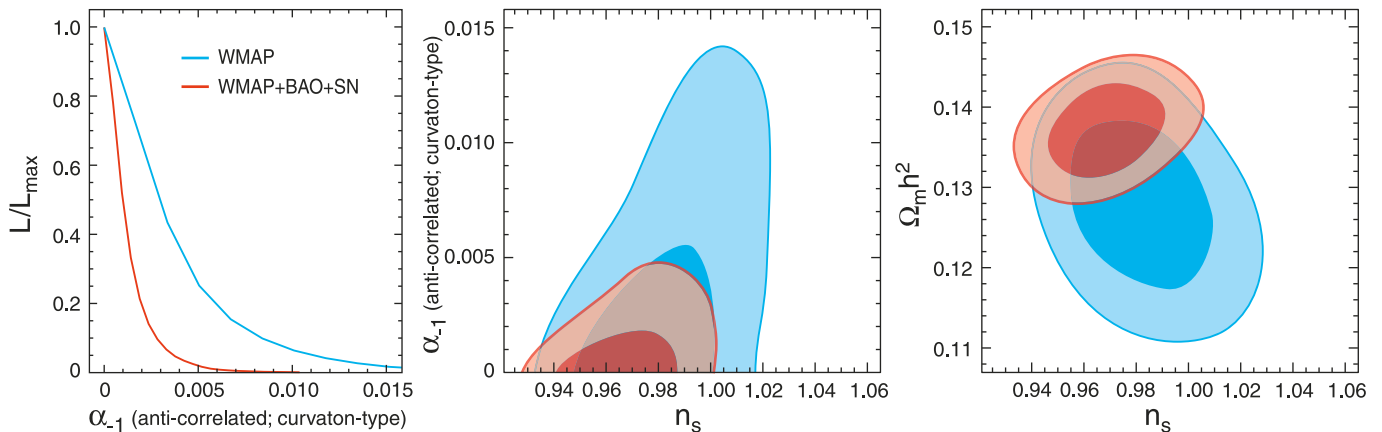
FIG. 8.— Constraint on the axion entropy perturbation fraction, α_0 (§ 3.6.3). In all panels we show the WMAP-only results in blue and WMAP+BAO+SN in red. (*Left*) One-dimensional marginalized constraint on α_0, showing WMAP-only and WMAP+BAO+SN. (*Middle*) Joint two-dimensional marginalized constraint (68% and 95% CL), showing the degeneracy between α_0 and n_s for WMAP-only and WMAP+BAO+SN. (*Right*) Degeneracy between n_s and $\Omega_m h^2$. The BAO and SN data help to break this degeneracy which, in turn, reduces degeneracy between α_0 and n_s, resulting in a factor of 2.4 better limit on α_0.

FIG. 9.— Constraint on the curvaton entropy perturbation fraction, α_{-1} (§ 3.6.4). In all panels we show the WMAP-only results in blue and WMAP+BAO+SN in red. (*Left*) One-dimensional marginalized constraint on α_{-1}, showing WMAP-only and WMAP+BAO+SN. (*Middle*) Joint two-dimensional marginalized constraint (68% and 95% CL), showing the degeneracy between α_{-1} and n_s for WMAP-only and WMAP+BAO+SN. (*Right*) Degeneracy between n_s and $\Omega_m h^2$. The BAO and SN data help to break this degeneracy which, in turn, reduces degeneracy between α_{-1} and n_s, resulting in a factor of 3 better limit on α_{-1}. These properties are similar to those of the axion dark matter presented in Fig. 8.

Therefore, in order to use the same sign convention for β as most of the previous work, we shall use Eq. (42), and call $\beta = +1$ "totally correlated," and $\beta = -1$ "totally anti-correlated," entropy perturbations.

It is also useful to understand how the correlation or anti-correlation affects the CMB power spectrum at low multipoles. By squaring equation (43) and taking the average, we obtain

$$\frac{\langle (\Delta T)^2 \rangle}{T^2} = \frac{1}{25}\left(P_{\tilde{\mathcal{R}}} + 4P_{\mathcal{S}} - 4\beta\sqrt{P_{\tilde{\mathcal{R}}} P_{\mathcal{S}}(k)} \right). \quad (45)$$

Therefore, the "correlation," $\beta > 0$, reduces the temperature power spectrum on low multipoles, whereas the "anti-correlation," $\beta < 0$, increases the power. This point will become important when we interpret our results: namely, models with $\beta < 0$ will result in a positive correlation between α and n_s (Gordon & Lewis 2003). Note that this property is similar to that of the tensor mode: as the tensor mode adds a significant power only to $l \lesssim 50$, the tensor-to-scalar ratio, r, is degenerate with n_s (see Fig. 3).

Finally, we specify the power spectrum of S as a pure power-law,

$$P_{\mathcal{S}}(k) \propto k^{m-4}, \qquad P_{\mathcal{S},\mathcal{R}}(k) \propto k^{(m+n_s)/2-4}, \quad (46)$$

in analogy to the curvature power spectrum, $P_{\mathcal{R}}(k) \propto k^{n_s-4}$. Note that β does not depend on k for this choice of $P_{\mathcal{S},\mathcal{R}}(k)$. With this parametrization, it is straightforward to compute the angular power spectra of the temperature and polarization of CMB.

In this paper we shall pay attention to two limiting cases that are physically motivated: totally uncorrelated ($\beta = 0$) entropy perturbations – axion-type (Seckel & Turner 1985; Linde 1985; Linde 1991; Turner & Wilczek 1991), and totally anti-correlated ($\beta = -1$) entropy perturbations – curvaton-type (Linde & Mukhanov 1997; Lyth & Wands 2003; Moroi & Takahashi 2001, 2002; Bartolo & Liddle 2002). Then, we shall use α_0 to denote α for $\beta = 0$ and α_{-1} for $\beta = -1$.

3.6.3. *Results: Implications for Axion*

First, let us consider the axion case in which $\mathcal{S}$ and $\mathcal{R}$ are totally uncorrelated, i.e., $\beta = 0$. This case represents the entropy perturbation between photons and axions,

with axions accounting for some fraction of dark matter in the universe. For simplicity, we take the axion perturbations to be scale invariant, i.e., $m = 1$. In Appendix B we show that this choice corresponds to taking one of the slow-roll parameters, ϵ, to be less than 10^{-2}, or adding a tiny amount of gravitational waves, $r \ll 0.1$, which justifies our ignoring gravitational waves in the analysis.

The left panel of Fig. 8 shows that we do not find any evidence for the axion entropy perturbations. The limits are $\alpha_0 < 0.16$ (95% CL) and $\alpha_0 < 0.067$ (95% CL) for the WMAP-only analysis and WMAP+BAO+SN, respectively. The latter limit is the most stringent to date, from which we find the adiabaticity deviation parameter of $\delta_{adi}^{c,\gamma} < 0.086$ (Eq. [39]); thus, we conclude that the axion dark matter and photons should obey the adiabatic relation (Eq. [36]) to 8.6%, at the 95% CL.

We find that n_s and α_0 are strongly degenerate (see the middle panel of Fig. 8). It is easy to understand the direction of degeneracy. As the entropy perturbation with a scale invariant spectrum adds power to the temperature anisotropy on large angular scales only, the curvature perturbation tries to compensate it by reducing power on large scales with a larger tilt, n_s. However, since a larger n_s produces too much power on small angular scales, the fitting tries to increase $\Omega_b h^2$ to suppress the second peak, and reduce $\Omega_c h^2$ to suppress the third peak. Overall, $\Omega_m h^2$ needs to be reduced to compensate an increase in n_s, as shown in the right panel of Fig. 8.

Adding the distance information from the BAO and SN helps to break the degeneracy between $\Omega_m h^2$ and n_s by constraining $\Omega_m h^2$, independent of n_s. Therefore, with WMAP+BAO+SN we find an impressive, factor of 2.4 improvement in the constraint on α_0.

What does this imply for the axions? It has been shown that the limit on the axion entropy perturbation can be used to place a constraint on the energy scale of inflation which, in turn, leads to a stringent constraint on the tensor-to-scalar ratio, r (Kain 2006; Beltran et al. 2007; Sikivie 2008; Kawasaki & Sekiguchi 2007).

In Appendix B we study a particular axion cosmology called the "misalignment angle scenario," in which the Pecci-Quinn symmetry breaking occurred during inflation, and *was never restored after inflation.* In other words, we assume that the Pecci-Quinn symmetry breaking scale set by the axion decay constant, f_a, which has been constrained to be greater than 10^{10} GeV from the supernova 1987A (Yao et al. 2006), is at least greater than the reheating temperature of the universe after inflation. This is a rather reasonable assumption, as the reheating temperature is usually taken to be as low as 10^8 GeV in order to avoid overproduction of unwanted relics (Pagels & Primack 1982; Coughlan et al. 1983; Ellis et al. 1986). Such a low reheating temperature is natural also because a coupling between inflaton and matter had to be weak; otherwise, it would terminate inflation prematurely.

In this scenario axions acquired quantum fluctuations during inflation, in the same way that inflaton fields would acquire fluctuations. These fluctuations were then converted to mass density fluctuations when axions acquired mass at the QCD phase transition at ~ 200 MeV. We observe a signature of the axion mass density fluctuations via CDM-photon entropy perturbations imprinted in the CMB temperature and polarization anisotropies.

We find that the tensor-to-scalar ratio r, the axion density, Ω_a, CDM density, Ω_c, the phase of the Pecci-Quinn field within our observable universe, θ_a, and α_0, are related as (for an alternative expression that has f_a left instead of θ_a, see Eq. [B7])

$$r = \frac{4.7 \times 10^{-12}}{\theta_a^{10/7}} \left(\frac{\Omega_c h^2}{\gamma}\right)^{12/7} \left(\frac{\Omega_c}{\Omega_a}\right)^{2/7} \frac{\alpha_0}{1-\alpha_0}, \quad (47)$$

$$< \frac{(0.99 \times 10^{-13})\alpha_0}{\theta_a^{10/7}\gamma^{12/7}} \left(\frac{\Omega_c}{\Omega_a}\right)^{2/7} \quad (48)$$

where $\gamma \leq 1$ is a "dilution factor" representing the amount by which the axion density parameter, $\Omega_a h^2$, would have been diluted due to a potential late-time entropy production by, e.g., decay of some (unspecified) heavy particles, between 200 MeV and the epoch of nucleosynthesis, 1 MeV. Here, we have used the limit on the CDM density parameter, $\Omega_c h^2$, from the axion entropy perturbation model that we consider here, $\Omega_c h^2 = 0.1052^{+0.0068}_{-0.0070}$, as well as the observational fact that $\alpha_0 \ll 1$.

With our limit, $\alpha_0 < 0.067$ (95% CL), we find a limit on r within this scenario as

$$r < \frac{6.6 \times 10^{-15}}{\theta_a^{10/7}\gamma^{12/7}} \left(\frac{\Omega_c}{\Omega_a}\right)^{2/7}. \quad (49)$$

Therefore, in order for the axion dark matter scenario that we have considered here to be compatible with $\Omega_c \sim \Omega_a$ and the limits on the non-adiabaticity and $\Omega_c h^2$, the energy scale of inflation should be low, and hence the gravitational waves are predicted to be negligible, *unless* the axion density was diluted severely by a late-time entropy production, $\gamma \sim 0.8 \times 10^{-7}$ (for $\theta_a \sim 1$), the axion phase (or the misalignment angle) within our observable universe was close to zero, $\theta_a \sim 3 \times 10^{-9}$ (for $\gamma \sim 1$), or both γ and θ_a were close to zero with lesser degree. All of these possibilities would give $r \sim 0.01$, a value that could be barely detectable in the foreseeable future. One can also reverse Eq. (49) to obtain

$$\frac{\Omega_a}{\Omega_c} < \frac{3.0 \times 10^{-39}}{\theta_a^5 \gamma^6} \left(\frac{0.01}{r}\right)^{7/2}. \quad (50)$$

Therefore, the axion density would be negligible for the detectable r, unless θ_a or γ or both are tuned to be small.

Whether such an extreme production of entropy is highly unlikely, or such a tiny angle is an undesirable fine-tuning, can be debated. In any case, it is clear that the cosmological observations, such as the CDM density, entropy perturbations, and gravitational waves, can be used to place a rather stringent limit on the axion cosmology based upon the misalignment scenario, one of the most popular scenarios for axions to become a dominant dark matter component in the universe.

3.6.4. *Results: Implications for Curvaton*

Next, let us consider one of the curvaton models in which $\mathcal{S}$ and $\tilde{\mathcal{R}}$ are totally anti-correlated, i.e., $\beta = -1$ (Lyth & Wands 2003; Moroi & Takahashi 2001, 2002; Bartolo & Liddle 2002). One can also write $\mathcal{S}$ as $\mathcal{S} = B\mathcal{R} = -B\tilde{\mathcal{R}}$ where $B > 0$; thus, $B^2 = \alpha_{-1}/(1 - \alpha_{-1})$.[38]

---

[38] This variable, B, is the same as B used in Gordon & Lewis (2003), including the sign convention.

We take the spectral index of the curvaton entropy perturbation, m, to be the same as that of the adiabatic perturbation, n_s, i.e., $n_s = m$.

The left panel of Figure 9 shows that we do not find any evidence for the curvaton entropy perturbations, either. The limits, $\alpha_{-1} < 0.011$ (95% CL) and $\alpha_{-1} < 0.0037$ (95% CL) for the WMAP-only analysis and WMAP+BAO+SN, respectively, are more than a factor of 10 better than those for the axion perturbations. The WMAP-only limit is better than the previous limit by a factor of 4 (Bean et al. 2006). From the WMAP+BAO+SN limit, we find the adiabaticity deviation parameter of $\delta_{adi}^{(c,\gamma)} < 0.020$ (Eq. [39]); thus, we conclude that the curvaton dark matter and photons should obey the adiabatic relation (Eq. [36]) to 2.0% at the 95% CL.

Once again, adding the distance information from the BAO and SN helps to break the degeneracy between n_s and $\Omega_m h^2$ (see the right panel of Fig. 9), and reduces the degeneracy between n_s and α_{-1}. The directions in which these parameters are degenerate are similar to those for the axion case (see Fig. 8), as the entropy perturbation with $\beta = -1$ also increases the CMB temperature power spectrum on large angular scales, as we described in § 3.6.2.

What is the implication for this type of curvaton scenario, in which $\beta = -1$? This scenario would arise when CDM was created from the decay products of the curvaton field. One then finds a prediction (Lyth et al. 2003)

$$\frac{\alpha_{-1}}{1 - \alpha_{-1}} \approx 9 \left(\frac{1 - \rho_{\text{curvaton}}/\rho_{\text{total}}}{\rho_{\text{curvaton}}/\rho_{\text{total}}} \right)^2, \qquad (51)$$

where ρ_{curvaton} and ρ_{total} are the curvaton density and total density at the curvaton decay, respectively. Note that there would be no entropy perturbation if curvaton dominated the energy density of the universe completely at the decay. The reason is simple: in such a case *all* of the curvaton perturbation would become the adiabatic perturbation, so would the CDM perturbation. Our limit, $\alpha_{-1} < 0.0037$ (95% CL), indicates that $\rho_{\text{curvaton}}/\rho_{\text{total}}$ is close to unity, which simplifies the relation (Eq. [51]) to give

$$\frac{\rho_{\text{curvaton}}}{\rho_{\text{total}}} \approx 1 - \frac{\sqrt{\alpha_{-1}}}{3} = 1 - \delta_{adi}^{(c,\gamma)}. \qquad (52)$$

Note that it is the adiabaticity deviation parameter given by Eq. (39) that gives the deviation of $\rho_{\text{curvaton}}/\rho_{\text{total}}$ from unity. From this result we find

$$1 \geq \frac{\rho_{\text{curvaton}}}{\rho_{\text{total}}} \gtrsim 0.98 \qquad (95\% \text{ CL}). \qquad (53)$$

As we mentioned in § 3.5.1, the curvaton scenario is capable of producing the local form of non-Gaussianity, and f_{NL}^{local} is given by (Lyth & Rodriguez 2005, and references therein[39])

$$f_{NL}^{\text{local}} = \frac{5\rho_{\text{total}}}{4\rho_{\text{curvaton}}} - \frac{5}{3} - \frac{5\rho_{\text{curvaton}}}{6\rho_{\text{total}}}, \qquad (54)$$

which gives $-1.25 \leq f_{NL}^{\text{local}}(\text{curvaton}) \lesssim -1.21$, for $\alpha_{-1} < 0.0037$ (95% CL). While we need to add additional contributions from post-inflationary, non-linear

---

[39] Note that the sign convention of f_{NL}^{local} in Lyth & Rodriguez (2005) is such that $f_{NL}^{\text{local}, WMAP} = -f_{NL}^{\text{local}}{}_{,\text{theirs}}$

gravitational perturbations of order unity to this value in order to compare with what we measure from CMB, the limit from the curvaton entropy perturbation is consistent with the limit from the measured f_{NL}^{local} (see § 3.5.3). For the other possibilities, including possible baryon entropy perturbations, see Gordon & Lewis (2003).

4. PROBING PARITY VIOLATION OF THE UNIVERSE: TB AND EB CORRELATION

4.1. *Motivation*

Since the temperature and E-mode polarization are parity-even and the B-mode polarization is parity-odd, the TB and EB correlations should vanish in a universe that conserves parity (Kamionkowski et al. 1997; Kamionkowski et al. 1997; Seljak & Zaldarriaga 1997; Zaldarriaga & Seljak 1997). For this reason the TB and EB correlations are usually used to check for systematics, and not widely used as a cosmological probe.

However, parity is violated in the weak interactions (Lee & Yang 1956; Wu et al. 1957). Why can't parity be violated at cosmological scales?

Polarization of photons offers a powerful way of probing the cosmological parity violation, or the "cosmological birefringence" (Carroll 1998). Let us consider a parity-violating interaction term in the Lagrangian such as the Chern-Simons term, $\mathcal{L}_{CS} = -(1/2)p_\alpha A_\beta \tilde{F}^{\alpha\beta}$, where $F^{\alpha\beta}$ and A_β are the usual electromagnetic tensor and vector potential, respectively, $\tilde{F}^{\alpha\beta} = (1/2)\epsilon^{\alpha\beta\mu\nu} F_{\mu\nu}$ is a dual tensor, and p_α is an arbitrary four-vector. Carroll et al. (1990) have shown that the Chern-Simons term makes two polarization states of photons propagate with different group velocities, *causing the polarization plane to rotate* by an angle $\Delta\alpha$.

What would p_α be? We may take this to be a derivative of a light scalar field, $p_\alpha = 2(\partial_\alpha\phi)/M$, where M is some unspecified energy scale. In this case, the rotation angle is given by $\Delta\alpha = \int \frac{dt}{a}\dot{\phi}/M = (\Delta\phi)/M$ (Carroll et al. 1990; Carroll 1998; Liu et al. 2006; Xia et al. 2007). Such a field might have something to do with dark energy, for example. We are therefore looking at a potential parity-violating interaction between the visible section (i.e., photons) and dark sector (i.e., dark energy).

Such an unusual rotation of polarization vectors has been constrained by observations of radio galaxies and quasars (Carroll 1998): one of the best data sets available today at a single redshift is 3C9 at $z = 2.012$, which gives a limit on the rotation angle, $\Delta\alpha = 2° \pm 3°$ (68% CL). There are about 10 measurements between $z = 0.425$ and $z = 2.012$, whose average is $\Delta\alpha = -0.6° \pm 1.5°$ (68% CL).

The rotation of polarization plane converts the E-mode polarization to the B-mode. As a result, B modes can be produced from E modes even if inflation did not produce much B modes. This is similar to the gravitational lensing effect, which also produces B modes from E modes (Zaldarriaga & Seljak 1998), but there is an important difference: the lensing does not violate parity, but this interaction does. As a result, the lensing does not yield non-zero TB or EB, but this interaction yields both TB and EB.

We shall constrain $\Delta\alpha$ between the reionization epoch $z \sim 10$ and the present epoch, as well as $\Delta\alpha$ between the decoupling epoch, $z \simeq 1090$, and the present epoch,
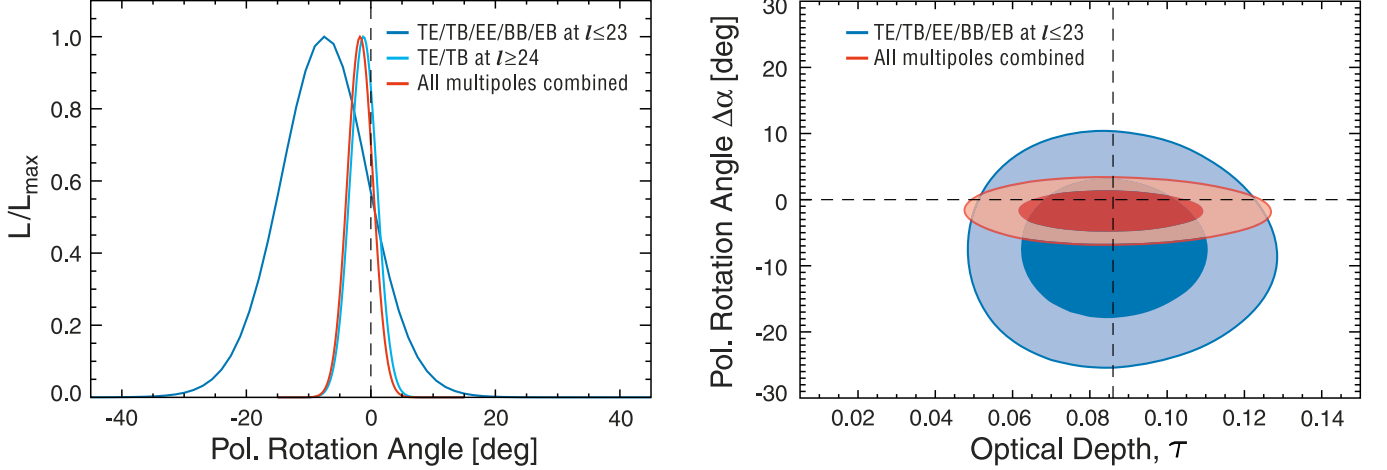
FIG. 10.— Constraint on the polarization rotation angle, $\Delta\alpha$, due to a parity-violating interaction that rotates the polarization angle of CMB (§ 4.3). We have used the polarization spectra (TE/TB/EE/BB/EB at $l \leq 23$, and TE/TB at $l \geq 24$), and did not use the TT power spectrum. (*Left*) One-dimensional marginalized constraint on $\Delta\alpha$ in units of degrees. The dark blue, light blue, and red curves show the limits from the low-l ($2 \leq l \leq 23$), high-l ($24 \leq l \leq 450$), and combined ($2 \leq l \leq 450$) analysis of the polarization data, respectively. (*Right*) Joint two-dimensional marginalized constraint on τ and $\Delta\alpha$ (68% and 95% CL). The bigger contours are from the low-l analysis, while the smaller ones are from the combined analysis. The vertical dotted line shows the best-fitting optical depth in the absence of parity violation ($\tau = 0.086$), whereas the horizontal dotted line shows $\Delta\alpha = 0$ to guide eyes.

using the TB and EB spectra that we measure from the *WMAP* 5-year data.

4.2. *Analysis*

Before we proceed, we should remember that the magnitude of polarization rotation angle, $\Delta\alpha$, depends on the path length over which photons experienced a parity-violating interaction. As pointed out by Liu et al. (2006), this leads to the polarization angle that depends on l. We can divide this l-dependence in two regimes:

- $l \lesssim 20$: the polarization signal was generated during reionization (Zaldarriaga 1997). We are sensitive only to the polarization rotation between the reionization epoch and present epoch.

- $l \gtrsim 20$: the polarization signal was generated at the decoupling epoch. We are sensitive to the polarization rotation between the decoupling epoch and present epoch; thus, we have the largest path length in this case.

Below, we shall explore two cases separately. Note that we shall use only the polarization spectra: TE, TB, EE, BB, and EB, and do not use the temperature spectrum, as the temperature spectrum is not affected by the parity-violating interaction.

Moreover, for the analysis at $l \leq 23$ we only vary the polarization angle $\Delta\alpha$, and the optical depth, τ, and fix the other parameters at $\Omega_k = 0$, $\Omega_b h^2 = 0.02265$, $\Omega_c h^2 = 0.1143$, $H_0 = 70.1$ km s^{-1} Mpc^{-1}, and $n_s = 0.960$. At each value of τ, we re-adjust the overall normalization of power spectra such that the first peak of the temperature spectrum is held fixed. For the analysis at $l \geq 24$ we fix τ at 0.085, and vary only $\Delta\alpha$, as there is no degeneracy between $\Delta\alpha$ and τ at high multipoles. We ignore EE, BB and EB at $l \geq 24$, as they are much noisier than TE and TB and thus do not add much information.

When the polarization plane is rotated by $\Delta\alpha$, the intrinsic (primordial) TE, EE, and BB spectra are converted into TE, TB, EE, BB, and EB spectra as (Lue

et al. 1999; Feng et al. 2005)

$$C_l^{TE,obs} = C_l^{TE} \cos(2\Delta\alpha), \tag{55}$$

$$C_l^{TB,obs} = C_l^{TE} \sin(2\Delta\alpha), \tag{56}$$

$$C_l^{EE,obs} = C_l^{EE} \cos^2(2\Delta\alpha) + C_l^{BB} \sin^2(2\Delta\alpha), \tag{57}$$

$$C_l^{BB,obs} = C_l^{EE} \sin^2(2\Delta\alpha) + C_l^{BB} \cos^2(2\Delta\alpha), \tag{58}$$

$$C_l^{EB,obs} = \frac{1}{2} \left(C_l^{EE} - C_l^{BB} \right) \sin(4\Delta\alpha), \tag{59}$$

where C_l's are the primordial power spectra in the absence of parity violation, while C_l^{obs}'s are what we would observe in the presence of parity violation. To simplify the problem and maximize our sensitivity to a potential signal of $\Delta\alpha$, we ignore the primordial BB, and use only a reduced set:

$$C_l^{TE,obs} = C_l^{TE} \cos(2\Delta\alpha), \tag{60}$$

$$C_l^{TB,obs} = C_l^{TE} \sin(2\Delta\alpha), \tag{61}$$

$$C_l^{EE,obs} = C_l^{EE} \cos^2(2\Delta\alpha), \tag{62}$$

$$C_l^{BB,obs} = C_l^{EE} \sin^2(2\Delta\alpha), \tag{63}$$

$$C_l^{EB,obs} = \frac{1}{2} C_l^{EE} \sin(4\Delta\alpha). \tag{64}$$

Therefore, TB and EB will be produced via the "leakage" from TE and EE. Note that E and B are totally correlated in this case: $(C_l^{EB,obs})^2 = C_l^{EE,obs} C_l^{BB,obs}$.

Several groups have constrained $\Delta\alpha$ from the *WMAP* 3-year data as well as from the BOOMERanG data (Feng et al. 2006; Liu et al. 2006; Cabella et al. 2007; Xia et al. 2007). All but Liu et al. (2006) assume that $\Delta\alpha$ is constant at all multipoles, which is acceptable when they consider the TB and EB data at $l \gtrsim 20$, i.e., the BOOMERanG data and high-l *WMAP* data. However, it requires care when one considers the low-l *WMAP* data. Moreover, all of the authors used a Gaussian form of the likelihood function for C_l, which is again acceptable at high multipoles, but it is inaccurate at low multipoles.

For the 5-year data release we have added capabilities of computing the likelihood of TB and EB spectra at

low multipoles, $2 \leq l \leq 23$, exactly, as well as that of TB spectrum at high multipoles, $24 \leq l \leq 450$, using the MASTER (pseudo-C_l) algorithm. We shall use this code to obtain the limit on $\Delta\alpha$ from the 5-year *WMAP* polarization data. For the low-l polarization we use the Ka, Q, and V band data, whereas for the high-l polarization we use the Q and V band data.

4.3. *Results*

Fig. 10 shows our limit on $\Delta\alpha$ between (i) the reionization epoch and present epoch from the low-l polarization data (dark blue), (ii) between the decoupling epoch and present epoch from the high-l polarization data (light blue), and (iii) combined constraints from the low-l and high-l data assuming a constant $\Delta\alpha$ across the entire multipole range (red). We find no evidence for parity-violating interactions: the 95% CL (68% CL) limits are $-22.2° < \Delta\alpha < 7.2°$ ($\Delta\alpha = -7.5° \pm 7.3°$) for (i), $-5.5° < \Delta\alpha < 3.1°$ ($\Delta\alpha = -1.2° \pm 2.2°$) for (ii), and $-5.9° < \Delta\alpha < 2.4°$ ($\Delta\alpha = -1.7° \pm 2.1°$) for (iii).

The previous 95% CL (68% CL) limits on $\Delta\alpha$ are largely based upon the high-l TB and EB data from the *WMAP* 3-year data and/or BOOMERanG: $-13.7° < \Delta\alpha < 1.9°$ ($\Delta\alpha = -6.0° \pm 4.0°$) (Feng et al. 2006), $-8.5° < \Delta\alpha < 3.5°$ ($\Delta\alpha = -2.5° \pm 3.0°$) (Cabella et al. 2007), and $-13.8° < \Delta\alpha < 1.4°$ ($\Delta\alpha = -6.2° \pm 3.8°$) (Xia et al. 2007). Our limits from the *WMAP* 5-year data are tighter than the previous ones by a factor of 1.5 to 2, and already comparable to those from the polarization data of radio galaxies and quasars (see § 4.1). Note that the radio galaxies and quasars measure the rotation of polarization between up to $z = 2$ and the present epoch, whereas our limits measure the rotation between the decoupling epoch, $z \simeq 1090$, and the present epoch.

These results show that the TB and EB polarization data can provide interesting limits on parity-violating interaction terms. The future data will be able to place more stringent limits (Xia et al. 2007). In particular, adding the Ka and W band data to the high-l polarization should improve our limit significantly.

5. DARK ENERGY

5.1. *Motivation*

Dark energy is one of the most mysterious observations in physics today. The issue is the following: when the luminosity distances out to Type Ia supernovae (Riess et al. 1998; Perlmutter et al. 1999) and the angular diameter distances measured from the BAO (Eisenstein et al. 2005) as well as CMB (Bennett et al. 2003b) are put together in the context of homogeneous and isotropic cosmological models, one cannot fit these distances without having an accelerated expansion of the universe today. A straightforward interpretation of this result is that we need an additional energy component in the universe that has a large negative pressure, which causes the expansion to accelerate.

However, we do not know much about dark energy. A study of review articles written over the past twenty years reveals a growing circle of ignorance (Weinberg 1989; Carroll et al. 1992; Sahni & Starobinsky 2000; Padmanabhan 2003; Peebles & Ratra 2003; Padmanabhan 2005; Copeland et al. 2006): physicists first struggled to understand why the cosmological constant or vacuum energy

term was so close to zero, then to understand why it was non-zero. Cosmologists then explored the possibility that dark energy was dynamical, e.g., in a form of some light scalar field (Ford 1987; Wetterich 1988; Ratra & Peebles 1988; Peebles & Ratra 1988; Fujii & Nishioka 1990; Chiba et al. 1997; Caldwell et al. 1998; Copeland et al. 1998; Ferreira & Joyce 1998; Zlatev et al. 1999). Recently, there has been significant interest in modifications to General Relativity, in the context of explaining the acceleration of the universe (Dvali et al. 2000; Deffayet et al. 2002).

Currently, the properties of dark energy are mainly constrained by the distance information. There are other promising ways of finding dark energy independent of distances: the expansion rate of the universe at higher ($z \gtrsim 0.5$) redshifts, the Integrated Sachs-Wolfe (ISW) effect, and a slow-down of the growth of large-scale structure in the universe due to dark energy. While these tools are powerful in principle, the current data are not accurate enough to distinguish between the effects of dark energy and spatial curvature of the universe, owing to the degeneracy between them (e.g., Nesseris & Perivolaropoulos 2008; Ho et al. 2008).

Indeed, the properties of dark energy, such as the present-day density and its evolution, e.g., the equation of state parameter w, are degenerate with the spatial curvature of the universe, Ω_k. In this section we shall explore both flat and curved universes when we report on our limits on the dark energy properties.

In § 5.2 and § 5.3 we explore constraints on time-independent (i.e., constant) equation of state, w, assuming flat ($\Omega_k = 0$) and curved ($\Omega_k \neq 0$) geometries, respectively. In § 5.4 we introduce a set of "*WMAP* distance priors," and use them to explore a wider range of model space that has time-dependent equation of state, $w = w(z)$. Throughout § 5.4 we use the distance information only to constrain the properties of dark energy. We thus assume the standard homogeneous and isotropic Friedmann-Lemaitre-Robertson-Walker universe, and do not consider modifications of gravity or local inhomogeneity, as the distance information alone cannot discriminate between these models and the accelerated expansion due to dark energy. Finally, in § 5.5 we introduce a "*WMAP* normalization prior."

5.2. *Constant equation of state: Flat universe*

What are we doing by assuming a flat universe, when we constrain the dark energy equation of state, w? Most inflation models in which the inflationary periods last for much longer than 60 e-folds predict $\Omega_k \sim 10^{-5}$, which is three orders of magnitude below the current constraint (see § 3.4). In this subsection, we use a "strong inflation prior," imposing a flatness prior, and explore dark energy models in the context of such inflation models. We shall explore curved universes in § 5.3.

Figure 11 shows the constraints on w and the present-day dark energy density, Ω_Λ. The *WMAP* data alone cannot constrain this parameter space very well, as certain combinations of w and Ω_Λ can produce very similar angular diameter distances out to the decoupling epoch.

The HST prior helps a little bit $-0.47 < 1 + w < 0.42$ (95% CL) by constraining Ω_Λ: the *WMAP* data measure $\Omega_m h^2$, and a flatness prior imposes a constraint, $\Omega_\Lambda = 1 - (\Omega_m h^2)/h^2$; thus, an additional constraint on
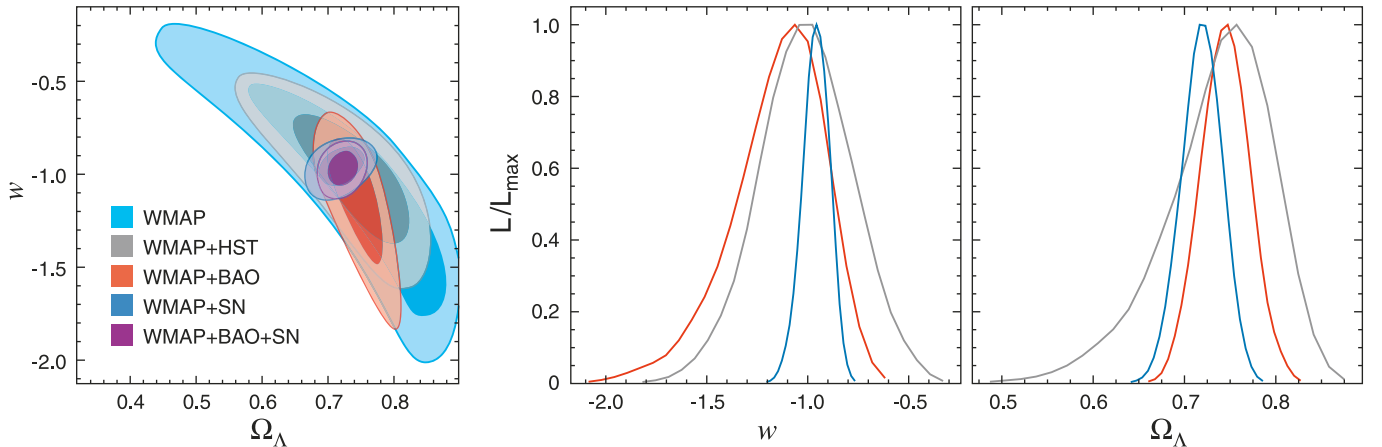
FIG. 11.— Constraint on the time-independent (constant) dark energy equation of state, w, and the present-day dark energy density, Ω_Λ, assuming a flat universe, $\Omega_k = 0$ (§ 5.2). Note that we have imposed a prior on w, $w > -2.5$. (*Left*) Joint two-dimensional marginalized distribution of w and Ω_Λ. The contours show the 68% and 95% CL. The WMAP-only constraint (light blue) is compared with WMAP+HST (gray), WMAP+BAO (red), WMAP+SN (dark blue), and WMAP+BAO+SN (purple). This figure shows how powerful a combination of the *WMAP* data and the current SN data is for constraining w. (*Middle*) One-dimensional marginalized constraint on w for a flat universe from WMAP+HST (gray), WMAP+BAO (red), and WMAP+SN (dark blue). The WMAP+BAO+SN result (not shown) is essentially the same as WMAP+SN. (*Right*) One-dimensional marginalized constraints on Ω_Λ for a flat universe from WMAP+HST (gray), WMAP+BAO (red), and WMAP+SN (dark blue). The WMAP+BAO+SN result (not shown) is essentially the same as WMAP+SN. See Fig. 12 for the constraints on w for non-flat universes.

h from the HST Key Project helps determine Ω_Λ better.

The current angular diameter distance measurements from the BAO do not quite break the degeneracy between w and Ω_Λ, as they constrain the distances at relatively low redshifts, $z = 0.2$ and 0.35, whereas the transition from matter to dark energy domination, which is sensitive to w, happens at earlier times. (Therefore, the future BAO surveys at higher redshifts should be more sensitive to w.) The WMAP+BAO yields $-0.68 < 1 + w < 0.21$ (95% CL).[40]

Finally, the Type Ia supernova data break the degeneracy nicely, as their constraint on this parameter space is nearly orthogonal to what is determined by the CMB data: WMAP+SN yields $-0.098 < 1 + w < 0.159$ (95% CL).[41]

With a flatness prior, the constraint on w from SN is so powerful that WMAP+SN is similar to WMAP+BAO+SN. We conclude that, when the equation of state does not depend on redshifts, dark energy is consistent with vacuum energy, with $-0.097 < 1 + w < 0.142$ (95% CL)[42] (from WMAP+BAO+SN), in the context of a flat universe at the level of curvature that is predicted by long-lasting inflation models.

5.3. *Constant equation of state: Curved universe*

In this subsection we do not assume a flat universe, but do assume a constant equation of state. (For time-dependent equation of state, see § 5.4.2.) As we discussed in § 3.4, the *WMAP* data alone are unable to place meaningful constraints on the spatial curvature of the universe; however, two or more distance or expansion rate measurements break the degeneracy between Ω_k and Ω_m. As Fig. 6 shows, the combination of the *WMAP* measurement of the distance to the decoupling epoch at $z \simeq 1090$, and the distance measurements out

to $z = 0.2$ and 0.35 from BAO, strongly constrains the curvature, at the level of 1–2%.

However, when dark energy is dynamical, we need three distance indicators that cover a wide range of redshift. As the current SN data cover a wider range in redshifts, $0.02 \lesssim z \leq 1.7$, than the BAO data, the SN data help to constrain the evolution of dark energy, i.e., w.

Figure 12 shows the constraints on w and Ω_k from the *WMAP* 5-year data alone, WMAP+HST, WMAP+BAO, WMAP+SN, as well as WMAP+BAO+SN. The middle panel is particularly illuminating. The WMAP+BAO combination fixes Ω_k, nearly independent of w. [43] The WMAP+SN combination yields a degeneracy line that is tilted with respect to the WMAP+BAO line. The WMAP+BAO and WMAP+SN lines intersect at $\Omega_k \sim 0$ and $w \sim -1$, and the combined constraints are $-0.0175 < \Omega_k < 0.0085$ (95% CL) and $-0.11 < 1 + w < 0.14$ (95% CL).[44] It is remarkable that the limit on Ω_k is as good as that for a vacuum energy model, $-0.0181 < \Omega_k < 0.0071$ (95% CL). This is because the BAO and SN yield constraints on Ω_k and w that are complementary to each other, breaking the degeneracy effectively.

These limits give the lower bounds to the curvature radii of the observable universe as $R_{\rm curv} > 33\ h^{-1}{\rm Gpc}$ and $R_{\rm curv} > 23\ h^{-1}{\rm Gpc}$ for negatively and positively curved universes, respectively.

Is the apparent "tension" between the WMAP+BAO limit and the WMAP+SN limit in Fig. 12 the signature of new physics? We have checked this by the BAO distance scale out to $z = 0.35$ from the SDSS LRG sam-

---

[40] The 68% limit is $w = -1.15^{+0.21}_{-0.22}$ (WMAP+BAO; $\Omega_k = 0$).

[41] The 68% limit is $w = -0.960^{+0.066}_{-0.064}$ (WMAP+SN; $\Omega_k = 0$).

[42] The 68% limit is $w = -0.972^{+0.061}_{-0.060}$ (WMAP+BAO+SN; $\Omega_k = 0$).

[43] For the WMAP+BAO limit, there is a long degenerate valley with a significant volume at $w < -1$. Models anywhere in this valley are good fits to both data sets. It is dangerous to marginalize over these degenerate parameters as conclusions are very sensitive to the choice and the form of priors.

[44] The 68% limits are $\Omega_k = -0.0046^{+0.0066}_{-0.0067}$ and $w = -0.984^{+0.065}_{-0.064}$ (WMAP+BAO+SN).
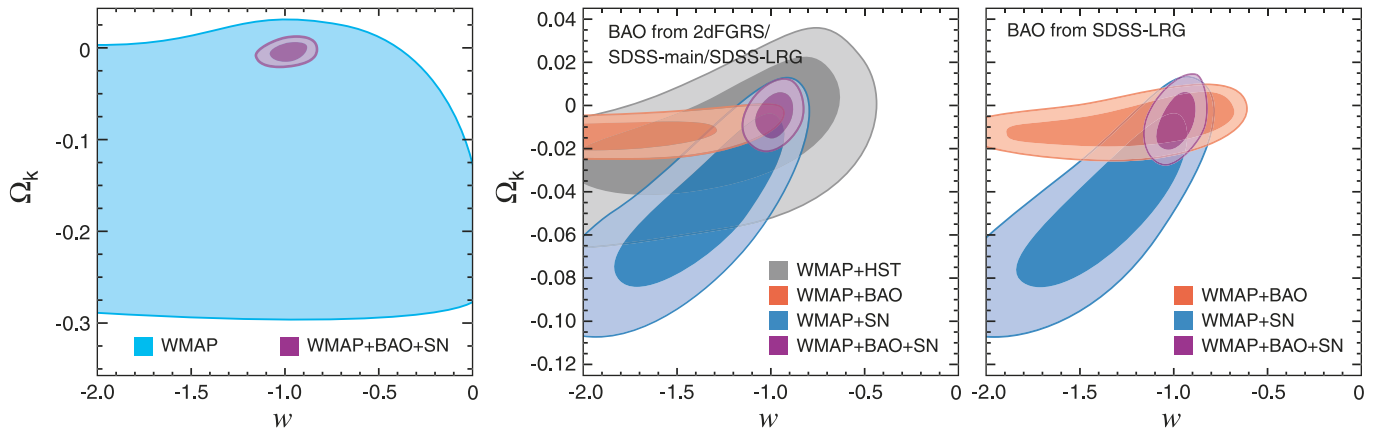
FIG. 12.— Joint two-dimensional marginalized constraint on the time-independent (constant) dark energy equation of state, w, and the curvature parameter, Ω_k (§ 5.3). Note that we have imposed a prior on w, $w > -2.5$. The contours show the 68% and 95% CL. (*Left*) The WMAP-only constraint (light blue; 95% CL) compared with WMAP+BAO+SN (purple; 68% and 95% CL). This figure shows how powerful the extra distance information from BAO and SN is for constraining Ω_k and w simultaneously. (*Middle*) A blow-up of the left panel, showing WMAP+HST (gray), WMAP+BAO (red), WMAP+SN (dark blue), and WMAP+BAO+SN (purple). This figure shows that we need both BAO and SN to constrain Ω_k and w simultaneously: WMAP+BAO fixes Ω_k, and WMAP+SN fixes w. (*Right*) The same as the middle panel, but with the BAO prior re-weighted by a weaker BAO prior from the SDSS LRG sample (Eisenstein et al. 2005). The BAO data used in the other panels combine the SDSS main and LRG, as well as the 2dFGRS data (Percival et al. 2007). The constraints from these are similar, and thus our results are not sensitive to the exact form of the BAO data sets.

ple, obtained by Eisenstein et al. (2005), instead of the $z = 0.2$ and $z = 0.35$ constraints based on the combination of SDSS LRGs with the SDSS main sample and 2dFGRS (Percival et al. 2007). While is it not an independent check, it does provide some measurement of the sensitivity of the constraints to the details of the BAO data set.

The right panel of Fig. 12 shows that the results are not sensitive to the exact form of the BAO data sets.[45] Eisenstein et al.'s BAO prior is a bit weaker than Percival et al.'s, and thus the WMAP+BAO contours extend more to $w \gtrsim -1$. The important point is that the direction of degeneracy does not change. Therefore, the combined limits from WMAP, SN and Eisenstein et al.'s BAO, $-0.11 < w < 0.14$ (95% CL) and $-0.0218 < \Omega_k < 0.0095$ (95% CL), are similar to those with Percival et al.'s BAO, $-0.11 < 1 + w < 0.14$ (95% CL), and $-0.0175 < \Omega_k < 0.0085$ (95% CL). As expected, a weaker BAO prior resulted in a weaker limit on Ω_k.

From these studies, we are able to place rather stringent, simultaneous limits on Ω_k (to 1–2% level, depending upon the sign), and w (to 14% level). The spatial curvature is consistent with zero, and the dark energy is consistent with vacuum energy. How does this conclusion change when we allow w to vary?

5.4. *WMAP distance priors for testing dark energy models*

5.4.1. *Motivation*

Dark energy influences the distance scales as well as the growth of structure. The CMB power spectra are sensitive to both, although sensitivity to the growth of structure is fairly limited, as it influences the CMB power spectrum via the ISW effect at low multipoles ($l \lesssim 10$),

---

[45] To obtain the WMAP+BAO contours in the right panel of Fig. 12, we have re-weighted the WMAP+BAO data in the middle panel of Fig. 12 by the likelihood ratio of L(Eisenstein's BAO)$/L$(Percival's BAO). As a result the contours do not extend to $w \sim 0$; however, the contours would extend more to $w \sim 0$ if we ran a Markov Chain Monte Carlo from the beginning with Eisenstein et al.'s BAO.

TABLE 10
WMAP DISTANCE PRIORS OBTAINED FROM THE WMAP 5-YEAR FIT TO MODELS WITH SPATIAL CURVATURE AND DARK ENERGY. THE CORRELATION COEFFICIENTS ARE: $r_{l_A,R} = 0.1109$, $r_{l_A,z_*} = 0.4215$, AND $r_{R,z_*} = 0.6928$.

	5-year ML[a]	5-year Mean[b]	Error, σ
$l_A(z_*)$	302.10	302.45	0.86
$R(z_*)$	1.710	1.721	0.019
z_*[e]	1090.04	1091.13	0.93

[a]Maximum likelihood values (recommended)
[b]Mean of the likelihood
[c]Maximum likelihood values (recommended)
[d]Mean of the likelihood
[e]Equation (66)

TABLE 11
INVERSE COVARIANCE MATRIX FOR THE WMAP DISTANCE PRIORS

	$l_A(z_*)$	$R(z_*)$	z_*
$l_A(z_*)$	1.800	27.968	-1.103
$R(z_*)$		5667.577	-92.263
z_*			2.923

whose precise measurement is hampered by a large cosmic variance.

On the other hand, CMB is sensitive to the distance to the decoupling epoch via the locations of peaks and troughs of the acoustic oscillations, which can be measured precisely. More specifically, CMB measures two distance ratios: (i) the angular diameter distance to the decoupling epoch divided by the sound horizon size at the decoupling epoch, $D_A(z_*)/r_s(z_*)$, and (ii) the angular diameter distance to the decoupling epoch divided by the Hubble horizon size at the decoupling epoch, $D_A(z_*)H(z_*)/c$. This consideration motivates our using these two distance ratios to constrain various dark energy models, in the presence of the spatial curvature,
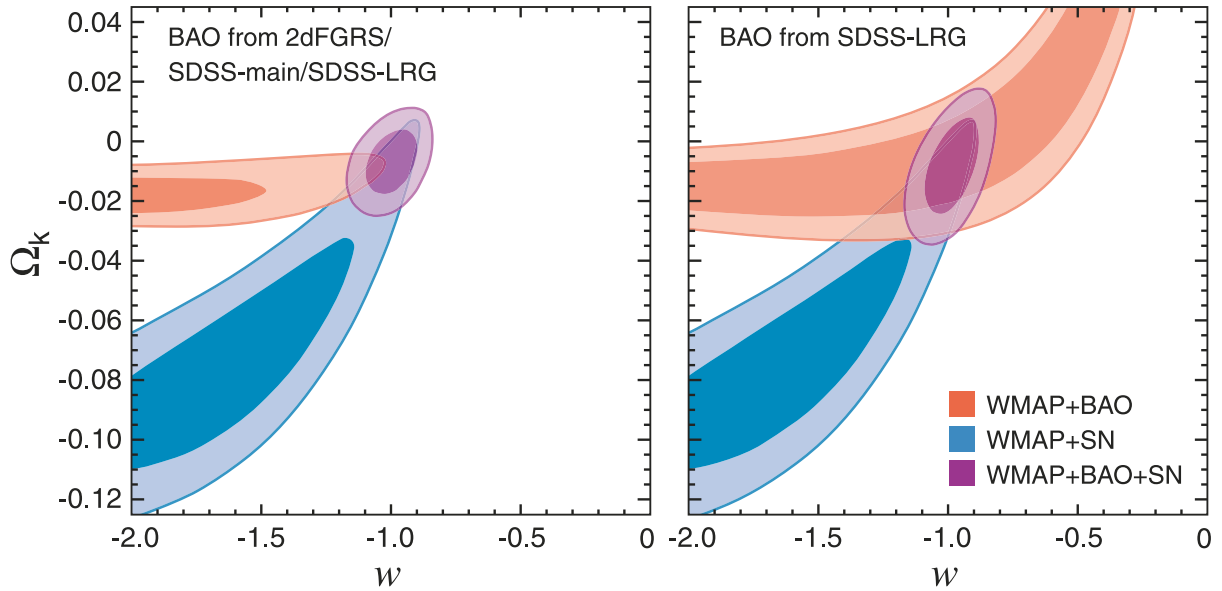
FIG. 13.— Joint two-dimensional marginalized constraint on the time-independent (constant) dark energy equation of state, w, and the curvature parameter, Ω_k, derived solely from the *WMAP* distance priors (l_A, R, z_*) (see § 5.4.1), combined with either BAO (red) or SN (dark blue) or both (purple). The contours show the $\Delta\chi^2_{\text{total}} = 2.30$ (68.3% CL) and $\Delta\chi^2_{\text{total}} = 6.17$ (95.4% CL). The left (BAO data from Percival et al. (2007)) and right (BAO data from Eisenstein et al. (2005)) panels should be compared with the middle and right panels of Fig. 12, respectively, which have been derived from the full *WMAP* data combined with the same BAO and SN data. While the *WMAP* distance priors capture most of the information in this parameter space, the constraint is somewhat weaker than that from the full analysis.

on the basis of distance information (Wang & Mukherjee 2007; Wright 2007).

We shall quantify the first distance ratio, $D_A(z_*)/r_s(z_*)$, by the "acoustic scale," l_A, defined by

$$l_A \equiv (1 + z_*) \frac{\pi D_A(z_*)}{r_s(z_*)}, \qquad (65)$$

where a factor of $(1 + z_*)$ arises because $D_A(z_*)$ is the proper (physical) angular diameter distance (Eq. [2]), whereas $r_s(z_*)$ is the comoving sound horizon at z_* (Eq. [6]). Here, we shall use the fitting function of z_* proposed by Hu & Sugiyama (1996):

$$z_* = 1048 \left[1 + 0.00124(\Omega_b h^2)^{-0.738}\right] \left[1 + g_1 \left(\Omega_m h^2\right)^{g_2}\right], \qquad (66)$$

where

$$g_1 = \frac{0.0783(\Omega_b h^2)^{-0.238}}{1 + 39.5(\Omega_b h^2)^{0.763}}, \qquad (67)$$

$$g_2 = \frac{0.560}{1 + 21.1(\Omega_b h^2)^{1.81}}. \qquad (68)$$

Note that one could also use the peak of the probability of last scattering of photons, i.e., the peak of the visibility function, to define the decoupling epoch, which we denote as z_{dec}. Both quantities yield similar values. We shall adopt z_* here because it is easier to compute, and therefore it allows one to implement the *WMAP* distance priors in a straightforward manner.

The second distance ratio, $D_A(z_*)H(z_*)/c$, is often called the "shift parameter," R, given by (Bond et al. 1997)

$$R(z_*) \equiv \sqrt{\Omega_m H_0^2}(1 + z_*)D_A(z_*). \qquad (69)$$

This quantity is different from $D_A(z_*)H(z_*)/c$ by a factor of $\sqrt{1 + z_*}$, and also ignores the contributions from

radiation, curvature, or dark energy to $H(z_*)$. Nevertheless, we shall use R to follow the convention in the literature.

We give the 5-year *WMAP* constraints on l_A, R, and z_* that we recommend as the *WMAP* distance priors for constraining dark energy models. However, we note an important caveat. As pointed out by Elgarøy & Multamäki (2007) and Corasaniti & Melchiorri (2007), the derivation of the *WMAP* distance priors requires us to assume the underlying cosmology first, as all of these quantities are *derived parameters* from fitting the CMB power spectra. Therefore, one must be careful about which model one is testing. Here, we give the *WMAP* distance priors, assuming the following model:

- The standard Friedmann-Lemaitre-Robertson-Walker universe with matter, radiation, dark energy, as well as spatial curvature.

- Neutrinos with the effective number of neutrinos equal to 3.04, and the minimal mass ($m_\nu \sim 0.05$ eV).

- Nearly power-law primordial power spectrum of curvature perturbations, $|dn_s/d\ln k| \ll 0.01$.

- Negligible primordial gravitational waves relative to the curvature perturbations, $r \ll 0.1$.

- Negligible entropy fluctuations relative to the curvature perturbations, $\alpha \ll 0.1$.

In Fig. 13 we show the constraints on w and Ω_k from the *WMAP* distance priors (combined with BAO and SN). We find a good agreement with the full MCMC results. (Compare the middle and right panels of Fig. 12 with the left and right panels of Fig. 13, respectively.) The constraints from the *WMAP* distance priors are

slightly weaker than the full MCMC, as the distance priors use only a part of the information contained in the *WMAP* data.

Of course, the agreement between Fig. 12 and 13 does not guarantee that these priors yield good results for the other, more complex dark energy models with a time-dependent w; however, the previous studies indicate that, under the assumptions given above, these priors can be used to constrain a wide variety of dark energy models (Wang & Mukherjee 2007; Elgarøy & Multamäki 2007; Corasaniti & Melchiorri 2007).

Here is the prescription for using the *WMAP* distance priors.

(1) For a given $\Omega_b h^2$ and $\Omega_m h^2$, compute z_* from Eq. (66).

(2) For a given H_0, $\Omega_m h^2$, $\Omega_r h^2$ (which includes $N_{\rm eff} = 3.04$), Ω_Λ, and $w(z)$, compute the expansion rate, $H(z)$, from Eq. (7), as well as the comoving sound horizon size at z_*, $r_s(z_*)$, from Eq. (6).

(3) For a given Ω_k and $H(z)$ from the previous step, compute the proper angular diameter distance, $D_A(z)$, from Eq. (2).

(4) Use Eq. (65) and (69) to compute $l_A(z_*)$ and $R(z_*)$, respectively.

(5) Form a vector containing $x_i = (l_A, R, z_*)$ in this order.

(6) Use Table 10 for the data vector, $d_i = (l_A^{WMAP}, R^{WMAP}, z_*^{WMAP})$. We recommend the maximum likelihood (ML) values.

(7) Use Table 11 for the inverse covariance matrix, $(C^{-1})_{ij}$.

(8) Compute the likelihood, L, as $\chi^2_{WMAP} \equiv -2 \ln L = (x_i - d_i)(C^{-1})_{ij}(x_j - d_j)$.

(9) Add this to the favorite combination of the cosmological data sets. In this paper we add χ^2_{WMAP} to the BAO and SN data, i.e., $\chi^2_{\rm total} = \chi^2_{WMAP} + \chi^2_{BAO} + \chi^2_{SN}$.

(10) Marginalize the posterior distribution over $\Omega_b h^2$, $\Omega_m h^2$, and H_0 with uniform priors. Since the *WMAP* distance priors combined with the BAO and SN data provide tight constraints on these parameters, the posterior distribution of these parameters is close to a Gaussian distribution. Therefore, the marginalization is equivalent to minimizing $\chi^2_{\rm total}$ with respect to $\Omega_b h^2$, $\Omega_m h^2$, and H_0 (see also Cash 1976; Wright 2007). We use a downhill simplex method for minimization (amoeba routine in Numerical Recipes (Press et al. 1992)). The marginalization over $\Omega_b h^2$, $\Omega_m h^2$, and H_0 leaves us with the the marginalized posterior distribution of the dark energy function, $w(a)$, and the curvature parameter, Ω_k.

Note that this prescription eliminates the need for running the Markov Chain Monte Carlo entirely, and thus the computational cost for evaluating the posterior distribution of $w(a)$ and Ω_k is not demanding. In § 5.4.2 we shall apply the *WMAP* distance priors to constrain the dark energy equation of state that depends on redshifts, $w = w(z)$.

5.4.2. *Application of the WMAP distance priors: Variable equation of state*

In this subsection we explore a time-dependent equation of state of dark energy, $w(z)$. We use the following parametrized form:

$$w(a) = \frac{a\tilde{w}(a)}{a + a_{\rm trans}} - \frac{a_{\rm trans}}{a + a_{\rm trans}}, \qquad (70)$$

where $\tilde{w}(a) = \tilde{w}_0 + (1 - a)\tilde{w}_a$. We give a motivation, derivation, and detailed discussion on this form of $w(a)$ in Appendix C. This form has a number of desirable properties:

- $w(a)$ approaches to -1 at early times, $a < a_{\rm trans}$, where $a_{\rm trans} = 1/(1 + z_{\rm trans})$ is the "transition epoch," and $z_{\rm trans}$ is the transition redshift. Therefore, the dark energy density tends to a constant value at $a < a_{\rm trans}$.

- The dark energy density remains totally subdominant relative to the matter density at the decoupling epoch.

- We recover the widely used linear form, $w(a) = w_0 + (1 - a)w_a$ (Chevallier & Polarski 2001; Linder 2003), at late times, $a > a_{\rm trans}$.

- The early-time behaviour is consistent with some of scalar field models classified as the "thawing models," (Caldwell & Linder 2005) in which a scalar field was moving very slowly at early times, and then began to move faster at recent times.

- Since the late-time form of $w(a)$ allows $w(a)$ to go below -1, our form is more general than models based upon a single scalar field.

- The form is simple enough to give a closed, analytical form of the effective equation of state, $w_{\rm eff}(a) = (\ln a)^{-1} \int_0^{\ln a} d\ln a'\, w(a')$ (Eq. C6), which determines the evolution of the dark energy density, $\rho_{\rm de}(a) = \rho_{\rm de}(0)a^{-3[1+w_{\rm eff}(a)]}$; thus, it allows one to compute the evolution of the expansion rate and cosmological distances easily.

While this form contains three free parameters, $\tilde{w}_0$, $\tilde{w}_a$ and $z_{\rm trans}$, we shall give constraints on the present-day value of w, $w_0 \equiv w(a)$, and the first derivative of w at present, $w' \equiv dw/dz|_{z=0}$, instead of $\tilde{w}_0$ and $\tilde{w}_a$, as they can be compared to the previous results in the literature more directly. We find that the results are not sensitive to the exact values of $z_{\rm trans}$.

In Fig. 14 we present the constraint on w_0 and w' that we have derived from the *WMAP* distance priors (l_A, R, z_*), combined with the BAO and SN data. Note that we have assumed a flat universe in this analysis, although it is straightforward to include the spatial curvature. Wang & Mukherjee (2007) and Wright (2007) show that the two-dimensional distribution extends more towards south-east, i.e., $w > -1$ and $w' < 0$, when the spatial curvature is allowed.
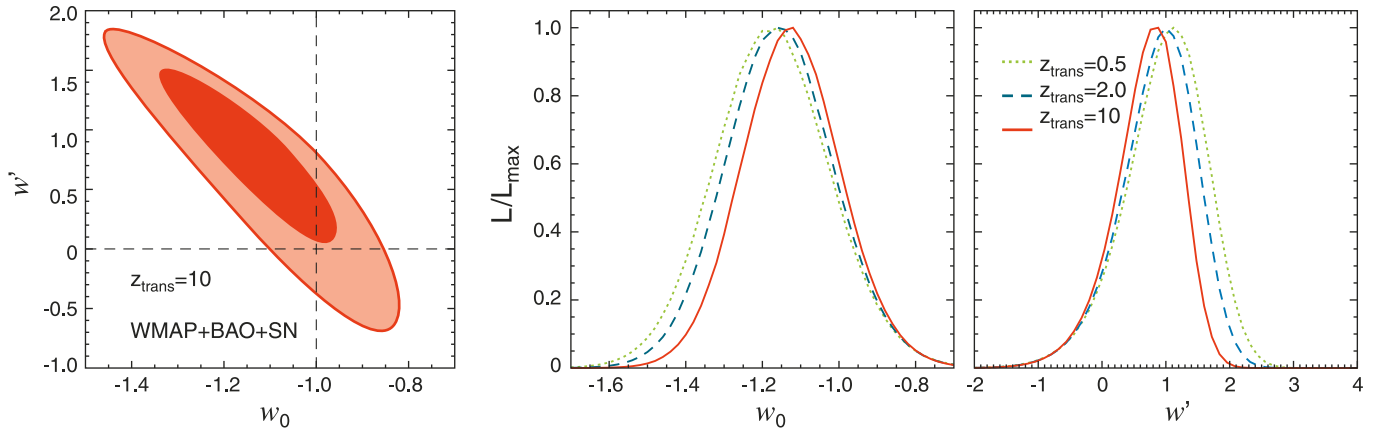
FIG. 14.— Constraint on models of time-dependent dark energy equation of state, $w(z)$ (Eq. [70]), derived from the *WMAP* distance priors $(l_A, R,$ and $z_*)$ combined with the BAO and SN distance data (§ 5.4.2). There are three parameters: w_0 is the value of w at the present epoch, $w_0 \equiv w(z=0)$, w' is the first derivative of w with respect to z at $z=0$, $w' \equiv dw/dz|_{z=0}$, and $z_{\rm trans}$ is the transition redshift above which $w(z)$ approaches to -1. Here, we assume flatness of the universe, $\Omega_k = 0$. (*Left*) Joint two-dimensional marginalized distribution of w_0 and w' for $z_{\rm trans} = 10$. The constraints are similar for the other values of $z_{\rm trans}$. The contours show the $\Delta\chi^2_{\rm total} = 2.30$ (68.3% CL) and $\Delta\chi^2_{\rm total} = 6.17$ (95.4% CL). (*Middle*) One-dimensional marginalized distribution of w_0 for $z_{\rm trans} = 0.5$ (dotted), 2 (dashed), and 10 (solid). (*Middle*) One-dimensional marginalized distribution of w' for $z_{\rm trans} = 0.5$ (dotted), 2 (dashed), and 10 (solid). The constraints are similar for all $z_{\rm trans}$. We do not find evidence for the evolution of dark energy.

FIG. 15.— Constraint on the linear evolution model of dark energy equation of state, $w(z) = w_0 + w'z/(1+z)$, derived from the *WMAP* distance priors $(l_A, R,$ and $z_*)$ combined with the BAO and SN distance data as well as the Big Bang Nucleosynthesis (BBN) prior (Eq. [71]). Here, we assume flatness of the universe, $\Omega_k = 0$. (*Left*) Joint two-dimensional marginalized distribution of w_0 and w'. The contours show the $\Delta\chi^2_{\rm total} = 2.30$ (68.3% CL) and $\Delta\chi^2_{\rm total} = 6.17$ (95.4% CL). (*Middle*) One-dimensional marginalized distribution of w_0. (*Middle*) One-dimensional marginalized distribution of w'. We do not find evidence for the evolution of dark energy. Note that Linder (2003) defines w' as the derivative of w at $z=1$, whereas we define it as the derivative at $z=0$. They are related by $w'_{\rm linder} = 0.5 w'_{WMAP}$.

The 95% limit on w_0 for $z_{\rm trans} = 10$ is $-0.38 < 1 + w_0 < 0.14$[46], whose upper limit is surprisingly close to the limit for a constant w model in a flat universe, $-0.097 < 1 + w < 0.142$ (95% CL). Therefore, we have a fairly robust upper limit on the present-day value of the equation of state, $1 + w_0 < 0.14$. (This statement is, however, true only for a flat universe.) On the other hand, the lower limit has weakened significantly – by a factor of about four. Our results are consistent with the previous work using the *WMAP* 3-year data (see Wang & Mukherjee 2007; Wright 2007, for recent work and references therein). We find that our upper limit on w_0 and lower limit on w' are better than the previous work by a factor of ~ 2.

Alternatively, one may take the linear form, $w(a) = w_0 + (1-a)w_a$, literally and extend it to an arbitrarily high redshift. This can result in an undesirable situation

[46] The 68% intervals are $w_0 = -1.12 \pm 0.13$ and $w' = 0.70 \pm 0.53$ (WMAP+BAO+SN; $\Omega_k = 0$).

in which the dark energy is as important as the radiation density at the epoch of the Big Bang Nucleosynthesis (BBN); however, one can constrain such a scenario severely using the limit on the expansion rate from BBN (Steigman 2007). We follow Wright (2007) to adopt a Gaussian prior on

$$\sqrt{1 + \frac{\Omega_\Lambda (1+z_{\rm BBN})^{3[1+w_{\rm eff}(z_{\rm BBN})]}}{\Omega_m (1+z_{\rm BBN})^3 + \Omega_r (1+z_{\rm BBN})^4 + \Omega_k (1+z_{\rm BBN})^2}}$$
$$= 0.942 \pm 0.030, \tag{71}$$

where we have kept Ω_m and Ω_k for definiteness, but they are entirely negligible compared to the radiation density at the redshift of BBN, $z_{\rm BBN} = 10^9$. Figure 15 shows the constraint on w_0 and w' for the linear evolution model derived from the *WMAP* distance priors, the BAO and SN data, and the BBN prior. The 95% limit on w_0 is

TABLE 12
Amplitude of curvature perturbations, $\mathcal{R}$,
measured by WMAP at $k_{WMAP} = 0.02$ Mpc^{-1}

Model	$10^9 \times \Delta^2_{\mathcal{R}}(k_{WMAP})$
$\Omega_k = 0$ and $w = -1$	2.211 ± 0.083
$\Omega_k \neq 0$ and $w = -1$	2.212 ± 0.084
$\Omega_k = 0$ and $w \neq -1$	2.208 ± 0.087
$\Omega_k \neq 0$ and $w \neq -1$	2.210 ± 0.084
$\Omega_k = 0$, $w = -1$ and $m_\nu > 0$	2.212 ± 0.083
$\Omega_k = 0$, $w \neq -1$ and $m_\nu > 0$	2.218 ± 0.085
WMAP Normalization Prior	2.21 ± 0.09

$-0.32 < 1 + w_0 < 0.14$[47], which is similar to what we have obtained above. Again the upper limit, $1 + w_0 < 0.14$, is robust.

5.5. WMAP normalization prior

So far, we have been mainly using the distance information to constrain the properties of dark energy; however, this is not the only information that one can use to constrain the properties of dark energy. The amplitude of fluctuations is a powerful tool for distinguishing between dark energy and modifications to gravity (Ishak et al. 2006; Koyama & Maartens 2006; Doré et al. 2007; Linder & Cahn 2007; Upadhye 2007; Zhang et al. 2007; Yamamoto et al. 2007; Chiba & Takahashi 2007; Bean et al. 2007; Hu & Sawicki 2007; Song et al. 2007; Daniel et al. 2008; Jain & Zhang 2007; Bertschinger & Zukin 2008; Amin et al. 2007; Hu 2008), as well as for determining the mass of neutrinos (Hu et al. 1998; Lesgourgues & Pastor 2006).

The microwave background observations measure the amplitude of fluctuations at the decoupling epoch. By combining this measurement with the amplitude measured from various low redshift tracers, one can learn more about the dark energy properties and the mass of neutrinos.

The overall amplitude of CMB anisotropy is set by the amplitude of primordial curvature perturbations, $\mathcal{R}$. For example, on very large angular scales where the Sachs–Wolfe limit can be used, the temperature anisotropy is given by $\Delta T/T = -\mathcal{R}/5$ or, in terms of the curvature perturbation during the matter era, Φ, it is given by $\Delta T/T = -\Phi/3$. On small angular scales where the acoustic physics must be taken into account, we have the acoustic oscillation whose amplitude is also given by $\mathcal{R}$.

This motivates our reporting the "WMAP normalization," a measurement of the overall normalization of the curvature perturbations expressed in terms of $\Delta^2_{\mathcal{R}}(k_{WMAP})$, where $\Delta^2_{\mathcal{R}}(k) \equiv k^3 P_{\mathcal{R}}(k)/(2\pi^2)$ is a contribution to the total variance of $\mathcal{R}$, $\langle \mathcal{R}^2 \rangle$, per logarithmic interval of k (see also Eq. [15] and descriptions below it).

Here, k_{WMAP} is different from $k_0 = 0.002$ Mpc^{-1} that we used to define n_s, $dn_s/d\ln k$, r, and $\Delta^2_{\mathcal{R}}(k_0)$ reported in Table 1 or 4. The goal in this subsection is to give the normalization that is *as model independent as possible*.

At $k_0 = 0.002$ Mpc^{-1}, for example, we find $10^9 \Delta^2_{\mathcal{R}}(k_0) = 2.48$, 2.41, and 2.46 for a flat ΛCDM model, a curved ΛCDM model, and a flat ΛCDM model

---

[47] The 68% intervals are $w_0 = -1.09 \pm 0.12$ and $w' = 0.52 \pm 0.46$ (WMAP+BAO+SN+BBN; $\Omega_k = 0$).

---

with massive neutrinos. The scatter between these values comes solely from the fact that $k_0 = 0.002$ Mpc^{-1} is not a right place to define the normalization. In other words, this is not the pivot scale of the WMAP data.

We find that $k_{WMAP} = 0.02$ Mpc^{-1}, i.e., a factor of 10 larger than k_0, gives similar values of $\Delta^2_{\mathcal{R}}(k_{WMAP})$ for a wide range of models, as summarized in Table 12. From these results, we give the WMAP normalization prior:

$$\Delta^2_{\mathcal{R}}(k_{WMAP}) = (2.21 \pm 0.09) \times 10^{-9}, \qquad (72)$$

which is valid for models with $\Omega_k \neq 0$, $w \neq -1$, or $m_\nu > 0$. However, we find that these normalizations cannot be used for the models that have the tensor modes, $r > 0$, or the running index, $dn_s/d\ln k \neq 0$. We failed to find a universal normalization for these models. Nevertheless, our WMAP normalization given by Eq. (72) is still valid for a wide range of cosmological models.

How can one use the WMAP normalization? In order to predict the linear matter density power spectrum, $P_{\mathrm{lin}}(k)$, one needs to relate the primordial curvature perturbations, $\mathcal{R}_{\mathbf{k}}$, to the linear matter density fluctuations at arbitrary redshifts, $\delta_{m,\mathbf{k}}(z)$. From Einstein's equations, we find (see e.g., Appendix C of Takada et al. 2006)

$$\delta_{m,\mathbf{k}}(z) = \frac{2k^3}{5H_0^2\Omega_m} \mathcal{R}_{\mathbf{k}} T(k) D(k,z), \qquad (73)$$

where $D(k,z)$ and $T(k)$ is the linear growth rate and the matter transfer function normalized such that $T(k) \to 1$ as $k \to 0$, and $(1+z)D(k,z) \to 1$ as $k \to 0$ during the matter era (e.g., $z = 30$, where the radiation density is less than 1% of the matter density), respectively. Note that $D(k,z)$ does not depend on k when neutrinos are massless; however, it depends on k when they are massive (e.g., Hu & Eisenstein 1998). The linear matter density power spectrum is given by

$$\frac{k^3 P_{\mathrm{lin}}(k,z)}{2\pi^2} = (2.21 \pm 0.09) \times 10^{-9} \left(\frac{2k^2}{5H_0^2\Omega_m} \right)^2$$
$$\times D^2(k,z) T^2(k) \left(\frac{k}{k_{WMAP}} \right)^{n_s - 1}. \quad (74)$$

One application of the WMAP normalization is the computation of the present-day normalization of matter fluctuations, which is commonly expressed in terms of σ_8, given by

$$\sigma_8^2 = (2.21 \pm 0.09) \times 10^{-9} \left(\frac{2}{5\Omega_m} \right)^2$$
$$\times \int \frac{dk}{k} D^2(k, z=0) T^2(k) \frac{k^4}{H_0^4} \left(\frac{k}{k_{WMAP}} \right)^{n_s - 1}$$
$$\times \left[\frac{3\sin(kR)}{(kR)^3} - \frac{3\cos(kR)}{(kR)^2} \right]^2, \qquad (75)$$

where $R = 8\ h^{-1}$Mpc. Both the dark energy properties (or modified gravity) and the mass of neutrinos change the value of $D(k, z=0)$. The transfer function, $T(k)$, is much less affected, as long as neutrinos were still relativistic at the decoupling epoch, and the dark energy or modified gravity effect was unimportant at the decoupling epoch.

Ignoring the mass of neutrinos and modifications to gravity, one can obtain the growth rate by solving the
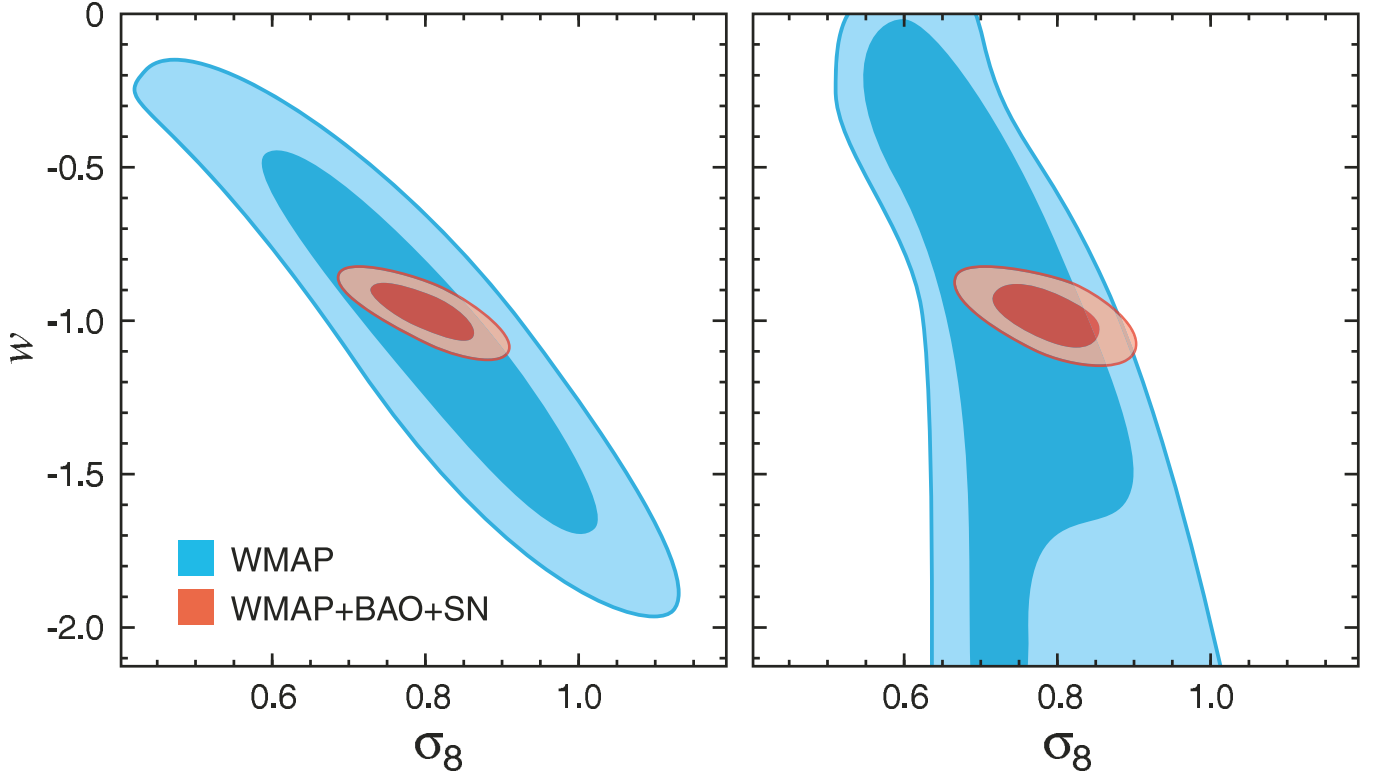
FIG. 16.— Predictions for the present-day amplitude of matter fluctuations, σ_8, as a function of the (constant) dark energy equation of state parameter, w, derived from the full *WMAP* data (blue) as well as from WMAP+BAO+SN (red). The contours show the 68% and 95% CL. (*Left*) Flat universe, $\Omega_k = 0$. (*Right*) Curved universe, $\Omega_k \neq 0$.

following differential equation (Wang & Steinhardt 1998; Linder & Jenkins 2003):

$$\frac{d^2g}{d\ln a^2} + \left[\frac{5}{2} + \frac{1}{2}\left(\Omega_k(a) - 3w_{\text{eff}}(a)\Omega_{de}(a)\right)\right]\frac{dg}{d\ln a}$$

$$+ \left[2\Omega_k(a) + \frac{3}{2}(1 - w_{\text{eff}}(a))\Omega_{de}(a)\right]g(a) = 0, \quad (76)$$

where

$$g(a) \equiv \frac{D(a)}{a} = (1 + z)D(z), \quad (77)$$

$$\Omega_k(a) \equiv \frac{\Omega_k H_0^2}{a^2 H^2(a)}, \quad (78)$$

$$\Omega_{de}(a) \equiv \frac{\Omega_\Lambda H_0^2}{a^{3[1+w_{\text{eff}}(a)]} H^2(a)}, \quad (79)$$

$$w_{\text{eff}}(a) \equiv \frac{1}{\ln a} \int_0^{\ln a} d\ln a' \; w(a'). \quad (80)$$

During the matter era, $g(a)$ does not depend on a; thus, the natural choice for the initial conditions are $g(a_{\text{initial}}) = 1$ and $dg/d\ln a|_{a=a_{\text{initial}}} = 0$, where a_{initial} must be taken during the matter era, e.g., $a_{\text{initial}} = 1/31$ (i.e., $z = 30$).

In Fig. 16 we show the predicted values of σ_8 as a function of w in a flat universe (left panel) and curved universes (right panel). (See the middle panel of Fig. 17 for σ_8 as a function of the mass of neutrinos.) Here, we have used the full information in the *WMAP* data. The normalization information alone is unable to give meaningful predictions for σ_8, which depends not only on $\Delta_\mathcal{R}^2(k_{WMAP})$, but also on the other cosmological parameters via $T(k)$ and $D(k, z = 0)$, especially w and $\Omega_m h^2$.

While the predictions from the *WMAP* data alone are still weak, adding the extra distance information from the BAO and SN data helps improve the predictions. We find $\sigma_8 = 0.799^{+0.044}_{-0.043}$ for a flat universe, and $\sigma_8 = 0.788^{+0.045}_{-0.044}$ for curved universes.

By combining these results with σ_8 measured from various low redshift tracers, one can break the remaining degeneracy between w and σ_8 to obtain a better limit on w. The precision of the current data from weak lensing surveys is comparable to these predictions, e.g., $\sigma_8(\Omega_m/0.25)^{0.64} = 0.785 \pm 0.043$ (Canada-France-Hawaii Telescope Legacy Survey (CFHTLS); Hoekstra et al. 2006). The weak lensing surveys will soon become powerful enough to yield smaller uncertainties in σ_8 than predicted from WMAP+BAO+SN.

6. NEUTRINOS

In this section, we shall use the *WMAP* data, combined with the distance information from BAO and SN observations, to place limits on the total mass of massive neutrino species (§ 6.1), as well as on the effective number of neutrino-like species that were still relativistic at the decoupling epoch (§ 6.2)

6.1. *Neutrino Mass*

6.1.1. *Motivation*

The existence of non-zero neutrino masses has been established firmly by the experiments detecting atmospheric neutrinos (Hirata et al. 1992; Fukuda et al. 1994, 1998; Allison et al. 1999; Ambrosio et al. 2001), solar neutrinos (Davis et al. 1968; Cleveland et al. 1998; Hampel et al. 1999; Abdurashitov et al. 1999; Fukuda et al. 2001b,a; Ahmad et al. 2002; Ahmed et al. 2004), reactor

neutrinos (Eguchi et al. 2003; Araki et al. 2005), and accelerator beam neutrinos (Ahn et al. 2003; Michael et al. 2006). These experiments have placed stringent limits on the squared mass *differences* between the neutrino mass eigenstates: $\Delta m_{21}^2 \simeq 8 \times 10^{-5}$ eV^2 from the solar and reactor experiments, and $\Delta m_{32}^2 \simeq 3 \times 10^{-3}$ eV^2 from the atmospheric and accelerator beam experiments.

One needs different experiments to measure the *absolute* masses. The next-generation tritium β-decay experiment, KATRIN[48], is expected to reach the electron neutrino mass of as small as ~ 0.2 eV. Cosmology has also been providing useful limits on the mass of neutrinos (see Dolgov 2002; Elgaroy & Lahav 2005; Tegmark 2005; Lesgourgues & Pastor 2006; Fukugita 2006; Hannestad 2006b, for reviews). Since the determination of the neutrino mass is of fundamental importance in physics, there is enough motivation to pursue cosmological constraints on the neutrino mass.

How well can CMB constrain the mass of neutrinos? We do not expect massive neutrinos to affect the CMB power spectra very much (except through the gravitational lensing effect), if they were still relativistic at the decoupling epoch, $z \simeq 1090$. This means that, for massive neutrinos to affect the CMB power spectra, *at least* one of the neutrino masses must be greater than the mean energy of relativistic neutrinos per particle at $z \simeq 1090$ when the photon temperature of the universe was $T_\gamma \simeq 3000$ K $\simeq 0.26$ eV. Since the mean energy of relativistic neutrinos is given by $\langle E \rangle = (7\pi^4 T_\nu)/(180\zeta(3)) \simeq 3.15 T_\nu = 3.15(4/11)^{1/3} T_\gamma$, we need *at least* one neutrino species whose mass satisfies $m_\nu > 3.15(4/11)^{1/3} T_\gamma \simeq 0.58$ eV; thus, it would not be possible to constrain the neutrino mass using the CMB data alone, if the mass of the heaviest neutrino species is below this value.

If the neutrino mass eigenstates are degenerate with the effective number of species equal to 3.04, this argument suggests that $\sum m_\nu \sim 1.8$ eV would be the limit to which the CMB data are sensitive. Ichikawa et al. (2005) argue that $\sum m_\nu \sim 1.5$ eV would be the limit for the CMB data alone, which is fairly close to the value given above.

In order to go beyond ~ 1.5 eV, therefore, one needs to combine the CMB data with the other cosmological probes. We shall combine the *WMAP* data with the distance information from BAO and SN to place a limit on the neutrino mass. We shall not use the galaxy power spectrum in this paper, and therefore our limit on the neutrino mass is free from the uncertainty in the galaxy bias. We discuss this in more detail in the Analysis section below.

6.1.2. *Analysis*

We assume that, for definiteness, the neutrino mass eigenstates are *degenerate*, which means that all of the three neutrino species have equal masses.[49] We measure

the neutrino mass density parameter, $\Omega_\nu h^2$, and convert it to the total mass, $\sum m_\nu$, via

$$\sum m_\nu \equiv N_\nu m_\nu = 94 \text{ eV}(\Omega_\nu h^2), \qquad (81)$$

where N_ν is the number of massive neutrino species. We take it to be 3.04. Note that in this case the mass density parameter is the sum of baryons, CDM, and neutrinos: $\Omega_m = \Omega_b + \Omega_c + \Omega_\nu$.

Since the release of the 1-year (Spergel et al. 2003) and 3-year (Spergel et al. 2007) results on the cosmological analysis of the *WMAP* data, there have been a number of studies with regard to the limits on the mass of neutrinos (Hannestad 2003; Elgarøy & Lahav 2003; Allen et al. 2003; Tegmark et al. 2004a; Barger et al. 2004; Hannestad & Raffelt 2004; Crotty et al. 2004; Seljak et al. 2005a,b; Ichikawa et al. 2005; Hannestad 2005; Lattanzi et al. 2005; Hannestad & Raffelt 2006; Goobar et al. 2006; Feng et al. 2006; Lesgourgues et al. 2007). These analyses reached different limits depending upon (1) the choice of data sets and (2) the parameters in the cosmological model.

The strongest limits quoted on neutrino masses come from combining CMB measurements with measurements of the amplitude of density fluctuations in the recent universe. Clustering of galaxies and Lyα forest observations have been used to obtain some of the strongest limits on neutrino masses (Seljak et al. 2005b; Seljak et al. 2006; Viel et al. 2006). As the neutrino mass increases, the amplitude of mass fluctuations on small scales decreases (Bond et al. 1980; Bond & Szalay 1983; Ma 1996, see also the middle panel of Fig. 17), which can be used to weigh neutrinos in the universe (Hu et al. 1998; Lesgourgues & Pastor 2006).

These analyses are sensitive to correctly calculating the relationship between the level of observed fluctuations in galaxies (or gas) and the mass fluctuation with the strongest limits coming from the smallest scales in the analyses. With the new *WMAP* data, these limits are potentially even stronger. There are, however, several potential concerns with this limit: there is already "tension" between the high level of fluctuations seen in the Lyman alpha forest and the amplitude of mass fluctuations inferred from *WMAP* (Lesgourgues et al. 2007); the relationship between gas temperature and density appears to be more complicated than assumed in the previous Lyα forest analysis (Kim et al. 2007; Bolton et al. 2007); and additional astrophysics could potentially be the source of some of the small scale fluctuations seen in the Lyα forest data. Given the power of the Lyα forest data, it is important to address these issues; however, they are beyond the scope of this paper.

In this paper, we take the more conservative approach and use only the *WMAP* data and the distance measures to place limits on the neutrino masses. Our approach is more conservative than Goobar et al. (2006), who have found a limit of 0.62 eV on the sum of the neutrino mass from the *WMAP* 3-year data, the SDSS-LRG BAO measurement, the SNLS supernova data, and the shape of the galaxy power spectra from the SDSS main sample and 2dFGRS. While we use the *WMAP* 5-year data, the SDSS+2dFGRS BAO measurements, and HST+SNLS+ESSENCE supernova data, we do not use the shape of the galaxy power spectra. See § 2.2 in this
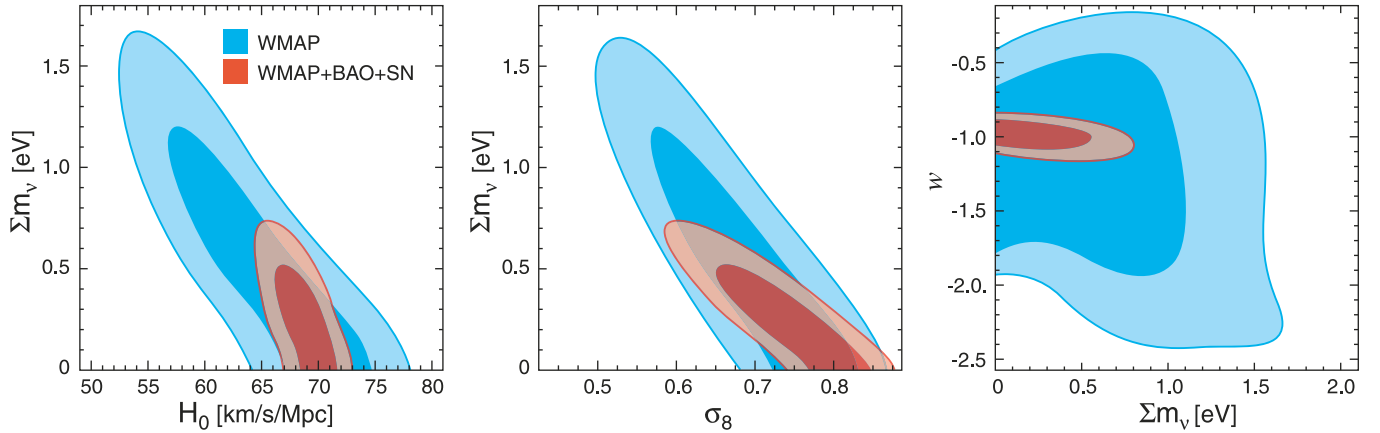
---

[48] http://www-ik.fzk.de/~katrin
[49] While the current cosmological data are not yet sensitive to the mass of *individual* neutrino species, i.e., the mass hierarchy, this situation may change in the future, with high-z galaxy redshift surveys or weak lensing surveys (Takada et al. 2006; Slosar 2006; Hannestad & Wong 2007; Kitching et al. 2008; Abdalla & Rawlings 2007).

FIG. 17.— Constraint on the total mass of neutrinos, $\sum m_\nu$ (§ 6.1.3). In all panels we show the WMAP-only results in blue and WMAP+BAO+SN in red. (*Left*) Joint two-dimensional marginalized distribution of H_0 and $\sum m_\nu$ (68% and 95% CL). The additional distance information from BAO helps reduce the degeneracy between H_0 and $\sum m_\nu$. (*Middle*) The *WMAP* data, combined with the distances from BAO and SN, predict the present-day amplitude of matter fluctuations, σ_8, as a function of $\sum m_\nu$. An independent determination of σ_8 will help determine $\sum m_\nu$ tremendously. (*Right*) Joint two-dimensional marginalized distribution of w and $\sum m_\nu$. No significant degeneracy is observed. Note that we have a prior on w, $w > -2.5$, and thus the WMAP-only lower limit on w in this panel cannot be trusted.

paper or Dunkley et al. (2008) for more detail on this choice.

In summary, we do not use the amplitude or shape of the matter power spectrum, but rely exclusively on the CMB data and the distance measurements. As a result our limits are weaker than the strongest limits in the literature.

Next, let us discuss (2), the choice of parameters. A few degeneracies between the neutrino mass and other cosmological parameters have been identified. Hannestad (2005) has found that the limit on the neutrino mass degrades significantly when the dark energy equation of state, w, is allowed to vary (see also Fig. 18 of Spergel et al. 2007). This degeneracy would arise only when the amplitude of the galaxy or Lyα forest power spectrum was included, as the dark energy equation of state influences the growth rate of the structure formation. Since we do not include them, our limit on the neutrino mass is not degenerate with w. We shall come back to this point later in the Results section. Incidentally, our limit is not degenerate with the running index, $dn_s/d\ln k$, or the tensor-to-scalar ratio, r.

6.1.3. *Results*

Figure 17 summarizes our limits on the sum of neutrino masses, $\sum m_\nu$.

With the *WMAP* data alone we find $\sum m_\nu < 1.3$ eV (95% CL) for the ΛCDM model in which $w = -1$, and $\sum m_\nu < 1.5$ eV (95% CL) for $w \neq -1$. (We assume a flat universe in both cases.) These constraints are very similar, which means that w and $\sum m_\nu$ are not degenerate. We show this more explicitly on the right panel of Fig. 17.

When the BAO and SN data are added, our limits improve significantly, by a factor 2, to $\sum m_\nu < 0.61$ eV (95% CL) for $w = -1$, and $\sum m_\nu < 0.66$ eV (95% CL) for $w \neq -1$. Again, we do not observe much degeneracy between w and $\sum m_\nu$. While the distances out to *either* BAO or SN cannot break degeneracy between Ω_m (or H_0) and w, a combination of the two can break this degeneracy effectively, leaving little degeneracy left on the right panel of Fig. 17.

What information do BAO and SN add to improve the

limit on $\sum m_\nu$? It's the Hubble constant, H_0, as shown in the left panel of Fig. 17. This effect has been explained by Ichikawa et al. (2005) as follows.

The massive neutrinos modify the CMB power spectrum by their changing the matter-to-radiation ratio at the decoupling epoch. If the sum of degenerate neutrino masses is below 1.8 eV, the neutrinos were still relativistic at the decoupling epoch. However, *they are definitely non-relativistic at the present epoch*, as the neutrino oscillation experiments have shown that at least one neutrino species is heavier than 0.05 eV. This means that the Ω_m that we measure must be the sum of Ω_b, Ω_c, and Ω_ν; however, at the decoupling epoch, neutrinos were still relativistic, and thus the matter density at the decoupling epoch was actually smaller than a naive extrapolation from the present value.

As the matter-to-radiation ratio was smaller than one would naively expect, it would accelerate the decay of gravitational potential around the decoupling epoch. This leads to an enhancement in the so-called early integrated Sachs–Wolfe (ISW) effect. The larger $\sum m_\nu$ is, the larger early ISW becomes, as long as the neutrinos were still relativistic at the decoupling epoch, i.e., $\sum m_\nu \lesssim 1.8$ eV.

The large ISW causes the first peak position to shift to lower multipoles by adding power at $l \sim 200$; however, this shift can be absorbed by a reduction in the value of H_0.[50] This is why $\sum m_\nu$ and H_0 are anti-correlated (see Ichikawa et al. 2005, for a further discussion on this subject).

It is the BAO distance that provides a better limit on H_0, as BAO is an absolute distance indicator. The SN is totally insensitive to H_0, as their absolute magnitudes have been marginalized over (SN is a relative distance indicator); however, the SN data do help break the degeneracy between w and H_0 when w is allowed to vary.

---

[50] This is similar to what happens to the curvature constraint from the CMB data alone. A positive curvature model, $\Omega_k < 0$, shifts the acoustic peaks to lower multipoles; however, this shift can be absorbed by a reduction in the value of H_0. As a result, a closed universe with $\Omega_k \sim -0.3$ and $\Omega_\Lambda \sim 0$ is still a good fit, if Hubble's constant is as low as $H_0 \sim 30$ km/s/Mpc (Spergel et al. 2007).

As a result, we have equally tight limits on $\sum m_\nu$ regardless of w.

Our limit, $\sum m_\nu < 0.61$ eV (95% CL) (for $w = -1$), is weaker than the best limit quoted in the literature, as we have not used the information on the amplitude of fluctuations traced by the large-scale structure. The middle panel of Fig. 17 shows how the *WMAP* data combined with BAO and SN predict the present-day amplitude of matter fluctuations, σ_8, as a function of $\sum m_\nu$. From this it is clear that an accurate, *independent* measurement of σ_8 will break the degeneracy between σ_8 and $\sum m_\nu$, and provide a significant improvement in the limit on $\sum m_\nu$.

Improving upon our understanding of non-linear astrophysical effects such as those raised by Bolton et al. (2007) for the Lyα forest data and Sanchez & Cole (2007) for the SDSS and 2dFGRS data is a promising way to improve upon the numerical value of the limit, as well as the robustness of the limit, on the mass of neutrinos.

6.2. *Effective number of neutrino species*

6.2.1. *Motivation*

While the absolute mass of neutrinos is unknown, the number of neutrino species is well known: it's three. The high precision measurement of the decay width of Z into neutrinos (the total decay width minus the decay width to quarks and charged leptons), carried out by LEP using the production of Z in e^+e^- collisions, has yielded $N_\nu = 2.984 \pm 0.008$ (Yao et al. 2006). However, are there any *other* particles that we do not know yet, and that were relativistic at the photon decoupling epoch?

Such extra relativistic particle species can change the expansion rate of the universe during the radiation era. As a result, they change the predictions from the Big Bang Nucleosynthesis (BBN) for the abundance of light elements such as helium and deuterium (Steigman et al. 1977). One can use this property to place a tight bound on the relativistic degrees of freedom, expressed in terms of the "effective number of neutrino species," $N_{\rm eff}$ (see Eq. [84] below for the precise definition). As the BBN occurred at the energy of ~ 0.1 MeV, which is later than the neutrino decoupling epoch immediately followed by e^+e^- annihilation, the value of $N_{\rm eff}$ for 3 neutrino species is slightly larger than 3. With other subtle corrections included, the current standard value is $N_{\rm eff}^{\rm standard} = 3.04$ (Dicus et al. 1982; Gnedin & Gnedin 1998; Dolgov et al. 1999; Mangano et al. 2002). The 2σ interval for $N_{\rm eff}$ from the observed helium abundance, $Y_P = 0.240 \pm 0.006$, is $1.61 < N_{\rm eff} < 3.30$ (see Steigman 2007, for a recent summary).

Many people have been trying to find evidence for the extra relativistic degrees of freedom in the universe, using the cosmological probes such as CMB and the large-scale structure (Pierpaoli 2003; Hannestad 2003; Crotty et al. 2003, 2004; Barger et al. 2003; Trotta & Melchiorri 2005; Lattanzi et al. 2005; Hannestad 2006a; Ichikawa et al. 2007; Mangano et al. 2007; Hamann et al. 2007; de Bernardis et al. 2007). There is a strong motivation to seek the answer for the following question, "can we detect the cosmic neutrino background, and confirm that the signal is consistent with the expected number of neutrino species that we know?" Although we cannot detect the cosmic neutrino background directly yet, there is a possibility that we can detect it indirectly by looking for the signatures of neutrinos in the CMB power spectrum.

In this section we shall revisit this classical problem by using the *WMAP* 5-year data as well as the distance information from BAO and SN, and Hubble's constant measured by HST.

6.2.2. *Analysis*

It is common to write the energy density of neutrinos (including anti-neutrinos), when they were still relativistic, in terms of the effective number of neutrino species, $N_{\rm eff}$, as

$$\rho_\nu = N_{\rm eff} \frac{7\pi^2}{120} T_\nu^4, \tag{82}$$

where T_ν is the temperature of neutrinos. How do we measure $N_{\rm eff}$ from CMB?

The way that we use CMB to determine $N_{\rm eff}$ is relatively simple. The relativistic particles that stream freely influence CMB in two ways: (1) their energy density changing the matter-radiation equality epoch, and (2) their anisotropic stress acting as an additional source for the gravitational potential via Einstein's equations. Incidentally, the relativistic particles that *do not* stream freely, but interact with matter frequently, do not have a significant anisotropic stress because they isotropize themselves via interactions with matter; thus, anisotropic stress of photons before the decoupling epoch was very small. Neutrinos, on the other hand, decoupled from matter much earlier (~ 2 MeV), and thus their anisotropic stress was significant at the decoupling epoch.

The amount of the early ISW effect changes as the equality redshift changes. The earlier the equality epoch is, the more the ISW effect CMB photons receive. This effect can be measured via the height of the third acoustic peak relative to the first peak. Therefore, the equality redshift, $z_{\rm eq}$, is one of the fundamental observables that one can extract from the CMB power spectrum.

One usually uses $z_{\rm eq}$ to determine $\Omega_m h^2$ from the CMB power spectrum, without noticing that it is actually $z_{\rm eq}$ that they are measuring. However, the conversion from $z_{\rm eq}$ to $\Omega_m h^2$ is automatic only when one knows the radiation content of the universe exactly – in other words, when one knows $N_{\rm eff}$ exactly:

$$1 + z_{\rm eq} = \frac{\Omega_m}{\Omega_r} = \frac{\Omega_m h^2}{\Omega_\gamma h^2} \frac{1}{1 + 0.2271 N_{\rm eff}}, \tag{83}$$

where $\Omega_\gamma h^2 = 2.469 \times 10^{-5}$ is the present-day photon energy density parameter for $T_{\rm cmb} = 2.725$ K. Here, we have used the standard relation between the photon temperature and neutrino temperature, $T_\nu = (4/11)^{1/3} T_\gamma$, derived from the entropy conservation across the electron-positron annihilation (see, e.g., Weinberg 1972; Kolb & Turner 1990).

However, if we do not know $N_{\rm eff}$ precisely, it is not possible to use $z_{\rm eq}$ to measure $\Omega_m h^2$. In fact, we lose our ability to measure $\Omega_m h^2$ from CMB almost completely if we do not know $N_{\rm eff}$. Likewise, if we do not know $\Omega_m h^2$ precisely, it is not possible to use $z_{\rm eq}$ to measure $N_{\rm eff}$. As a result, $N_{\rm eff}$ and $\Omega_m h^2$ are linearly correlated (degenerate), with the width of the degeneracy line given by the uncertainty in our determination of $z_{\rm eq}$.

The distance information from BAO and SN provides us with an independent constraint on $\Omega_m h^2$, which helps to reduce the degeneracy between $z_{\rm eq}$ and $\Omega_m h^2$.
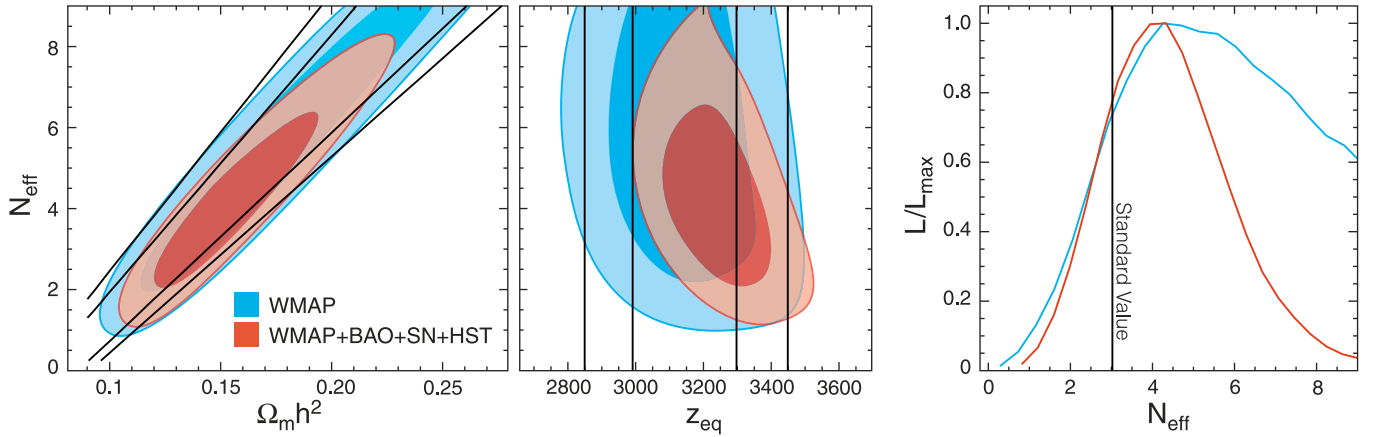
FIG. 18.— Constraint on the effective number of neutrino species, $N_{\rm eff}$ (§ 6.2.3). Note that we have imposed a prior on $N_{\rm eff}$, $0 < N_{\rm eff} < 10$. In all panels we show the WMAP-only results in blue and WMAP+BAO+SN in red. (*Left*) Joint two-dimensional marginalized distribution (68% and 95% CL), showing a strong degeneracy between $\Omega_m h^2$ and $N_{\rm eff}$. This degeneracy line is given by the equality redshift, $1 + z_{\rm eq} = \Omega_m/\Omega_r = (4.050 \times 10^4)\Omega_m h^2/(1 + 0.2271N_{\rm eff})$. The thick solid lines show the 68% and 95% limits calculated from the WMAP-only limit on $z_{\rm eq}$: $z_{\rm eq} = 3141^{+154}_{-157}$ (68% CL). The 95% CL contours do not follow the lines below $N_{\rm eff} \sim 1.5$ but close there, which shows a strong evidence for the cosmic neutrino background from its effects on the CMB power spectrum via the neutrino anisotropic stress. The BAO and SN provide an independent constraint on $\Omega_m h^2$, which helps reduce the degeneracy between $N_{\rm eff}$ and $\Omega_m h^2$. (*Middle*) When we transform the horizontal axis of the left panel to $z_{\rm eq}$, we observe no degeneracy. The vertical solid lines show the one-dimensional marginalized 68% and 95% distribution calculated from the WMAP-only limit on $z_{\rm eq}$: $z_{\rm eq} = 3141^{+154}_{-157}$ (68% CL). Therefore, the left panel is simply a rotation of this panel using a relation between $z_{\rm eq}$, $\Omega_m h^2$, and $N_{\rm eff}$. (*Right*) One-dimensional marginalized distribution of $N_{\rm eff}$ from WMAP-only and WMAP+BAO+SN+HST. Note that a gradual decline of the likelihood toward $N_{\rm eff} \gtrsim 6$ for the WMAP-only constraint should not be trusted, as it is affected by the hard prior, $N_{\rm eff} < 10$. The WMAP+BAO+SN+HST constraint is robust. This figure shows that the lower limit on $N_{\rm eff}$ is coming solely from the *WMAP* data. The 68% interval from WMAP+BAO+SN+HST, $N_{\rm eff} = 4.4 \pm 1.5$, is consistent with the standard value, 3.04, which is shown by the vertical line.

The anisotropic stress of neutrinos also leaves distinct signatures in the CMB power spectrum, which is not degenerate with $\Omega_m h^2$ (Hu et al. 1995; Bashinsky & Seljak 2004). Trotta & Melchiorri (2005) (see also Melchiorri & Serra 2006) have reported on evidence for the neutrino anisotropic stress at slightly more than 95% CL. They have parametrized the anisotropic stress by the viscosity parameter, $c^2_{\rm vis}$ (Hu 1998), and found $c^2_{\rm vis} > 0.12$ (95% CL). However, they had to combine the *WMAP* 1-year data with the SDSS data to see the evidence for non-zero $c^2_{\rm vis}$.

In Dunkley et al. (2008) we report on the lower limit to $N_{\rm eff}$ solely from the *WMAP* 5-year data. In this paper we shall combine the *WMAP* data with the distance information from BAO and SN as well as Hubble's constant from HST to find the best-fitting value of $N_{\rm eff}$.

6.2.3. *Results*

Figure 18 shows our constraint on $N_{\rm eff}$. The contours in the left panel lie on the expected linear correlation between $\Omega_m h^2$ and $N_{\rm eff}$ given by

$$N_{\rm eff} = 3.04 + 7.44 \left(\frac{\Omega_m h^2}{0.1308} \frac{3139}{1 + z_{\rm eq}} - 1 \right), \quad (84)$$

which follows from equation (83). (Here, $\Omega_m h^2 = 0.1308$ and $z_{\rm eq} = 3138$ are the maximum likelihood values from the simplest ΛCDM model.) The width of the degeneracy line is given by the accuracy of our determination of $z_{\rm eq}$, which is given by $z_{\rm eq} = 3141^{+154}_{-157}$ (WMAP-only) for this model. Note that the mean value of $z_{\rm eq}$ for the simplest ΛCDM model with $N_{\rm eff} = 3.04$ is $z_{\rm eq} = 3176^{+151}_{-150}$, which is close. This confirms that $z_{\rm eq}$ is one of the fundamental observables, and $N_{\rm eff}$ is merely a secondary parameter that can be derived from $z_{\rm eq}$. The middle panel of Fig. 18 shows this clearly: $z_{\rm eq}$ is determined independently of $N_{\rm eff}$. For each value of $N_{\rm eff}$ along a constant $z_{\rm eq}$

line, there is a corresponding $\Omega_m h^2$ that gives the same value of $z_{\rm eq}$ along the line.

However, the contours do not extend all the way down to $N_{\rm eff} = 0$, although equation (84) predicts that $N_{\rm eff}$ should go to zero when $\Omega_m h^2$ is sufficiently small. This indicates that we are seeing the effect of the neutrino anisotropic stress at a high significance. While we need to repeat the analysis of Trotta & Melchiorri (2005) in order to prove that our finding of $N_{\rm eff} > 0$ comes from the neutrino anisotropic stress, we believe that there is a strong evidence that we see non-zero $N_{\rm eff}$ via the effect of neutrino anisotropic stress, rather than via $z_{\rm eq}$.

While the *WMAP* data alone can give a lower limit on $N_{\rm eff}$ (Dunkley et al. 2008), they cannot give an upper limit owing to the strong degeneracy with $\Omega_m h^2$. Therefore, we use the BAO, SN, and HST data to break the degeneracy. We find $N_{\rm eff} = 4.4 \pm 1.5$ (68%) from WMAP+BAO+SN+HST, which is fully consistent with the standard value, 3.04 (see the right panel of Fig. 18).

7. CONCLUSION

With 5 years of integration, the *WMAP* temperature and polarization data have improved significantly. An improved determination of the third acoustic peak has enabled us to reduce the uncertainty in the amplitude of matter fluctuation, parametrized by σ_8, by a factor of 1.4 from the *WMAP* 3-year result. The E-mode polarization is now detected at 5 standard deviations (c.f., 3.0 standard deviations for the 3-year data; Page et al. 2007), which rules out an instantaneous reionization at $z_{\rm reion} = 6$ at the 3.5σ level. Overall, the *WMAP* 5-year data continue to support the simplest, 6-parameter ΛCDM model (Dunkley et al. 2008).

In this paper, we have explored our ability to limit deviations from the simplest picture, namely, non-Gaussianity, non-adiabatic fluctuations, non-zero grav-
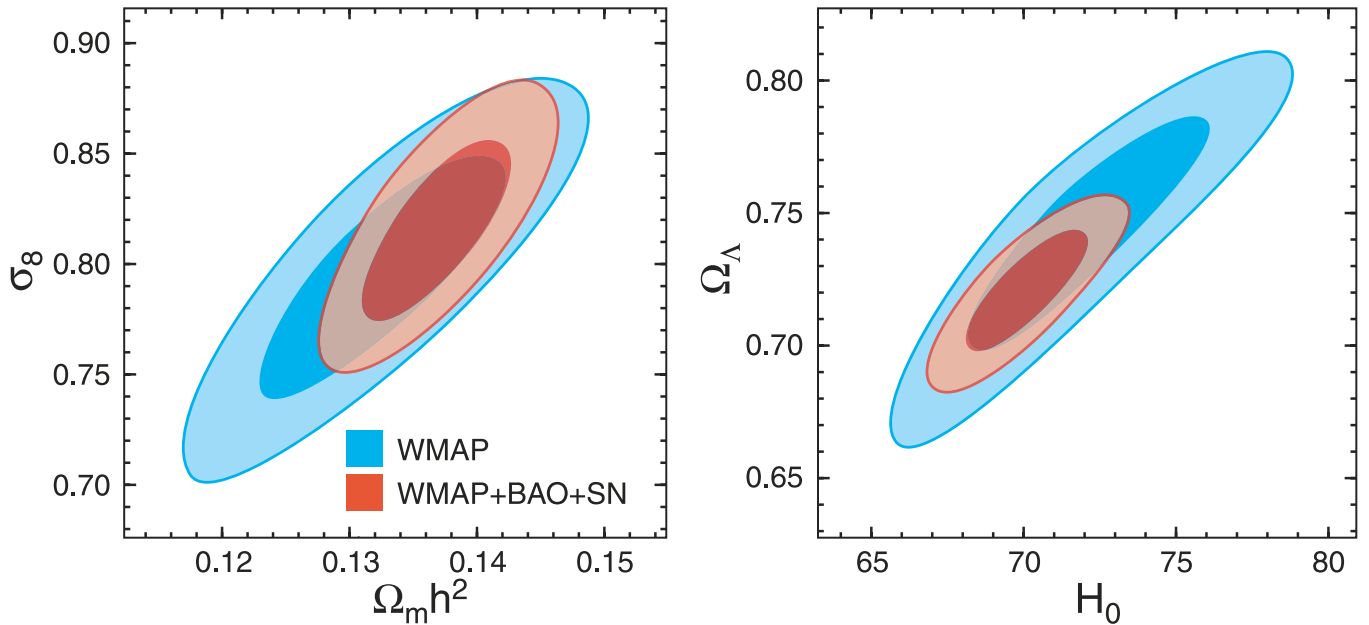
FIG. 19.— Four representative cosmological parameters that have improved significantly by adding the BAO and SN data. (See also Table 1.) The contours show the 68% and 95% CL. The WMAP-only constraint is shown in blue, while WMAP+BAO+SN in red. (*Left*) The distance information from BAO and SN provides a better determination of $\Omega_m h^2$, which results in 40% better determination of σ_8. (*Right*) The BAO data, being the absolute distance indicator, provides a better determination of H_0, which results in a factor of 2 better determination of Ω_Λ, Ω_b, and Ω_c.

itational waves, non-power-law spectrum, non-zero curvature, dynamical dark energy, parity-violating interactions, non-zero neutrino mass, and non-standard number of neutrino species. Detection of any of these items will lead us immediately to the new era in cosmology, and a better understanding of the physics of our universe.

From these studies, we conclude that we have not detected any convincing deviations from the simplest 6-parameter ΛCDM model at the level greater than 99% CL. By combining *WMAP* data with the distance information from BAO and SN, we have improved the accuracy of the derived cosmological parameters. As the distance information provides strong constraints on the matter density (both BAO and SN) and Hubble's constant (BAO), the uncertainties in $\Omega_m h^2$ and H_0 have been reduced by a factor of 1.7 and 2, respectively, from the WMAP-only limits. The better determination of H_0 reduces the uncertainty in Ω_Λ (as well as Ω_b and Ω_c) by a factor of 2, and the better determination of $\Omega_m h^2$ reduces the uncertainty in σ_8 by a factor of 1.4. These results are presented visually in Fig. 19. See also Table 1 for the summary of the cosmological parameters of the ΛCDM model. The addition of BAO and SN does not improve determinations of $\Omega_b h^2$ or τ as expected. Since n_s is mainly degenerate with $\Omega_b h^2$ and τ, with the former being more degenerate, the addition of BAO and SN does not improve our determination of n_s, when we consider the simplest 6-parameter ΛCDM model.

To find the limits on various deviations from the simplest model, we have explored the parameter space by combining the *WMAP* 5-year data with the distance measurements from the Baryon Acoustic Oscillations (BAO) and Type Ia supernova (SN) observations. Here, we summarize significant findings from our analysis (see also Table 2):

- *Gravitational waves and primordial power spec-*

trum: Improved simultaneous constraint on the amplitude of primordial gravitational waves and the shape of the primordial power spectrum (from WMAP+BAO+SN). In terms of the tensor-to-scalar ratio, r, we have found $r < 0.20$ (95% CL), which is the tightest bound to date. A blue primordial spectrum index, $n_s > 1$, now begins to be disfavoured even in the presence of gravitational waves, $0.0014 < 1 - n_s < 0.0608$ (95% CL). We find no evidence for the running index, $dn_s/d\ln k$. The parameter space allowed for inflation models has shrunk significantly since the 3-year data release (§ 3.3), most notably for models that produce significant gravitational waves, such as chaotic or power-law inflation models, and models that produce $n_s > 1$, such as hybrid inflation models.

- *Dark energy and curvature*: Improved simultaneous constraint on the dark energy equation of state, w, and the spatial curvature of the universe, Ω_k (from WMAP+BAO+SN). We find $-0.0175 < \Omega_k < 0.0085$ (95% CL) and $-0.11 < 1 + w < 0.14$ (95% CL). The curvature radius of the universe should be greater than $R_{\rm curv} > 23$ and $33 \ h^{-1}{\rm Gpc}$ for positive and negative curvature, respectively. The combination of *WMAP*, BAO, and SN is particularly powerful for constraining w and Ω_k simultaneously.

- *Time-dependent equation of state*: Using the *WMAP* distance priors (l_A, R, z_*) combined with the BAO and SN distance data, we have constrained time-dependent w. The present-day value of w, w_0, is constrained as $-0.38 < 1 + w_0 < 0.14$ (95% CL), for a flat universe. Our upper limit on w_0 and lower limit on the derivative of w, w', are better than the previous limits from the *WMAP* 3-year data by a factor of about two.

- *Non-Gaussianity*: Improved constraints on primordial non-Gaussianity parameters, $-9 < f_{NL}^{\text{local}} < 111$ and $-151 < f_{NL}^{\text{equil}} < 253$ (95% CL), from the *WMAP* temperature data. The Gaussianity tests show that the primordial fluctuations are Gaussian to the 0.1% level, which provides the strongest evidence for the quantum origin of the primordial fluctuations.

- *Non-adiabaticity*: Improved constraints on non-adiabatic fluctuations. The photon and matter fluctuations are found to obey the adiabatic relation to 8.6% and 2.0% for axion- and curvaton-type non-adiabatic fluctuations, respectively.

- *Parity violation*: *WMAP*'s limits on the TB and EB correlations indicate that parity-violating interactions that couple to photons could not have rotated the polarization angle by more than $-5.9° < \Delta\alpha < 2.4°$ between the decoupling epoch and present epoch.

- *Neutrino mass*: With the *WMAP* data combined with the distance information from BAO and SN, we find a limit on the neutrino mass, $\sum m_\nu < 0.61$ eV (95% CL), which is better than the WMAP-only limit by a factor of 2, owing to an additional constraint on H_0 provided by BAO. The limit does not get worse very much even when w is allowed to vary, as the SN data break degeneracy between H_0 and w effectively. Since we rely only on the CMB data and distance information, our limit is not sensitive to our understanding of non-linear astrophysical effects in the large-scale structure data.

- *Number of neutrino species*: With the *WMAP* data alone we find evidence for non-zero N_{eff} (Dunkley et al. 2008), which is likely coming from our measurement of the effect of neutrino anisotropic stress on the CMB power spectrum. With the BAO, SN, and HST added, we break the degeneracy between $\Omega_m h^2$ and N_{eff}, and find $N_{\text{eff}} = 4.4 \pm 1.5$ (68% CL) and $1.9 < N_{\text{eff}} < 7.8$ (95% CL), which are consistent with the standard value, $N_{\text{eff}} = 3.04$; thus, we do not find any evidence for the extra relativistic species in the universe.

The limits that we have obtained from our analysis in this paper are already quite stringent; however, we emphasize that they should still be taken as a prototype of what we can achieve in the future, including more integration of the *WMAP* observations.

A smaller noise level in the temperature data will reduce the uncertainty in non-Gaussianity parameters. An improved determination of the TE spectrum increases our sensitivity to non-adiabatic fluctuations as well as to the primordial gravitational waves. The E-mode polarization will be more dominated by the signal, to the point where we begin to constrain the detailed history of the reionization of the universe beyond a simple parametrization. Our limit on the B-mode polarization continues to improve, which will provide us with a better understanding of the polarized foreground. The improved TB and EB correlations will provide better limits on the cosmological birefringence.

While we have chosen to combine the *WMAP* data mainly with the distance indicators, one should be able to put even more stringent limits on important parameters such as r, n_s, $dn_s/d\ln k$, $w(z)$, m_ν, and N_{eff}, by including the other data sets that are sensitive to the *amplitude* of density fluctuations, such as the amplitude of the galaxy power spectrum, Lyα forest, weak lensing, and cluster abundance. With the Lyα forest data from Seljak et al. (2006), for example, the limit on the running index improves from $-0.0728 < dn_s/d\ln k < 0.0087$ (95% CL) to $-0.034 < dn_s/d\ln k < 0.011$ (95% CL) for $r = 0$, and $-0.1186 < dn_s/d\ln k < -0.0051$ (95% CL) to $-0.0411 < dn_s/d\ln k < 0.0067$ (95% CL) for $r \neq 0$. Better understanding of systematic errors in these methods will be crucial in improving our understanding of the physics of our universe. Hints for new physics may well be hidden in the deviations from the simplest 6-parameter ΛCDM model.

APPENDIX

FAST CUBIC ESTIMATORS

We use the following estimators for f_{NL}^{local}, f_{NL}^{equil}, and b_{src} (the amplitude of the point-source bispectrum):

$$f_{NL}^{\text{local}} = (F^{-1})_{11}S_1 + (F^{-1})_{12}S_2 + (F^{-1})_{13}S_3, \tag{A1}$$

$$f_{NL}^{\text{equil}} = (F^{-1})_{21}S_1 + (F^{-1})_{22}S_2 + (F^{-1})_{23}S_3, \tag{A2}$$

$$b_{src} = (F^{-1})_{31}S_1 + (F^{-1})_{32}S_2 + (F^{-1})_{33}S_3, \tag{A3}$$

where F_{ij} is the Fisher matrix given by

$$F_{ij} \equiv \sum_{2 \leq l_1 \leq l_2 \leq l_3} \frac{B^{(i)}_{l_1 l_2 l_3} B^{(j)}_{l_1 l_2 l_3}}{\tilde{C}_{l_1} \tilde{C}_{l_2} \tilde{C}_{l_3}}. \tag{A4}$$

Here, $B^{(i)}_{l_1 l_2 l_3}$ are theoretically calculated angular bispectra (given below), where $i = 1$ is used for f_{NL}^{local}, $i = 2$ for f_{NL}^{equil}, and $i = 3$ for b_{src}. The denominator of F_{ij} contains the total power spectrum including the CMB signal (C_l^{cmb}) and noise (N_l), $\tilde{C}_l \equiv C_l^{cmb} b_l^2 + N_l$, and b_l is the beam transfer function given in Hill et al. (2008).

While this formula allows one to estimate f_{NL}^{local}, f_{NL}^{equil}, and b_{src} simultaneously, we find that a simultaneous estimation does not change the results significantly. Therefore, we use

$$f_{NL}^{\text{local}} = S_1/F_{11}, \qquad f_{NL}^{\text{equil}} = S_2/F_{22}, \qquad b_{src} = S_3/F_{33}, \tag{A5}$$

to simplify the analysis, as well as to make the comparison with the previous work easier. However, we do take into account a potential leakage of the point sources into f_{NL}^{local} and f_{NL}^{equil} by using the Monte Carlo simulation of point sources, as described later. These Monte-Carlo estimates of the bias in f_{NL}^{local} and f_{NL}^{equil} due to the source contamination agree roughly with contributions from the off-diagonal terms in Eq. (A1) and (A2).

Assuming white noise, which is a good approximation at high multipoles in which noise becomes important, one can compute the noise power spectrum analytically as

$$N_l = \Omega_{\text{pix}} \int \frac{d^2\hat{\mathbf{n}}}{4\pi f_{\text{sky}}} \frac{\sigma_0^2 M(\hat{\mathbf{n}})}{N_{\text{obs}}(\hat{\mathbf{n}})}, \tag{A6}$$

where $\Omega_{\text{pix}} \equiv 4\pi/N_{\text{pix}}$ is the solid angle per pixel, $M(\hat{\mathbf{n}})$ is the *KQ75* mask, $f_{\text{sky}} = 0.718$ is the fraction of sky retained by the *KQ75* mask, σ_0 is the rms noise per observation, and $N_{\text{obs}}(\hat{\mathbf{n}})$ is the number of observations per pixel.

The angular bispectra are given by

$$B^{(1)}_{l_1 l_2 l_3} = 2 I_{l_1 l_2 l_3} \int_0^\infty r^2 dr \left[\alpha_{l_1}(r) \beta_{l_2}(r) \beta_{l_3}(r) + (\text{cyc.}) \right], \tag{A7}$$

$$B^{(2)}_{l_1 l_2 l_3} = -3 B^{(1)}_{l_1 l_2 l_3} + 6 I_{l_1 l_2 l_3} \int_0^\infty r^2 dr \left\{ [\beta_{l_1}(r) \gamma_{l_2}(r) \delta_{l_3}(r) + (\text{cyc.})] - 2 \delta_{l_1}(r) \delta_{l_2}(r) \delta_{l_3}(r) \right\}, \tag{A8}$$

$$B^{(3)}_{l_1 l_2 l_3} = I_{l_1 l_2 l_3} b_{src}, \tag{A9}$$

where

$$I_{l_1 l_2 l_3} \equiv \sqrt{\frac{(2l_1 + 1)(2l_2 + 1)(2l_3 + 1)}{4\pi}} \begin{pmatrix} l_1 & l_1 & l_3 \\ 0 & 0 & 0 \end{pmatrix}. \tag{A10}$$

Various functions in $B^{(i)}_{l_1 l_2 l_3}$ are given by

$$\alpha_l(r) \equiv \frac{2}{\pi} \int k^2 dk\, g_{Tl}(k) j_l(kr), \tag{A11}$$

$$\beta_l(r) \equiv \frac{2}{\pi} \int k^2 dk\, P_\Phi(k) g_{Tl}(k) j_l(kr), \tag{A12}$$

$$\gamma_l(r) \equiv \frac{2}{\pi} \int k^2 dk\, P_\Phi^{1/3}(k) g_{Tl}(k) j_l(kr), \tag{A13}$$

$$\delta_l(r) \equiv \frac{2}{\pi} \int k^2 dk\, P_\Phi^{2/3}(k) g_{Tl}(k) j_l(kr). \tag{A14}$$

Here, $P_\Phi(k) \propto k^{n_s - 4}$ is the primordial power spectrum of Bardeen's curvature perturbations, and $g_{Tl}(k)$ is the radiation transfer function that gives the angular power spectrum as $C_l = (2/\pi) \int k^2 dk\, P_\Phi(k) g_{Tl}^2(k)$.

The skewness parameters, S_i, are given by (Komatsu et al. 2005; Creminelli et al. 2006; Yadav et al. 2007)

$$S_1 \equiv 4\pi \int r^2 dr \int \frac{d^2\hat{\mathbf{n}}}{w_3} \left[A(\hat{\mathbf{n}}, r) B^2(\hat{\mathbf{n}}, r) \right.$$
$$\left. -2B(\hat{\mathbf{n}}, r) \langle A_{\text{sim}}(\hat{\mathbf{n}}, r) B_{\text{sim}}(\hat{\mathbf{n}}, r) \rangle_{\text{MC}} - A(\hat{\mathbf{n}}, r) \langle B_{\text{sim}}^2(\hat{\mathbf{n}}, r) \rangle_{\text{MC}} \right], \tag{A15}$$

$$S_2 \equiv -3S_1 + 24\pi \int r^2 dr \int \frac{d^2\hat{\mathbf{n}}}{w_3} \left\{ [B(\hat{\mathbf{n}}, r) C(\hat{\mathbf{n}}, r) D(\hat{\mathbf{n}}, r) - B(\hat{\mathbf{n}}, r) \langle C_{\text{sim}}(\hat{\mathbf{n}}, r) D_{\text{sim}}(\hat{\mathbf{n}}) \rangle_{\text{MC}} \right.$$
$$\left. -C(\hat{\mathbf{n}}, r) \langle B_{\text{sim}}(\hat{\mathbf{n}}, r) D_{\text{sim}}(\hat{\mathbf{n}}) \rangle_{\text{MC}} - D(\hat{\mathbf{n}}, r) \langle B_{\text{sim}}(\hat{\mathbf{n}}, r) C_{\text{sim}}(\hat{\mathbf{n}}, r) \rangle_{\text{MC}}] \right.$$
$$\left. -\frac{1}{3} \left[D^3(\hat{\mathbf{n}}, r) - 3D(\hat{\mathbf{n}}, r) \langle D_{\text{sim}}^2(\hat{\mathbf{n}}, r) \rangle_{\text{MC}} \right] \right\} \tag{A16}$$

$$S_3 \equiv \frac{2\pi}{3} \int \frac{d^2\hat{\mathbf{n}}}{w_3} \left[E^3(\hat{\mathbf{n}}) - 3E(\hat{\mathbf{n}}) \langle E_{\text{sim}}^2(\hat{\mathbf{n}}) \rangle_{\text{MC}} \right], \tag{A17}$$

where w_3 is the sum of the weighting function cubed:

$$w_3 \equiv \int d^2\hat{\mathbf{n}} \, W^3(\hat{\mathbf{n}}). \tag{A18}$$

For a uniform weighting, the weighting function is simply given by the *KQ75* mask, i.e., $W(\hat{\mathbf{n}}) = M(\hat{\mathbf{n}})$, which gives $w_3 = 4\pi f_{\text{sky}}$. For our measurements of f_{NL}^{local}, f_{NL}^{equil}, and b_{src}, we shall use a "combination signal-plus-noise weight," given by

$$W(\mathbf{n}) = \frac{M(\hat{\mathbf{n}})}{\sigma_{\text{cmb}}^2 + \sigma_0^2/N_{\text{obs}}(\hat{\mathbf{n}})}, \tag{A19}$$

where $\sigma_{\text{cmb}}^2 \equiv (1/4\pi)\sum_l(2l+1)C_l^{\text{cmb}}b_l^2$ is the CMB signal variance, σ_0 is the rms noise per observation, and $N_{\text{obs}}(\hat{\mathbf{n}})$ is the number of observations per pixel. This combination weighting yields a nearly optimal performance for b_{src} and f_{NL}^{equil}, whereas it results in a minor improvement in f_{NL}^{local} over the uniform weighting. The bracket, $\langle\rangle_{\text{MC}}$, denotes the average over Monte Carlo realizations, and "sim" denotes that these are the filtered maps of the Monte Carlo realizations.

The filtered temperature maps, A, B, C, D, and E, are given by

$$A(\hat{\mathbf{n}}, r) \equiv \sum_{l=2}^{l_{\max}}\sum_{m=-l}^{l} \alpha_l(r)\frac{b_l}{\tilde{C}_l}a_{lm}Y_{lm}(\hat{\mathbf{n}}), \tag{A20}$$

$$B(\hat{\mathbf{n}}, r) \equiv \sum_{l=2}^{l_{\max}}\sum_{m=-l}^{l} \beta_l(r)\frac{b_l}{\tilde{C}_l}a_{lm}Y_{lm}(\hat{\mathbf{n}}), \tag{A21}$$

$$C(\hat{\mathbf{n}}, r) \equiv \sum_{l=2}^{l_{\max}}\sum_{m=-l}^{l} \gamma_l(r)\frac{b_l}{\tilde{C}_l}a_{lm}Y_{lm}(\hat{\mathbf{n}}), \tag{A22}$$

$$D(\hat{\mathbf{n}}, r) \equiv \sum_{l=2}^{l_{\max}}\sum_{m=-l}^{l} \delta_l(r)\frac{b_l}{\tilde{C}_l}a_{lm}Y_{lm}(\hat{\mathbf{n}}), \tag{A23}$$

$$E(\hat{\mathbf{n}}) \equiv \sum_{l=2}^{l_{\max}}\sum_{m=-l}^{l} \frac{b_l}{\tilde{C}_l}a_{lm}Y_{lm}(\hat{\mathbf{n}}), \tag{A24}$$

respectively. Here, $l_{\max}$ is the maximum multipole that we use in the analysis. We vary $l_{\max}$ to see how much the results depend on $l_{\max}$.

Eq. (A15) and (A16) involve the integrals over the conformal distances, r. We evaluate these integrals as

$$\int r^2 dr[\ldots](r) = \sum_i (w_i)_{\text{opt}} r_i^2 \Delta r_i [\ldots](r_i). \tag{A25}$$

We use the bispectrum optimization algorithm described in Smith & Zaldarriaga (2006) to compute the optimal weights, $(w_i)_{\text{opt}}$, and decide on which quadrature points, r_i, to keep. We choose the number of quadrature points such that the bispectrum computed in this way agrees with that from more dense sampling in r to 10^{-5}, which typically gives ~ 5 quadrature points for f_{NL}^{local} and ~ 15 points for f_{NL}^{equil}.[51]

The measurement of these estimators proceeds as follows:

1. Generate the simulated realizations of CMB signal maps, T_S, from the input signal power spectrum, C_l^{cmb}, and the beam transfer function, b_l. We have generated 300 realizations for the analysis given in this paper.

2. Add random noise, T_N, using the rms noise per pixel given by $\sigma_0/\sqrt{N_{\text{obs}}(\hat{\mathbf{n}})}$.

3. Add point sources. We use a simplified treatment for the source simulation,

$$\frac{T_{\text{src}}(\hat{\mathbf{n}})}{2.725 \text{ K}} = \left[\frac{\sinh^2(x/2)}{x^4}\frac{F_{\text{src}}/\Omega_{pix}}{67.55 \text{ MJy}}\right]\epsilon, \tag{A26}$$

where Ω_{pix} is the solid angle of pixel, $x = h\nu/(k_B T_{\text{cmb}}) = 56.80$ GHz (for $T_{\text{cmb}} = 2.725$ K), ϵ is a Poisson random variable with the mean of $\langle\epsilon\rangle = n_{\text{src}}\Omega_{pix}$, and n_{src} is the average number of sources per steradians. This simplified model assumes that there is only one population of sources with a fixed flux, F_{src}, and each source's flux is independent of frequency. We choose $n_{\text{src}} = 0.85$ sr^{-1} and $F_{\text{src}} = 0.5$ Jy, which yields the source power spectrum in Q band of $C_{ps} = 8.7\times10^{-3}$ μK^2 sr and the source bispectrum in Q band of $b_{src} = 8.7\times10^{-5}$ μK^3 sr^2,

---

[51] Note that Smith & Zaldarriaga (2006) use 10^{-6} as a criterion, which gives more quadrature points to evaluate. We find that 10^{-5} is sufficient for the size of statistical and systematic errors in the current measurements.

which roughly reproduce the measured values. However, this model does not reproduce the source counts very well. (The source density of $n_{\rm src} = 0.85$ sr^{-1} at 0.5 Jy is too low.) The main purpose of this phenomenological model is to reproduce the power spectrum and bispectrum – we include point sources in the simulations, in order to take into account the potential effects of the unresolved sources on primordial non-Gaussianity, $f_{NL}^{\rm local}$ and $f_{NL}^{\rm equil}$.

4. Coadd them to create the simulated temperature maps, $T(\hat{\bf n}) = T_S(\hat{\bf n}) + T_N(\hat{\bf n}) + T_{\rm src}(\hat{\bf n})$.

5. Mask and weight the temperature maps, $T(\hat{\bf n}) \to \tilde{T}(\hat{\bf n}) = W(\hat{\bf n})T(\hat{\bf n})$, where $W(\hat{\bf n})$ is given by Eq. (A19).

6. Remove the monopole and dipole from $\tilde{T}(\hat{\bf n})$.

7. Compute the harmonic coefficients as

$$a_{lm} = \int d^2\hat{\bf n} \ \tilde{T}(\hat{\bf n})Y_{lm}^*(\hat{\bf n}). \tag{A27}$$

8. Generate the filtered maps, $A_{\rm sim}$, $B_{\rm sim}$, $C_{\rm sim}$, $D_{\rm sim}$, and $E_{\rm sim}$, and compute the appropriate Monte-Carlo averages such as $\langle A_{\rm sim}B_{\rm sim}\rangle_{\rm MC}$, etc. This is the most time consuming part.

9. Compute the filtered maps from the *WMAP* data. When we coadd the V and W band data, we weight them as $T_{\rm V+W} = (T_{\rm V}+0.9T_{\rm W})/1.9$. The beam transfer function of the coadded map is given by $b_l^{\rm V+W} = (b_l^{\rm V}+0.9b_l^{\rm W})/1.9$, and $\sigma_0/N_{\rm obs}$ of the coadded map is given by

$$\frac{(\sigma_0^{\rm V+W})^2}{N_{\rm obs}^{\rm V+W}(\hat{\bf n})} = \frac{1}{1.9^2}\left[\frac{(\sigma_0^{\rm V})^2}{N_{\rm obs}^{\rm V}(\hat{\bf n})} + \frac{(0.9\sigma_0^{\rm W})^2}{N_{\rm obs}^{\rm W}(\hat{\bf n})}\right]. \tag{A28}$$

10. Compute the skewness parameters, S_i, from the filtered *WMAP* data, and obtain $f_{NL}^{\rm local}$, $f_{NL}^{\rm equil}$, and b_{src}, either jointly or separately.

11. Compute these parameters from the simulated realizations as well, and obtain the uncertainties.

For the computations of $g_{Tl}(k)$ and generation of Monte Carlo realizations, we have used the maximum-likelihood values of the *WMAP* 3-year data (the power-law ΛCDM model fit by the *WMAP* data alone with the Sunyaev–Zel'dovich effect marginalized): $\Omega_b = 0.0414$, $\Omega_{cdm} = 0.1946$, $\Omega_\Lambda = 0.7640$, $H_0 = 73.2$ km/s/Mpc, $\tau = 0.091$, and $n_s = 0.954$ (Spergel et al. 2007). These parameters yield the conformal distance to $t = 0$ as $c\tau_0 = 14.61$ Gpc.

AXION

In this Appendix we derive relations between the tensor-to-scalar ratio r, the axion mass density $\Omega_a h^2$, the entropy-to-curvature perturbation ratio α, the phase of the Pecci-Quinn field θ_a, and the axion decay constant f_a.

Let us write the expectation value of the complex Pecci-Quinn field, $\psi_{\rm PQ}$, as

$$\langle\psi_{\rm PQ}\rangle = \frac{f_a}{\sqrt{2}}e^{i\theta_a}, \tag{B1}$$

where f_a is the axion decay constant, and θ_a is the phase. Quantum fluctuations during inflation generate fluctuations in the phase, $\delta\theta_a$, as

$$\delta\theta_a = \frac{H}{2\pi f_a}. \tag{B2}$$

As the number density of axions scales as the phase squared, $n_a \propto \theta_a^2$, the mass density fluctuation is given by

$$\frac{\delta\rho_a}{\rho_a} = 2\frac{\delta\theta_a}{\theta_a} = \frac{H}{\pi\theta_a f_a}. \tag{B3}$$

As the energy density of axions was negligible during inflation, the axion density perturbation, $\delta\rho_a/\rho_a$, would produce the isocurvature perturbation. While radiation (including photons) is generated by decay of inflaton fields, (some of) dark matter is in the form of axions whose generation is independent of photons; thus, the entropy perturbation between photons and axions would be generated. We assume that axions were not in thermal equilibrium with photons in the subsequent evolution of the universe.

The entropy perturbations and curvature perturbations are given, respectively, by

$$\frac{k^3 P_\mathcal{S}(k)}{2\pi^2} = \frac{\Omega_a^2}{\Omega_c^2}\frac{H_k^2}{\pi^2\theta_a^2 f_a^2}, \qquad \frac{k^3 P_\mathcal{R}(k)}{2\pi^2} = \frac{H_k^4}{4\pi^2\dot{\phi}_k^2} \approx \frac{H_k^2}{8\pi^2 M_{\rm pl}^2\epsilon} \tag{B4}$$

where $\Omega_a \leq \Omega_c$ is the axion mass density, H_k is the expansion rate during inflation at which the wavenumber k went outside of the horizon, ϕ_k is the value of inflation at the same time, $\epsilon \equiv -\dot{H}/H \approx (M_{\rm pl}^2/2)(V'/V)^2$ is the usual slow-roll

parameter, $V(\phi)$ is the inflaton potential, and $M_{\rm pl} = 1/\sqrt{8\pi G}$ is the reduced Planck mass. We have used the slow-roll approximation, $\dot{\phi} \approx -V'/(3H)$ and $H^2 \approx V/(3M_{\rm pl}^2)$.

Here, let us comment on our choice of $m = 1$, which makes $k^3 P_{\mathcal{S}} \propto k^{m-1}$ independent of k. Since $k^3 P_{\mathcal{S}} \propto H_k^2 \propto k^{-2\epsilon}$, where $\epsilon = -\dot{H}/H^2$, this choice corresponds to having a very small slow-roll parameter, $\epsilon \ll 1$. This is consistent with our limit on the curvature power spectrum, $n_s = 1 + 6\epsilon - 4\eta \simeq 1 - 4\eta < 1$, where η is another slow-roll parameter. As the current limit is $1 - n_s \approx 4\eta \simeq 0.04$, our approximation, $m = 1$, is valid for $\epsilon < 0.01$. It should be straightforward to extend our analysis to the case in which $m \neq 1$.

By dividing $P_{\mathcal{S}}(k)$ by $P_{\mathcal{R}}(k)$, we find the entropy-to-curvature perturbation ratio for axions, $\alpha_0(k)$, as

$$\frac{\alpha_0(k)}{1 - \alpha_0(k)} \equiv \frac{P_{\mathcal{S}}(k)}{P_{\mathcal{R}}(k)} = \frac{\Omega_a^2}{\Omega_c^2} \frac{8\epsilon}{\theta_a^2(f_a/M_{\rm pl})^2}. \tag{B5}$$

At this point, it is clear that one cannot solve this constraint uniquely for any of ϵ, f_a, or θ_a.

In order to break the degeneracy, we use the axion mass density (Kawasaki & Sekiguchi 2007, and references therein)

$$\Omega_a h^2 = 1.0 \times 10^{-3} \gamma \theta_a^2 \left(\frac{f_a}{10^{10}\ {\rm GeV}}\right)^{7/6}, \tag{B6}$$

where γ is a dilution factor, representing the amount by which the axion density could have been diluted by a late-time entropy production between the QCD phase transition at ~ 200 MeV and the epoch of nucleosynthesis at ~ 1 Mpc.

Combining equation (B5) and (B6) to eliminate the phase, θ_a, and using the relation between the tensor-to-scalar ratio r and the slow-roll parameter ϵ, $r = 16\epsilon$, we find

$$r = (1.6 \times 10^{-12}) \left(\frac{\Omega_c h^2}{\gamma}\right) \left(\frac{\Omega_c}{\Omega_a}\right) \left(\frac{f_a}{10^{12}\ {\rm GeV}}\right)^{5/6} \frac{\alpha_0}{1 - \alpha_0}. \tag{B7}$$

Alternatively, we can eliminate the axion decay constant, f_a, to obtain

$$r = \frac{4.7 \times 10^{-12}}{\theta_a^{10/7}} \left(\frac{\Omega_c h^2}{\gamma}\right)^{12/7} \left(\frac{\Omega_c}{\Omega_a}\right)^{2/7} \frac{\alpha_0}{1 - \alpha_0}. \tag{B8}$$

This is equation (48).

EQUATION OF STATE OF DARK ENERGY: A NEW PARAMETRIZED FORM

In this Appendix, we describe the models of dark energy that we explore in § 5.4. Our goal is to obtain a sensible form of time-dependent dark energy equation of state, $w(a)$. One of the most commonly used form of $w(a)$ is a linear form (Chevallier & Polarski 2001; Linder 2003)

$$w(a) = w_0 + (1 - a)w_a, \tag{C1}$$

where w_0 and w_a parametrize the present-day value of w and the first derivative. However, this form cannot be adopted as it is when one uses the CMB data to constrain $w(a)$. Since this form is basically the leading-order term of a Taylor series expansion, the value of $w(a)$ can become unreasonably too large or too small when extrapolated to the decoupling epoch at $z_* \simeq 1090$ (or $a_* \simeq 9.17 \times 10^{-4}$), and thus one cannot extract meaningful constraints on the quantities such as w_0 and w_a that are defined at the *present epoch*.

To avoid this problem, yet to keep a close contact with the previous work in the literature, we shall consider an alternative parametrized form. Our idea is the following: we wish to keep the form given by Eq. (C1) at low redshifts, lower than some transition redshift, $z_{\rm trans}$. However, we demand $w(a)$ approach to -1 at higher redshifts, $z > z_{\rm trans}$. This form of $w(a)$ therefore has the following property: at early times, before the transition redshift, $z_{\rm trans}$, dark energy was just like a cosmological constant, and thus the dark energy density was nearly constant, i.e., $\rho_{\rm de}(z > z_{\rm trans}) \approx$ constant. Then, dark energy began to become dynamical at $z \sim z_{\rm trans}$, with the equation of state given by the conventional linear form, Eq. (C1).

Some of the properties of our form of $w(a)$ are similar to those of "thawing models," (Caldwell & Linder 2005) in which a scalar field was moving very slowly initially, giving $w(a) \approx -1$ at early times, and then began to move faster towards low redshifts, causing $w(a)$ to deviate more and more from -1 at low redshifts. Our parametrization can describe more general class of models than single scalar field models, as it allows for w to go below -1. On the other hand, models that are based upon a single scalar field cannot have $w < -1$ (e.g., Hu 2005). The "Forever regular" parametrization explored in Wang & Tegmark (2004) also approaches to a constant density at early times, if the late-time equation of state is $w < -1$. Our parametrization is more general than theirs, as their form allows only for a constant equation of state at late times.

We wish to find a smooth interpolation between $w_{\rm early} = -1$ and $w_{\rm late} = w_0 + (1 - a)w_a$. We begin by writing

$$w(a) = \tilde{w}(a)f(a/a_{\rm trans}) + (-1)\left[1 - f(a/a_{\rm trans})\right], \tag{C2}$$

where $a_{\rm trans} = 1/(1 + z_{\rm trans})$, and the function $f(x)$ goes to zero for $x \ll 1$, and to unity for $x \gg 1$. Here, $\tilde{w}(a)$ is the form of w at low redshifts. Any function that has this property is adequate for $f(x)$. We choose:

$$f(x) = \frac{1}{2}\left[\tanh(\ln x) + 1\right] = \frac{x}{x + 1}, \tag{C3}$$
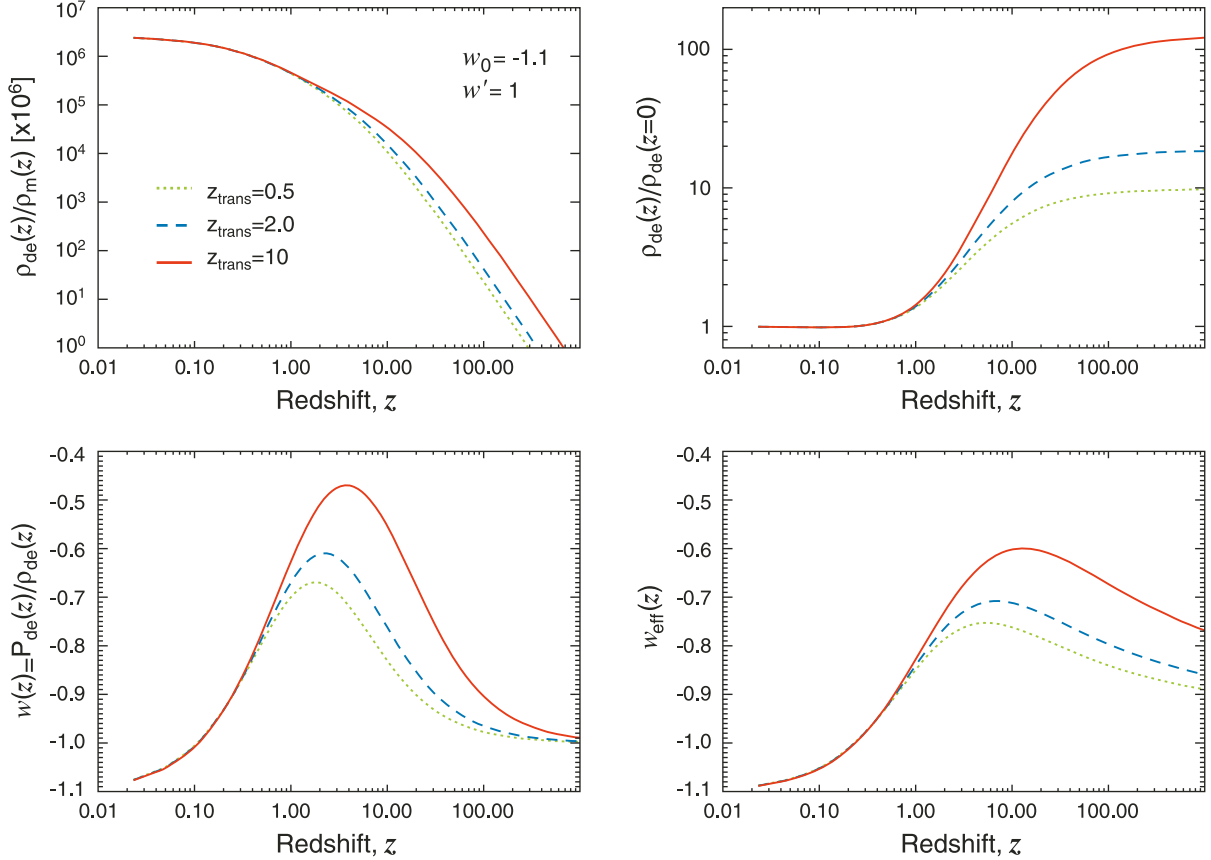
FIG. C1.— Evolution of dark energy for $w_0 = -1.1$ and $w' = 1$, and various transition redshifts, $z_{\rm trans} = 0.5$, 2, and 10, above which $w(z)$ approaches to -1. (*Top Left*) Evolution of the dark energy to matter density ratio as a function of z. Note that the vertical axis has been multiplied by 10^6. (*Top Right*) Evolution of the dark energy density relative to the dark energy density at present. The dark energy density was nearly constant at high redshifts above $z_{\rm trans}$; thus, these models can describe the "thawing models," (Caldwell & Linder 2005) in which dark energy was nearly constant at early times, and had become dynamical at lower redshifts. (*Bottom Left*) Evolution of the equation of state, $w(z) = P_{\rm de}(z)/\rho_{\rm de}(z)$. By construction of the model, $w(z)$ approaches to -1 beyond $z_{\rm trans}$. (*Bottom Right*) Evolution of the effective equation of state, $w_{\rm eff}(z)$, which determines the evolution of dark energy density as $\rho_{\rm de}(z) = \rho_{\rm de}(0)(1+z)^{3[1+w_{\rm eff}(z)]}$.

which gives the desired form of the equation of state of dark energy,

$$w(a) = \frac{a\tilde{w}(a)}{a + a_{\rm trans}} - \frac{a_{\rm trans}}{a + a_{\rm trans}}, \tag{C4}$$

where

$$\tilde{w}(a) = \tilde{w}_0 + (1 - a)\tilde{w}_a. \tag{C5}$$

One nice property of this form is that it allows one to obtain a closed, analytical form of the effective equation of state, $w_{\rm eff}(a)$, which gives the evolution of dark energy density, $\rho_{\rm de}(a) = \rho(0)a^{-3[1+w_{\rm eff}(a)]}$:

$$
\begin{aligned}
w_{\rm eff}(a) &= \frac{1}{\ln a} \int_0^{\ln a} d\ln a' \; w(a') \\
&= -1 + \frac{(1-a)\tilde{w}_a}{\ln a} + \frac{1 + \tilde{w}_0 + (1 + a_{\rm trans})\tilde{w}_a}{\ln a} \ln \frac{a + a_{\rm trans}}{1 + a_{\rm trans}}.
\end{aligned} \tag{C6}
$$

This property allows one to compute the expansion rate, $H(a)$ (Eq. [7]), and hence the distance (Eq. [2]), easily.

Finally, we use the present-day value of w, $w_0 \equiv w(z = 0)$, and the first derivative, $w' \equiv dw/dz|_{z=0}$, as free parameters. They are related to $\tilde{w}_0$ and $\tilde{w}_a$ as

$$1 + w_0 = \frac{1 + \tilde{w}_0}{1 + a_{\rm trans}}, \tag{C7}$$

$$w' = \frac{\tilde{w}_a}{1 + a_{\rm trans}} + \frac{a_{\rm trans}(1 + \tilde{w}_0)}{(1 + a_{\rm trans})^2}. \tag{C8}$$

The inverse relations are

$$1 + \tilde{w}_0 = (1 + a_{\rm trans})(1 + w_0), \tag{C9}$$

$$\tilde{w}_a = (1 + a_{\rm trans})w' - a_{\rm trans}(1 + w_0). \tag{C10}$$

In the limit of very early transition, $a_{\text{trans}} \ll 1$, one finds $w_0 \approx \tilde{w}_0$ and $w' \approx \tilde{w}_a$, as expected. This completes the description of our form of $w(a)$.

Figure C1 shows the evolution of dark energy density, $\rho_{\text{de}}(z) = \rho(0)(1+z)^{3[1+w_{\text{eff}}(a)]}$, the equation of state, $w(z)$, and the effective equation of state, $w_{\text{eff}}(z)$, computed from Eq. (C4) and (C6). We choose $w_0 = -1.1$ and $w' = 1$, which are close to the best-fitting values that we find in § 5.4 (see Fig. 14). We show three curves for the transition redshifts of $z_{\text{trans}} = 0.5, 2$, and 10. We find that the form of $w(z)$ that we have derived achieves our goal: $w(z)$ approaches to -1 and the dark energy density tends to a constant value at high redshifts, giving sensible results at the decoupling epoch. The dark energy density is totally sub-dominant compared to the matter density at high redshifts, which is also desirable.

The constraints that we have obtained for w_0 and w' are not sensitive to the exact values of z_{trans} (see the right panel of Fig. 14). This is because all of the curves shown in Fig. C1 are very similar at $z \lesssim 1$, where the BAO and SN data are currently available.

REFERENCES

Abbott, L. F., & Wise, M. B. 1984, Nucl. Phys., B244, 541

Abdalla, F. B., & Rawlings, S. 2007, MNRAS, 381, 1313

Abdurashitov, J. N., et al. 1999, Phys. Rev., C60, 055801

Accetta, F. S., Zoller, D. J., & Turner, M. S. 1985, Phys. Rev., D31, 3046

Acquaviva, V., Bartolo, N., Matarrese, S., & Riotto, A. 2003, Nucl. Phys., B667, 119

Adams, F. C., Bond, J. R., Freese, K., Frieman, J. A., & Olinto, A. V. 1993, Phys. Rev., D47, 426

Ahmad, Q. R., et al. 2002, Phys. Rev. Lett., 89, 011301

Ahmed, S. N., et al. 2004, Phys. Rev. Lett., 92, 181301

Ahn, M. H., et al. 2003, Phys. Rev. Lett., 90, 041801

Alabidi, L., & Lyth, D. H. 2006a, JCAP, 0608, 013

Alabidi, L., & Lyth, D. H. 2006b, JCAP, 0605, 016

Albrecht, A., & Steinhardt, P. J. 1982, Phys. Rev. Lett., 48, 1220

Alishahiha, M., Silverstein, E., & Tong, D. 2004, Phys. Rev. D, 70, 123505

Allen, S. W., Schmidt, R. W., & Bridle, S. L. 2003, MNRAS, 346, 593

Allison, W. W. M., et al. 1999, Phys. Lett., B449, 137

Ambrosio, M., et al. 2001, Phys. Lett., B517, 59

Amin, M. A., Wagoner, R. V., & Blandford, R. D. 2007, ArXiv e-prints, 708

Araki, T., et al. 2005, Phys. Rev. Lett., 94, 081801

Argüeso, F., González-Nuevo, J., & Toffolatti, L. 2003, ApJ, 598, 86

Arkani-Hamed, N., Creminelli, P., Mukohyama, S., & Zaldarriaga, M. 2004, JCAP, 0404, 001

Armendariz-Picon, C., Damour, T., & Mukhanov, V. F. 1999, Phys. Lett., B458, 209

Arroja, F., & Koyama, K. 2008, ArXiv e-prints, 802

Astier, P., et al. 2006, A&A, 447, 31

Babich, D., Creminelli, P., & Zaldarriaga, M. 2004, JCAP, 0408, 009

Bardeen, J. M., Steinhardt, P. J., & Turner, M. S. 1983, Phys. Rev. D, 28, 679

Barger, V., Kneller, J. P., Lee, H.-S., Marfatia, D., & Steigman, G. 2003, Phys. Lett., B566, 8

Barger, V., Marfatia, D., & Tregre, A. 2004, Phys. Lett., B595, 55

Bartolo, N., Komatsu, E., Matarrese, S., & Riotto, A. 2004, Phys. Rept., 402, 103

Bartolo, N., & Liddle, A. R. 2002, Phys. Rev. D, 65, 121301

Bartolo, N., Matarrese, S., & Riotto, A. 2006, JCAP, 0606, 024

Bartolo, N., Matarrese, S., & Riotto, A. 2007, JCAP, 0701, 019

Bashinsky, S., & Seljak, U. 2004, Phys. Rev. D, 69, 083002

Basko, M. M., & Polnarev, A. G. 1980, MNRAS, 191, 207

Bassett, B. A., Tsujikawa, S., & Wands, D. 2006, Rev. Mod. Phys., 78, 537

Bean, R., Bernat, D., Pogosian, L., Silvestri, A., & Trodden, M. 2007, Phys. Rev. D, 75, 064020

Bean, R., Chen, X., Peiris, H. V., & Xu, J. 2008, Phys. Rev., D77, 023527

Bean, R., Dunkley, J., & Pierpaoli, E. 2006, Phys. Rev., D74, 063503

Bean, R., Shandera, S. E., Henry Tye, S. H., & Xu, J. 2007, JCAP, 0705, 004

Beltran, M., Garcia-Bellido, J., & Lesgourgues, J. 2007, Phys. Rev., D75, 103507

Beltrán, M., García-Bellido, J., Lesgourgues, J., Liddle, A. R., & Slosar, A. 2005, Phys. Rev. D, 71, 063532

Beltran, M., Garcia-Bellido, J., Lesgourgues, J., & Riazuelo, A. 2004, Phys. Rev., D70, 103530

Beltran, M., Garcia-Bellido, J., Lesgourgues, J., & Viel, M. 2005, Phys. Rev., D72, 103515

Bennett, C. L., et al. 1996, ApJ, 464, L1

Bennett, C. L., et al. 2003a, ApJ, 583, 1

Bennett, C. L., et al. 2003b, ApJS, 148, 1

Bennett, C. L., et al. 2003c, ApJS, 148, 97

Bennett, C. L., et al. 1994, ApJ, 436, 423

Bernui, A., Mota, B., Rebouças, M. J., & Tavakol, R. 2007, A&A, 464, 479

Bertschinger, E., & Zukin, P. 2008, ArXiv e-prints, 801

Bielewicz, P., Eriksen, H. K., Banday, A. J., Górski, K. M., & Lilje, P. B. 2005, ApJ, 635, 750

Bolton, J. S., Viel, M., Kim, T. ., Haehnelt, M. G., & Carswell, R. F. 2007, ArXiv e-prints, 711

Bond, J. R., & Efstathiou, G. 1984, ApJ, 285, L45

Bond, J. R., Efstathiou, G., & Silk, J. 1980, Physical Review Letters, 45, 1980

Bond, J. R., Efstathiou, G., & Tegmark, M. 1997, MNRAS, 291, L33

Bond, J. R., & Szalay, A. S. 1983, ApJ, 274, 443

Boubekeur, L., & Lyth, D. H. 2006, Phys. Rev. D, 73, 021301

Bridges, M., McEwen, J. D., Cruz, M., Hobson, M. P., Lasenby, A. N., Vielva, P., & Martinez-Gonzalez, E. 2007, ArXiv e-prints, 712

Bridle, S. L., Lewis, A. M., Weller, J., & Efstathiou, G. 2003, MNRAS, 342, L72

Buchbinder, E. I., Khoury, J., & Ovrut, B. A. 2007, Phys. Rev., D76, 123503

Buchbinder, E. I., Khoury, J., & Ovrut, B. A. 2007, ArXiv e-prints, 710

Bucher, M., Dunkley, J., Ferreira, P. G., Moodley, K., & Skordis, C. 2004, Physical Review Letters, 93, 081301

Byrnes, C. T., Sasaki, M., & Wands, D. 2006, Phys. Rev. D, 74, 123519

Cabella, P., Hansen, F., Marinucci, D., Pagano, D., & Vittorio, N. 2004, Phys. Rev. D, 69, 063007

Cabella, P., Hansen, F. K., Liguori, M., Marinucci, D., Matarrese, S., Moscardini, L., & Vittorio, N. 2006, MNRAS, 369, 819

Cabella, P., Natoli, P., & Silk, J. 2007, Phys. Rev. D, 76, 123014

Caldwell, R. R., Dave, R., & Steinhardt, P. J. 1998, Phys. Rev. Lett., 80, 1582

Caldwell, R. R., & Linder, E. V. 2005, Phys. Rev. Lett., 95, 141301

Carroll, S. M. 1998, Phys. Rev. Lett., 81, 3067

Carroll, S. M., Field, G. B., & Jackiw, R. 1990, Phys. Rev., D41, 1231

Carroll, S. M., Press, W. H., & Turner, E. L. 1992, ARA&A, 30, 499

Cash, W. 1976, A&A, 52, 307

Cayón, L., Jin, J., & Treaster, A. 2005, MNRAS, 362, 826

Chambers, A., & Rajantie, A. 2008, Phys. Rev. Lett., 100, 041302

Chen, G., & Szapudi, I. 2005, ApJ, 635, 743

Chen, G., & Szapudi, I. 2006, ApJ, 647, L87

Chen, X., Easther, R., & Lim, E. A. 2007, JCAP, 0706, 023

Chen, X., Easther, R., & Lim, E. A. 2008, ArXiv e-prints, 801

Chen, X., Huang, M.-x., Kachru, S., & Shiu, G. 2007, JCAP, 0701, 002

Cheung, C., Creminelli, P., Fitzpatrick, A. L., Kaplan, J., & Senatore, L. 2007, ArXiv e-prints, 709

Chevallier, M., & Polarski, D. 2001, Int. J. Mod. Phys., D10, 213

Chiang, L., Naselsky, P. D., Verkhodanov, O. V., & Way, M. J. 2003, ApJ, 590, L65

Chiang, L.-Y., Naselsky, P. D., & Coles, P. 2007, ApJ, 664, 8

Chiba, T., Sugiyama, N., & Nakamura, T. 1997, Mon. Not. Roy. Astron. Soc., 289, L5

Chiba, T., & Takahashi, R. 2007, Phys. Rev. D, 75, 101301

Cleveland, B. T., et al. 1998, Astrophys. J., 496, 505

Cole, S., et al. 2005, MNRAS, 362, 505

Copeland, E. J., Liddle, A. R., & Wands, D. 1998, Phys. Rev., D57, 4686

Copeland, E. J., Sami, M., & Tsujikawa, S. 2006, Int. J. Mod. Phys., D15, 1753

Copi, C. J., Huterer, D., Schwarz, D. J., & Starkman, G. D. 2006, MNRAS, 367, 79

Copi, C. J., Huterer, D., Schwarz, D. J., & Starkman, G. D. 2007, Phys. Rev. D, 75, 023507

Copi, C. J., Huterer, D., & Starkman, G. D. 2004, Phys. Rev. D, 70, 043515

Corasaniti, P. S., & Melchiorri, A. 2007, ArXiv e-prints

Coughlan, G. D., Fischler, W., Kolb, E. W., Raby, S., & Ross, G. G. 1983, Phys. Lett., B131, 59

Coulson, D., Crittenden, R. G., & Turok, N. G. 1994, Phys. Rev. Lett., 73, 2390

Covi, L., Hamann, J., Melchiorri, A., Slosar, A., & Sorbera, I. 2006, Phys. Rev. D, 74, 083509

Creminelli, P., Nicolis, A., Senatore, L., Tegmark, M., & Zaldarriaga, M. 2006, JCAP, 0605, 004

Creminelli, P., & Senatore, L. 2007, JCAP, 0711, 010

Creminelli, P., Senatore, L., Zaldarriaga, M., & Tegmark, M. 2007, JCAP, 0703, 005

Crittenden, R., Bond, J. R., Davis, R. L., Efstathiou, G., & Steinhardt, P. J. 1993, Phys. Rev. Lett., 71, 324

Crittenden, R., Davis, R. L., & Steinhardt, P. J. 1993, ApJ, 417, L13

Crittenden, R. G., Coulson, D., & Turok, N. G. 1995, Phys. Rev. D, 52, 5402

Crotty, P., Garcia-Bellido, J., Lesgourgues, J., & Riazuelo, A. 2003, Phys. Rev. Lett., 91, 171301

Crotty, P., Lesgourgues, J., & Pastor, S. 2003, Phys. Rev., D67, 123005

Crotty, P., Lesgourgues, J., & Pastor, S. 2004, Phys. Rev., D69, 123007

Cruz, M., Cayón, L., Martínez-González, E., Vielva, P., & Jin, J. 2007a, ApJ, 655, 11

Cruz, M., Martínez-González, E., Vielva, P., & Cayón, L. 2005, MNRAS, 356, 29

Cruz, M., Tucci, M., Martínez-González, E., & Vielva, P. 2006, MNRAS, 369, 57

Cruz, M., Turok, N., Vielva, P., Martínez-González, E., & Hobson, M. 2007b, Science, 318, 1612

Curto, A., Aumont, J., Macías-Pérez, J. F., Martínez-González, E., Barreiro, R. B., Santos, D., Désert, F. X., & Tristram, M. 2007, A&A, 474, 23

Daniel, S. F., Caldwell, R. R., Cooray, A., & Melchiorri, A. 2008, ArXiv e-prints, 802

Davis, J., Raymond, Harmer, D. S., & Hoffman, K. C. 1968, Phys. Rev. Lett., 20, 1205

de Bernardis, F., Melchiorri, A., Verde, L., & Jimenez, R. 2007, ArXiv e-prints, 707

de Bernardis, P., et al. 2000, Nature, 404, 955

de Oliveira-Costa, A., Tegmark, M., Zaldarriaga, M., & Hamilton, A. 2004, Phys. Rev., D69, 063516

De Troia, G., et al. 2007, ApJ, 670, L73

Deffayet, C., Dvali, G., & Gabadadze, G. 2002, Phys. Rev. D, 65, 44023

Destri, C., de Vega, H. J., & Sanchez, N. G. 2008, Phys. Rev. D, 77, 043509

Dickinson, C., et al. 2004, MNRAS, 353, 732

Dicus, D. A., et al. 1982, Phys. Rev., D26, 2694

Dimopoulos, S., Kachru, S., McGreevy, J., & Wacker, J. 2005, ArXiv High Energy Physics - Theory e-prints

Dodelson, S., Kinney, W. H., & Kolb, E. W. 1997, Phys. Rev., D56, 3207

Dolgov, A. D. 2002, Phys. Rept., 370, 333

Dolgov, A. D., Hansen, S. H., & Semikoz, D. V. 1999, Nucl. Phys., B543, 269

Doré, O., et al. 2007, ArXiv e-prints, 712

Dunkley, J., et al. 2008, ApJS

Dunkley, J., Bucher, M., Ferreira, P. G., Moodley, K., & Skordis, C. 2005, Phys. Rev. Lett., 95, 261303

Dvali, G., Gruzinov, A., & Zaldarriaga, M. 2004a, Phys. Rev. D, 69, 083505

Dvali, G., Gruzinov, A., & Zaldarriaga, M. 2004b, Phys. Rev. D, 69, 023505

Dvali, G. R., Gabadadze, G., & Porrati, M. 2000, Phys. Lett., B485, 208

Easther, R., & McAllister, L. 2006, JCAP, 0605, 018

Easther, R., & Peiris, H. 2006, JCAP, 0609, 010

Eguchi, K., et al. 2003, Phys. Rev. Lett., 90, 021802

Eisenstein, D. J., & Hu, W. 1998, ApJ, 496, 605

Eisenstein, D. J., et al. 2005, ApJ, 633, 560

Elgarøy, Ø., & Lahav, O. 2003, Journal of Cosmology and Astro-Particle Physics, 4, 4

Elgaroy, O., & Lahav, O. 2005, New J. Phys., 7, 61

Elgarøy, O., & Multamäki, T. 2007, A&A, 471, 65

Ellis, J. R., Nanopoulos, D. V., & Quiros, M. 1986, Phys. Lett., B174, 176

Enqvist, K., Jokinen, A., Mazumdar, A., Multamäki, T., & Väihkönen, A. 2005, Phys. Rev. Lett., 94, 161301

Eriksen, H. K., Banday, A. J., Górski, K. M., Hansen, F. K., & Lilje, P. B. 2007a, ApJ, 660, L81

Eriksen, H. K., Hansen, F. K., Banday, A. J., Górski, K. M., & Lilje, P. B. 2004, ApJ, 605, 14

Eriksen, H. K., et al. 2007b, ApJ, 656, 641

Eriksen, H. K., Novikov, D. I., Lilje, P. B., Banday, A. J., & Gorski, K. M. 2004, Astrophys. J., 612, 64

Fabbri, R., & Pollock, M. d. 1983, Phys. Lett., B125, 445

Falk, T., Rangarajan, R., & Srednicki, M. 1993, ApJ, 403, L1

Feng, B., Li, H., Li, M.-z., & Zhang, X.-m. 2005, Phys. Lett., B620, 27

Feng, B., Li, M., Xia, J.-Q., Chen, X., & Zhang, X. 2006, Phys. Rev. Lett., 96, 221302

Ferreira, P. G., & Joyce, M. 1998, Phys. Rev. D, 58, 023503

Ford, L. H. 1987, Phys. Rev., D35, 2339

Freedman, W. L., et al. 2001, ApJ, 553, 47

Freese, K., Frieman, J. A., & Olinto, A. V. 1990, Phys. Rev. Lett., 65, 3233

Fujii, Y., & Nishioka, T. 1990, Phys. Rev., D42, 361

Fukuda, S., et al. 2001a, Phys. Rev. Lett., 86, 5656

Fukuda, S., et al. 2001b, Phys. Rev. Lett., 86, 5651

Fukuda, Y., et al. 1994, Phys. Lett., B335, 237

Fukuda, Y., et al. 1998, Phys. Rev. Lett., 81, 1562

Fukugita, M. 2006, Nucl. Phys. Proc. Suppl., 155, 10

Futamase, T., & Maeda, K.-i. 1989, Phys. Rev., D39, 399

Gangui, A., Lucchin, F., Matarrese, S., & Mollerach, S. 1994, ApJ, 430, 447

Garriga, J., & Mukhanov, V. F. 1999, Phys. Lett., B458, 219

Gaztañaga, E., & Wagg, J. 2003, Phys. Rev. D, 68, 021302

Gnedin, N. Y., & Gnedin, O. Y. 1998, ApJ, 509, 11

Gold, B., et al. 2008, ApJS

Goobar, A., Hannestad, S., Mortsell, E., & Tu, H. 2006, JCAP, 0606, 019

Gordon, C., Hu, W., Huterer, D., & Crawford, T. 2005, Phys. Rev. D, 72, 103002

Gordon, C., & Lewis, A. 2003, Phys. Rev., D67, 123513

Gordon, C., & Malik, K. A. 2004, Phys. Rev., D69, 063508

Gordon, C., Wands, D., Bassett, B. A., & Maartens, R. 2001, Phys. Rev., D63, 023506

Gott, J. R., Colley, W. N., Park, C.-G., Park, C., & Mugnolo, C. 2007, MNRAS, 377, 1668

Gott, J. R. I., Park, C., Juszkiewicz, R., Bies, W. E., Bennett, D. P., Bouchet, F. R., & Stebbins, A. 1990, ApJ, 352, 1

Grishchuk, L. P. 1975, Sov. Phys. JETP, 40, 409

Grivell, I. J., & Liddle, A. R. 2000, Phys. Rev. D, 61, 081301

Guth, A. H. 1981, Phys. Rev. D, 23, 347

Guth, A. H., & Pi, S. Y. 1982, Phys. Rev. Lett., 49, 1110

Hajian, A., & Souradeep, T. 2003, Astrophys. J., 597, L5

Hajian, A., & Souradeep, T. 2006, Phys. Rev. D, 74, 123521

Hajian, A., Souradeep, T., & Cornish, N. 2005, ApJ, 618, L63

Hamann, J., Hannestad, S., Raffelt, G. G., & Wong, Y. Y. Y. 2007, JCAP, 0708, 021

Hampel, W., et al. 1999, Phys. Lett., B447, 127

Hanany, S., et al. 2000, ApJ, 545, L5

Hannestad, S. 2003, JCAP, 0305, 004

Hannestad, S. 2004, JCAP, 0404, 002

Hannestad, S. 2005, Phys. Rev. Lett., 95, 221301
Hannestad, S. 2006a, JCAP, 0601, 001
Hannestad, S. 2006b, Ann. Rev. Nucl. Part. Sci., 56, 137
Hannestad, S., & Raffelt, G. 2004, JCAP, 0404, 008
Hannestad, S., & Raffelt, G. G. 2006, JCAP, 0611, 016
Hannestad, S., & Wong, Y. Y. Y. 2007, JCAP, 0707, 004
Hansen, F. K., Banday, A. J., & Gorski, K. M. 2004, MNRAS, 354, 641
Hansen, F. K., Cabella, P., Marinucci, D., & Vittorio, N. 2004, ApJ, 607, L67
Hawking, S. W. 1982, Phys. Lett., B115, 295
Hikage, C., Komatsu, E., & Matsubara, T. 2006, ApJ, 653, 11
Hikage, C., Matsubara, T., Coles, P., Liguori, M., Hansen, F. K., & Matarrese, S. 2008, ArXiv e-prints, 802
Hill, R., et al. 2008, ApJS
Hinshaw, G., et al. 2008, ApJS
Hinshaw, G., et al. 2007, ApJS, 170, 288
Hirata, K. S., et al. 1992, Phys. Lett., B280, 146
Ho, S., Hirata, C. M., Padmanabhan, N., Seljak, U., & Bahcall, N. 2008, ArXiv e-prints, 801
Hoekstra, H., et al. 2006, ApJ, 647, 116
Holman, R., & Tolley, A. J. 2007, ArXiv e-prints, 710
Hu, W. 1998, ApJ, 506, 485
Hu, W. 2005, Phys. Rev., D71, 047301
Hu, W. 2008, ArXiv e-prints, 801
Hu, W., & Eisenstein, D. J. 1998, ApJ, 498, 497
Hu, W., Eisenstein, D. J., & Tegmark, M. 1998, Phys. Rev. Lett., 80, 5255
Hu, W., & Okamoto, T. 2004, Phys. Rev., D69, 043004
Hu, W., & Sawicki, I. 2007, Phys. Rev. D, 76, 104043
Hu, W., Scott, D., Sugiyama, N., & White, M. 1995, Phys. Rev. D, 52, 5498
Hu, W., & Sugiyama, N. 1996, ApJ, 471, 542
Huang, M.-X., & Shiu, G. 2006, Phys. Rev. D, 74, 121301
Huffenberger, K. M., Eriksen, H. K., & Hansen, F. K. 2006, ApJ, 651, L81
Hwang, J., & Noh, H. 1998, Physical Review Letters, Volume 81, Issue 24, December 14, 1998, pp.5274-5277, 81, 5274
Ichikawa, K., Fukugita, M., & Kawasaki, M. 2005, Phys. Rev. D, 71, 043001
Ichikawa, K., Kawasaki, M., & Takahashi, F. 2007, JCAP, 0705, 007
Ishak, M., Upadhye, A., & Spergel, D. N. 2006, Phys. Rev., D74, 043513
Jaffe, T. R., Banday, A. J., Eriksen, H. K., Górski, K. M., & Hansen, F. K. 2005, ApJ, 629, L1
Jaffe, T. R., Banday, A. J., Eriksen, H. K., Górski, K. M., & Hansen, F. K. 2006, A&A, 460, 393
Jain, B., & Zhang, P. 2007, ArXiv e-prints, 709
Jokinen, A., & Mazumdar, A. 2006, JCAP, 0604, 003
Jones, W. C., et al. 2006, ApJ, 647, 823
Kadota, K., Dodelson, S., Hu, W., & Stewart, E. D. 2005, Phys. Rev. D, 72, 023510
Kain, B. 2006, Phys. Rev., D73, 123521
Kalara, S., Kaloper, N., & Olive, K. A. 1990, Nucl. Phys., B341, 252
Kamionkowski, M., Kosowsky, A., & Stebbins, A. 1997, Phys. Rev. Lett., 78, 2058
Kamionkowski, M., Kosowsky, A., & Stebbins, A. 1997, Phys. Rev. D, 55, 7368
Kawasaki, M., & Sekiguchi, T. 2007, ArXiv e-prints, 705
Kazanas, D. 1980, ApJ, 241, L59
Keskitalo, R., Kurki-Suonio, H., Muhonen, V., & Valiviita, J. 2007, JCAP, 0709, 008
Khoury, J., Ovrut, B. A., Seiberg, N., Steinhardt, P. J., & Turok, N. 2002a, Phys. Rev., D65, 086007
Khoury, J., Ovrut, B. A., Steinhardt, P. J., & Turok, N. 2001, Phys. Rev., D64, 123522
Khoury, J., Ovrut, B. A., Steinhardt, P. J., & Turok, N. 2002b, Phys. Rev., D66, 046005
Khoury, J., Steinhardt, P. J., & Turok, N. 2003, Phys. Rev. Lett., 91, 161301
Kim, T.-S., Bolton, J. S., Viel, M., Haehnelt, M. G., & Carswell, R. F. 2007, MNRAS, 382, 1657
Kinney, W. H. 1998, Phys. Rev., D58, 123506
Kinney, W. H., Kolb, E. W., Melchiorri, A., & Riotto, A. 2006, Phys. Rev., D74, 023502

Kitching, T. D., Heavens, A. F., Verde, L., Serra, P., & Melchiorri, A. 2008, ArXiv e-prints, 801
Knox, L. 2006, Phys. Rev., D73, 023503
Kodama, H., & Sasaki, M. 1984, Prog. Theor. Phys. Suppl., 78, 1
Kofman, L., Blumenthal, G. R., Hodges, H., & Primack, J. R. 1991, in ASP Conf. Ser. 15: Large-scale Structures and Peculiar Motions in the Universe, pp.339
Kogo, N., & Komatsu, E. 2006, Phys. Rev., D73, 083007
Kogo, N., Matsumiya, M., Sasaki, M., & Yokoyama, J. 2004, ApJ, 607, 32
Kogo, N., Sasaki, M., & Yokoyama, J. 2005, Prog. Theor. Phys., 114, 555
Kolb, E. W., & Turner, M. S. 1990, The Early Universe (New York, NY: Addison-Wesley)
Komatsu, E. 2001, ArXiv Astrophysics e-prints, Ph.D. thesis at Tohoku University (astro-ph/0206039)
Komatsu, E., & Futamase, T. 1999, Phys. Rev., D59, 064029
Komatsu, E., et al. 2003, ApJS, 148, 119
Komatsu, E., & Seljak, U. 2002, MNRAS, 336, 1256
Komatsu, E., & Spergel, D. N. 2001, Phys. Rev. D, 63, 63002
Komatsu, E., Spergel, D. N., & Wandelt, B. D. 2005, ApJ, 634, 14
Komatsu, E., Wandelt, B. D., Spergel, D. N., Banday, A. J., & Górski, K. M. 2002, ApJ, 566, 19
Kosowsky, A., & Turner, M. S. 1995, Phys. Rev. D, 52, 1739
Koyama, K., & Maartens, R. 2006, Journal of Cosmology and Astro-Particle Physics, 1, 16
Koyama, K., Mizuno, S., Vernizzi, F., & Wands, D. 2007, ArXiv e-prints, 708
Koyama, K., & Wands, D. 2007, JCAP, 0704, 008
Kuo, C. L., et al. 2007, ApJ, 664, 687
Kuo, C. L., et al. 2004, ApJ, 600, 32
Kurki-Suonio, H., Muhonen, V., & Valiviita, J. 2005, Phys. Rev., D71, 063005
La, D., & Steinhardt, P. J. 1989, Phys. Rev. Lett., 62, 376
Land, K., & Magueijo, J. 2005a, MNRAS, 357, 994
Land, K., & Magueijo, J. 2005b, Physical Review Letters, 95, 071301
Land, K., & Magueijo, J. 2007, MNRAS, 378, 153
Langlois, D. 1999, Phys. Rev., D59, 123512
Langlois, D., & Riazuelo, A. 2000, Phys. Rev., D62, 043504
Larson, D. L., & Wandelt, B. D. 2004, ApJ, 613, L85
Lattanzi, M., Ruffini, R., & Vereshchagin, G. V. 2005, Phys. Rev. D, 72, 063003
Lazarides, G. 2005, Nucl. Phys. Proc. Suppl., 148, 84
Lazarides, G., de Austri, R. R., & Trotta, R. 2004, Phys. Rev., D70, 123527
Lee, T. D., & Yang, C.-N. 1956, Phys. Rev., 104, 254
Lehners, J.-L., & Steinhardt, P. J. 2007, ArXiv e-prints, 712
Lesgourgues, J., & Pastor, S. 2006, Phys. Rept., 429, 307
Lesgourgues, J., & Valkenburg, W. 2007, Phys. Rev. D, 75, 123519
Lesgourgues, J., Viel, M., Haehnelt, M. G., & Massey, R. 2007, JCAP, 0711, 008
Lewis, A., & Challinor, A. 2006, Phys. Rep., 429, 1
Liddle, A. R., & Leach, S. M. 2003, Phys. Rev., D68, 103503
Liddle, A. R., & Lyth, D. H. 2000, Cosmological inflation and large-scale structure (Cambridge University Press)
Liddle, A. R., Mazumdar, A., & Schunck, F. E. 1998, Phys. Rev., D58, 061301
Lidsey, J. E., Liddle, A. R., Kolb, E. W., Copeland, E. J., Barreiro, T., & Abney, M. 1997, Rev. Mod. Phys., 69, 373
Linde, A. 2008, Lect. Notes Phys., 738, 1
Linde, A., & Mukhanov, V. 1997, Phys. Rev. D, 56, 535
Linde, A. D. 1982, Phys. Lett., B108, 389
Linde, A. D. 1983, Phys. Lett., B129, 177
Linde, A. D. 1985, Physics Letters B, 158, 375
Linde, A. D. 1991, Phys. Lett., B259, 38
Linde, A. D. 1994, Phys. Rev., D49, 748
Linder, E. V. 2003, Phys. Rev. Lett., 90, 091301
Linder, E. V., & Cahn, R. N. 2007, Astropart. Phys., 28, 481
Linder, E. V., & Jenkins, A. 2003, MNRAS, 346, 573
Liu, G.-C., Lee, S., & Ng, K.-W. 2006, Phys. Rev. Lett., 97, 161303
Lucchin, F., & Matarrese, S. 1985, Phys. Rev., D32, 1316
Lue, A., Wang, L., & Kamionkowski, M. 1999, Physical Review Letters, 83, 1506
Lyth, D. H., Malik, K. A., & Sasaki, M. 2005, JCAP, 0505, 004
Lyth, D. H., & Rodriguez, Y. 2005, Phys. Rev. Lett., 95, 121302
Lyth, D. H., Ungarelli, C., & Wands, D. 2003, Phys. Rev. D, 67, 23503

Lyth, D. H., & Wands, D. 2003, Phys. Rev., D68, 103516
Ma, C.-P. 1996, ApJ, 471, 13
Maldacena, J. M. 2003, JHEP, 05, 013
Mangano, G., Melchiorri, A., Mena, O., Miele, G., & Slosar, A. 2007, JCAP, 0703, 006
Mangano, G., Miele, G., Pastor, S., & Peloso, M. 2002, Phys. Lett., B534, 8
Mason, B. S., et al. 2003, ApJ, 591, 540
Matsumiya, M., Sasaki, M., & Yokoyama, J. 2002, Phys. Rev. D, 65, 083007
Matsumiya, M., Sasaki, M., & Yokoyama, J. 2003, JCAP, 2, 3
McAllister, L., & Silverstein, E. 2008, General Relativity and Gravitation, 32
Mecke, K. R., Buchert, T., & Wagner, H. 1994, A&A, 288, 697
Melchiorri, A., & Serra, P. 2006, Phys. Rev., D74, 127301
Michael, D. G., et al. 2006, Phys. Rev. Lett., 97, 191801
Miller, A. D., et al. 1999, ApJ, 524, L1
Miller, A. D., et al. 2002, ApJS, 140, 115
Miller, N. J., Keating, B. G., & Polnarev, A. G. 2007, ArXiv e-prints, 710
Mollerach, S., & Matarrese, S. 1997, Phys. Rev., D56, 4494
Montroy, T. E., et al. 2006, ApJ, 647, 813
Moodley, K., Bucher, M., Dunkley, J., Ferreira, P. G., & Skordis, C. 2004, Phys. Rev., D70, 103520
Moroi, T., & Takahashi, T. 2001, Phys. Lett., B522, 215
Moroi, T., & Takahashi, T. 2002, Phys. Rev., D66, 063501
Moss, I. G., & Graham, C. M. 2007, JCAP, 0711, 004
Moss, I. G., & Xiong, C. 2007, JCAP, 0704, 007
Mukhanov, V. F., & Chibisov, G. V. 1981, JETP Letters, 33, 532
Mukherjee, P., & Wang, Y. 2003a, ApJ, 598, 779
Mukherjee, P., & Wang, Y. 2003b, ApJ, 599, 1
Mukherjee, P., & Wang, Y. 2003c, ApJ, 593, 38
Mukherjee, P., & Wang, Y. 2004, ApJ, 613, 51
Naselsky, P. D., Christensen, P. R., Coles, P., Verkhodanov, O., Novikov, D., & Kim, J. 2007, ArXiv e-prints, 712
Nesseris, S., & Perivolaropoulos, L. 2008, Phys. Rev. D, 77, 023504
Netterfield, C. B., et al. 2002, ApJ, 571, 604
Nolta, M. R., et al. 2008, ApJS
Okamoto, T., & Hu, W. 2002, Phys. Rev. D, 66, 063008
Okumura, T., Matsubara, T., Eisenstein, D. J., Kayo, I., Hikage, C., Szalay, A. S., & Schneider, D. P. 2007, ArXiv e-prints, 711
Padmanabhan, T. 2003, Phys. Rept., 380, 235
Padmanabhan, T. 2005, Curr. Sci., 88, 1057
Page, L., et al. 2007, ApJS, 170, 335
Pagels, H., & Primack, J. R. 1982, Phys. Rev. Lett., 48, 223
Park, C. 2004, MNRAS, 349, 313
Park, C.-G., Park, C., & Gott, J. R. I. 2007, ApJ, 660, 959
Parkinson, D., Tsujikawa, S., Bassett, B. A., & Amendola, L. 2005, Phys. Rev., D71, 063524
Pearson, T. J., et al. 2003, ApJ, 591, 556
Peebles, P. J., & Ratra, B. 2003, Rev. Mod. Phys., 75, 559
Peebles, P. J. E., & Ratra, B. 1988, ApJ, 325, L17
Peiris, H., & Easther, R. 2006a, JCAP, 0607, 002
Peiris, H., & Easther, R. 2006b, JCAP, 0610, 017
Peiris, H. V., et al. 2003, ApJS, 148, 213
Percival, W. J., Cole, S., Eisenstein, D. J., Nichol, R. C., Peacock, J. A., Pope, A. C., & Szalay, A. S. 2007, MNRAS, 381, 1053
Perlmutter, S., et al. 1999, ApJ, 517, 565
Piacentini, F., et al. 2006, ApJ, 647, 833
Pierpaoli, E. 2003, Mon. Not. Roy. Astron. Soc., 342, L63
Polarski, D., & Starobinsky, A. A. 1992, Nucl. Phys., B385, 623
Polarski, D., & Starobinsky, A. A. 1994, Phys. Rev., D50, 6123
Polnarev, A. G. 1985, AZh, 62, 1041
Polnarev, A. G., Miller, N. J., & Keating, B. G. 2007, ArXiv e-prints, 710
Powell, B. A., & Kinney, W. H. 2007, JCAP, 0708, 006
Press, W. H., Teukolsky, S. A., Vetterling, W. T., & Flannery, B. P. 1992, Numerical Recipes in C (second ed.) (Cambridge, UK: Cambridge University Press)
Prunet, S., Uzan, J.-P., Bernardeau, F., & Brunier, T. 2005, Phys. Rev. D, 71, 083508
Pyne, T., & Carroll, S. M. 1996, Phys. Rev., D53, 2920
Rakić, A., & Schwarz, D. J. 2007, Phys. Rev. D, 75, 103002
Räth, C., Schuecker, P., & Banday, A. J. 2007, MNRAS, 380, 466
Ratra, B., & Peebles, P. J. E. 1988, Phys. Rev. D, 37, 3406
Readhead, A. C. S., et al. 2004, ApJ, 609, 498
Refregier, A., Spergel, D. N., & Herbig, T. 2000, ApJ, 531, 31
Reichardt, C. L., et al. 2008, ArXiv e-prints, 801

Riess, A. G., et al. 1998, AJ, 116, 1009
Riess, A. G., et al. 2004, ApJ, 607, 665
Riess, A. G., et al. 2007, ApJ, 659, 98
Rubakov, V. A., Sazhin, M. V., & Veryaskin, A. V. 1982, Phys. Lett., B115, 189
Ruhl, J. E., et al. 2003, ApJ, 599, 786
Sachs, R. K., & Wolfe, A. M. 1967, ApJ, 147, 73
Sahni, V., & Starobinsky, A. A. 2000, Int. J. Mod. Phys., D9, 373
Saito, S., Ichiki, K., & Taruya, A. 2007, JCAP, 0709, 002
Salopek, D. S., & Bond, J. R. 1990, Phys. Rev. D, 42, 3936
Sanchez, A. G., & Cole, S. 2007, ArXiv e-prints, 708
Santos, M. G., et al. 2003, MNRAS, 341, 623
Sasaki, M., & Stewart, E. D. 1996, Prog. Theor. Phys., 95, 71
Sato, K. 1981, MNRAS, 195, 467
Savage, C., Freese, K., & Kinney, W. H. 2006, Phys. Rev. D, 74, 123511
Schmalzing, J., & Buchert, T. 1997, ApJ, 482, L1
Schmalzing, J., & Gorski, K. M. 1998, MNRAS, 297, 355
Schwarz, D. J., Starkman, G. D., Huterer, D., & Copi, C. J. 2004, Physical Review Letters, 93, 221301
Sealfon, C., Verde, L., & Jimenez, R. 2005, Phys. Rev. D, 72, 103520
Seckel, D., & Turner, M. S. 1985, Phys. Rev. D, 32, 3178
Seery, D., & Lidsey, J. E. 2005, JCAP, 0506, 003
Seery, D., & Lidsey, J. E. 2007, JCAP, 0701, 008
Seery, D., Lidsey, J. E., & Sloth, M. S. 2007, JCAP, 0701, 027
Seljak, U., et al. 2005a, Phys. Rev. D, 71, 043511
Seljak, U., et al. 2005b, Phys. Rev. D, 71, 103515
Seljak, U., Slosar, A., & McDonald, P. 2006, JCAP, 0610, 014
Seljak, U., & Zaldarriaga, M. 1997, Phys. Rev. Lett., 78, 2054
Serra, P., & Cooray, A. 2008, ArXiv e-prints, 801
Shafieloo, A., & Souradeep, T. 2004, Phys. Rev. D, 70, 043523
Shafieloo, A., & Souradeep, T. 2007, ArXiv e-prints, 709
Sievers, J. L., et al. 2007, ApJ, 660, 976
Sievers, J. L., et al. 2003, ApJ, 591, 599
Sikivie, P. 2008, Lect. Notes Phys., 741, 19
Silk, J., & Turner, M. S. 1987, Phys. Rev., D35, 419
Silverstein, E., & Tong, D. 2004, Phys. Rev. D, 70, 103505
Slosar, A. 2006, Phys. Rev., D73, 123501
Smith, K. M., & Zaldarriaga, M. 2006, ArXiv Astrophysics e-prints
Smith, S., et al. 2004, MNRAS, 352, 887
Smoot, G. F., et al. 1992, ApJ, 396, L1
Song, Y.-S., Hu, W., & Sawicki, I. 2007, Phys. Rev. D, 75, 044004
Spergel, D. N., et al. 2007, ApJS, 170, 377
Spergel, D. N., et al. 2003, ApJS, 148, 175
Spergel, D. N., & Zaldarriaga, M. 1997, Phys. Rev. Lett., 79, 2180
Starobinsky, A. A. 1979, ZhETF Pis ma Redaktsiiu, 30, 719
Starobinsky, A. A. 1982, Phys. Lett., B117, 175
Starobinsky, A. A. 1985, Sov. Astron. Lett., 11, 133
Steigman, G. 2007, Annual Review of Nuclear and Particle Science, 57, 463
Steigman, G., Schramm, D. N., & Gunn, J. E. 1977, Phys. Lett., B66, 202
Steinhardt, P. J., & Accetta, F. S. 1990, Phys. Rev. Lett., 64, 2740
Stompor, R., & Efstathiou, G. 1999, MNRAS, 302, 735
Takada, M., Komatsu, E., & Futamase, T. 2006, Phys. Rev. D, 73, 083520
Tegmark, M. 2005, Phys. Scripta, T121, 153
Tegmark, M., et al. 2004a, ApJ, 606, 702
Tegmark, M., de Oliveira-Costa, A., & Hamilton, A. J. 2003, Phys. Rev. D, 68, 123523
Tegmark, M., et al. 2006, Phys. Rev. D, 74, 123507
Tegmark, M., et al. 2004b, Phys. Rev. D, 69, 103501
Tocchini-Valentini, D., Douspis, M., & Silk, J. 2005, MNRAS, 359, 31
Tocchini-Valentini, D., Hoffman, Y., & Silk, J. 2006, MNRAS, 367, 1095
Trotta, R. 2007, Mon. Not. Roy. Astron. Soc. Lett., 375, L26
Trotta, R., & Melchiorri, A. 2005, Phys. Rev. Lett., 95, 011305
Tsujikawa, S., & Gumjudpai, B. 2004, Phys. Rev., D69, 123523
Turner, M. S., & Wilczek, F. 1991, Phys. Rev. Lett., 66, 5
Upadhye, A. 2007, Nucl. Phys. Proc. Suppl., 173, 11
Verde, L., & Peiris, H. V. 2008, ArXiv e-prints, 802
Verde, L., Wang, L., Heavens, A. F., & Kamionkowski, M. 2000, MNRAS, 313, 141
Viel, M., Haehnelt, M. G., & Lewis, A. 2006, MNRAS, 370, L51
Vielva, P., Martínez-González, E., Barreiro, R. B., Sanz, J. L., & Cayón, L. 2004, ApJ, 609, 22

Wandelt, B. D., Larson, D. L., & Lakshminarayanan, A. 2004, Phys. Rev. D, 70, 083511

Wang, L., & Kamionkowski, M. 2000, Phys. Rev. D, 61, 63504

Wang, L., & Steinhardt, P. J. 1998, ApJ, 508, 483

Wang, Y., & Mukherjee, P. 2007, Phys. Rev. D, 76, 103533

Wang, Y., & Tegmark, M. 2004, Phys. Rev. Lett., 92, 241302

Weinberg, S. 1972, Gravitation and Cosmology (New York, NY: John Wiley)

Weinberg, S. 1978, Phys. Rev. Lett., 40, 223

Weinberg, S. 1989, Rev. Mod. Phys., 61, 1

Weinberg, S. 2003, Phys. Rev. D, 67, 123504

Weinberg, S. 2004, Phys. Rev., D70, 083522

Weinberg, S. 2008, Cosmology (Oxford, UK: Oxford University Press)

Wetterich, C. 1988, Nucl. Phys., B302, 668

Wiaux, Y., Vielva, P., Barreiro, R. B., Martínez-González, E., & Vandergheynst, P. 2008, MNRAS, 217

Wilczek, F. 1978, Phys. Rev. Lett., 40, 279

Winitzki, S., & Kosowsky, A. 1998, New Astronomy, 3, 75

Wood-Vasey, W. M., et al. 2007, ApJ, 666, 694

Wright, E. L. 2007, ApJ, 664, 633

Wright, E. L., et al. 2008, ApJS

Wu, C. S., Ambler, E., Hayward, R. W., Hoppes, D. D., & Hudson, R. P. 1957, Phys. Rev., 105, 1413

Xia, J.-Q., Li, H., Wang, X., & Zhang, X. 2007, ArXiv e-prints, 710

Yadav, A. P. S., Komatsu, E., Wandelt, B. D., Liguori, M., Hansen, F. K., & Matarrese, S. 2007, ArXiv e-prints, 711

Yadav, A. P. S., & Wandelt, B. D. 2007, ArXiv e-prints, 712

Yamamoto, K., Parkinson, D., Hamana, T., Nichol, R. C., & Suto, Y. 2007, Phys. Rev. D, 76, 023504

Yao, W. M., et al. 2006, J. Phys., G33, 1

Zaldarriaga, M. 1997, Phys. Rev. D, 55, 1822

Zaldarriaga, M., & Seljak, U. 1997, Phys. Rev. D, 55, 1830

Zaldarriaga, M., & Seljak, U. 1998, Phys. Rev., D58, 023003

Zhang, P., Liguori, M., Bean, R., & Dodelson, S. 2007, Phys. Rev. Lett., 99, 141302

Zlatev, I., Wang, L., & Steinhardt, P. J. 1999, Phys. Rev. Lett., 82, 896